COO-1112-7

THE UNIVERSITY OF MICHIGAN

COLLEGE OF LITERATURE, SCIENCE, AND THE ARTS

Department of Physics

Technical Report

PION DEUTERON ELASTIC SCATTERING AND BREAK UP AT 3.65 BEV/C

Hsien-chih Hsiung

ORA Project 04938

Under contract with:

U. S. ATOMIC ENERGY COMMISSION
CHICAGO OPERATIONS OFFICE
CONTRACT NO. AT(11-1)-1112
ARGONNE, ILLINOIS

Administered through:

OFFICE OF RESEARCH ADMINISTRATION ANN ARBOR

March 1969

This report was also a dissertation submitted in partial fulfillment of the requirements for the degree of Doctor of Philosophy in The University of Michigan, 1969.

TABLE OF CONTENTS

TABLE OF CONTENTS (Concluded)

LIST OF TABLES

LIST OF FIGURES

LIST OF FIGURES (Continued)

LIST OF FIGURES (Continued)

LIST OF FIGURES (Concluded)

ABSTRACT

PION DEUTERON ELASTIC SCATTERING AND
BREAK UP AT 3.65 BEV/C

by

Hsien-chih Hsiung

Chairman: Byron P. Roe

An experimental and theoretical investigation of pion-deuteron elastic scattering and deuteron break up reaction is presented.

The differential cross section for the elastic scattering of positive pions from deuterons at 3.65 BeV/c has been measured. Measurements were made for -t, the four momentum transfer squared, in the range 0.043-1.0 $(BeV/c)^2$. The data were obtained in a 222,000 picture exposure of the 20-inch deuteron bubble chamber at Brookhaven National Laboratory AGS. Experimental results are compared with calculations based on the Glauber high-energy approximation, utilizing the total $^3S_1 + {}^3D_1$ deuteron wave function and pion-nucleon scattering amplitudes. The experimental data do not show evidence for a pronounced dip. The agreement between experimental data and theoretical prediction is good.

The differential cross section for the deuteron break up reaction, $\pi^+ + d \rightarrow \pi^+ + p + n$, at 3.65 BeV/c has also been measured for -t in the range 0.0625-0.30 $(BeV/c)^2$. A theoretical prediction, based on Glauber's approximation, was calculated for a particular final state, $E_p = E_n$, and compared with the experimental results.

CHAPTER I

INTRODUCTION

The problem of coherent elastic scattering of high energy particles from bound states has received a good deal of attention in past years. The deuteron can be considered to be a non-relativistic bound state of a neutron and a proton. The weak binding of the deuteron and the large distance (3 fermi) between its components compared to the range of the neutron-proton interaction ($\hbar/m_\pi c$ = 1.4 fermi) encourage one to believe that it is a good approximation to treat the neutron and the proton in the deuteron as free particles[1] and thus, calculate the hadron deuteron elastic scattering cross section by using hadron nucleon elastic scattering amplitudes. For the pion-deuteron elastic scattering calculation, we will require pion-nucleon scattering amplitudes. Fortunately, a large amount of information about these amplitudes is available.[2]

The pion-deuteron elastic scattering differential cross section for pions with laboratory energies 61[3], 85[4], 140[5], 142[6], and 300[7] MeV havebeen measured. Above 300 MeV, pion-deuteron elastic scattering data has been scarce. Vegni et al.[8] have determined the differential cross section at a pion momentum of 6 BeV/c for values of four momentum transfer square (-t) out to 0.14 $(BeV/c)^2$. In the present experiment the elastic differential cross section for an incident pion

momentum of 3.65 BeV/c has been measured for (-t) out to 1.0 $(BeV/c)^2$, corresponding to a cosine of the center-of-mass scattering angle of 0.861. The differential cross section for the deuteron break up reaction has also been measured for (-t) out to 0.30 $(BeV/c)^2$.

The dynamical model used here for theoretical predictions is the multiple scattering model proposed many years ago by Glauber[9-14]. This is described in detail in Chapter II. In Chapter III the experimental techniques and results of elastic scattering and deuteron break up reaction are presented. In Chapter IV a comparison of the experimental elastic scattering cross section with the prediction based on the Glauber formalism is discussed. Finally in Chapter V a comparison of the experimental deuteron break up reaction result with the theoretical prediction is given.

CHAPTER II

MULTIPLE DIFFRACTION THEORY OF HIGH-ENERGY COLLISIONS

A. HIGH ENERGY APPROXIMATION BY GLAUBER

The common characteristic of high energy scattering of strongly interacting particles is a very strong forward diffraction peak. The description of this characteristic on the basis of a partial wave expansion would require a large number of terms with delicate cancellations. This characteristic occurs naturally in the semi-classical theory of scattering, which bears a certain family resemblance to the diffraction theory of physical optics. However, the situations encountered in scattering theory are usually quite different from those of optics. For example, the target particles in a nucleus are free to move about a bound state while the particles in a diffraction theory are always stationary. Therefore it is necessary to develop mathematical methods which are more general than those of physical optics. In diffraction theory one assumes that the incident plane wave sweeps, virtually undeviated, through the region of interaction, and emerges suffering only a position dependent change of phase and amplitude. When one makes use of a co-ordinate frame in which the target particle is displaced from the origin, the scattering interaction loses its azimuthal symmetry about the axis parallel to the direction of incident particle. Near the forward direction, the scattering amplitude

at high energy is given by

$$f(\vec{k}',\vec{k}) = \frac{k}{2\pi i}\int \exp i(\vec{k}-\vec{k}')\cdot\vec{b}\{\exp[i\chi(\vec{b})]-1\}d^2\vec{b} \qquad (2\text{-}1)$$

where $\vec{b}$ is the impact-parameter in the plane perpendicular to the direction of incidence, $\chi(\vec{b})$ is the phase shift, $\vec{k}$ is the initial propagation vector, $\vec{k}'$ the deflected one, k is the magnitude of $\vec{k}$, and $d^2\vec{b}$ is an element of area in the impact vector plane. For an axially symmetric region of interaction centered at b = 0, the expression for the scattering amplitude reduces to

$$f(\vec{k}',\vec{k}) = ik\int_0^\infty J_0(|\vec{k}-\vec{k}'|b)[1-e^{i\chi(\vec{b})}]bdb \qquad (2\text{-}2)$$

in which the Bessel function J_0 may be recognized as the asymptotic form of a Legendre polynomial valid for small scattering angles. A general expression for this amplitude is shown in Appendix A. It will be convenient to employ an abbreviation by defining a profile function

$$\Gamma(\vec{b}) = 1 - e^{i\chi(\vec{b})} \quad . \qquad (2\text{-}3)$$

Then the scattering amplitude for momentum transfer $\hbar\vec{q}$ is the Fourier transform of the profile function,

$$f(\vec{q}) = \frac{ik}{2\pi} \int e^{i\vec{q}\cdot\vec{b}} \Gamma(\vec{b}) d^2\vec{b} \quad . \tag{2-4}$$

Conversely, the profile function is the inverse transform

$$\Gamma(\vec{b}) = \frac{1}{2\pi ik} \int e^{-i\vec{q}\cdot\vec{b}} f(\vec{q}) d^2\vec{q} \tag{2-5}$$

where the integration is over a plane perpendicular to $\vec{k}$. The integration over a plane is approximately correct. A precise way would involve integration over the surface of a sphere which more accurately represents the locus of $\vec{q}$ for fixed energy and varying angle. However, the correction due to this approximation can be considered small because of the fact that $f(\vec{q})$ is sharply peaked forward and we don't look at large angles.

The formulas we have written for the scattering amplitude are the correct form for describing the collision of the incident and the target particles in their center-of-mass system. In order to compare cross-sections of nuclei (e.g., deuteron) with those of free nucleons by calculating scattering amplitudes in center-of-mass systems, however, we should have to make use of at least two such systems. It is considerably simpler to do the calculation in the laboratory system. In fact, it is shown in Appendix B that expressions (2-1) and (2-2) can be easily transformed to the laboratory

system. Because of the simple geometry and small recoil effect which are associated with the nearly forward scattering we simply substitute laboratory values for $\vec{k}$ and $\vec{k}'$ into Equations (2-1) and (2-2) to obtain the scattering amplitude in the laboratory system.

For a target particle (nucleus) consisting of a total of A nucleons with coordinates $\vec{r}_1$, ... $\vec{r}_A$, assuming that the incident particle interacts with the target particles by means of two-body forces, the total phase shift is the sum of the phase shifts by the individual particles,

$$\chi_{tot}(\vec{b},\vec{r}_1, \ldots \vec{r}_A) = \sum_{j=1}^{A} \chi_j(\vec{b} - \vec{s}_j) \qquad (2\text{-}5)$$

where $\vec{s}$ is the projection of the position coordinates on a plane perpendicular to the incident beam.

The optical analogy of this approximation can be seen as follows. The total phase shift as a photon passes through a lens is simply the sum of the infinitesimal phase shifts along the trajectory r. That is,

$$\delta\chi = n(r)\vec{k}(r) \cdot \delta\vec{r} \qquad (2\text{-}6)$$

where n(r) is the local index of refraction, $\vec{k}$ is the local propagation vector of the wave. Glauber's theory assumes that it is a good approximation to obtain the total phase

shift not by adding up the infinitesimal phase shifts along the true trajectory of the photon, but rather along a straight line, in the undeviated beam direction. The Glauber approximation takes advantage of the fact that the motion of a nucleon that is a part of the target particle is characteristically rather slow in comparison to that of a high energy incident particle. Therefore, the nucleons are fixed in their instantaneous positions during the passage of the incident particle through the nucleus. This approximation amounts to neglecting the energy communicated to the target nucleons by the incident particle. In a nonrelativistic picture, however, the interactions between the incident particle and the nucleons are determined by the cloud of virtual particles surrounding the nucleons' cores, and these clouds might reasonably be expected to be distorted when the nucleons are brought together. If the distortion is significant one can hardly believe that treating nucleons in a nucleus as if they are free nucleons is correct. However, for a nucleus which has open structure (e.g., deuteron) the nucleon clouds overlap only slightly, and the approximation, assuming the total phase shift is the sum of the phase shifts of the individual particles, might well give a good approximation.

By expressions (2-3) and (2-4) the scattering amplitude for the fixed configuration of the nucleons is

$$\frac{ik}{2\pi} \int \exp[i(\vec{q}) \cdot (\vec{b})] \, \Gamma_{tot}(\vec{b}, \vec{s}_1, \ldots \vec{s}_A) d^2\vec{b} \qquad (2\text{-}7)$$

where

$$\Gamma_{+\sigma}(\vec{b},\vec{s}_1, \ldots \vec{s}_A) = 1 - \exp[i\chi_{tot}(\vec{b},\vec{s}_1, \ldots \vec{s}_A)]. \quad (2\text{-}8)$$

One may consider that the nucleons are not rigidly fixed in the positions $\vec{r}_1 \ldots \vec{r}_A$ by noting that $\Gamma_{tot}(\vec{b},\vec{r}_1, \ldots \vec{r}_A)$ can be regarded as an operator. Since one does not observe the positions of the nucleons one must average the scattering operator Γ_{tot} over the positions of the A nucleons.

The scattering amplitude for a collision process in which the incident particle suffers a momentum transfer $\hbar\vec{q} = \hbar(\vec{k}' - \vec{k})$ while the target nucleus undergoes a transition from the initial state $|i\rangle$ to final state $\langle f|$ may be written as

$$F_{fi}(\vec{q}) = \frac{ik}{2\pi} \int \exp[i\vec{q} \cdot \vec{b}]$$

$$x \langle f|\Gamma_{tot}(\vec{b},\vec{s}_1, \ldots \vec{s}_A)|i\rangle d^2\vec{b} \quad . \quad (2\text{-}9)$$

The initial state $|i\rangle$ is usually a nuclear ground state, but the final state $\langle f|$ may be the ground state (elastic scattering) or any excited state (inelastic scattering).

If ψ_i and ψ_f are the wave functions of the target particles for the initial and final states respectively, then one may write the scattering amplitude as

$$F_{fi}(\vec{q}) = \frac{ik}{2\pi} \int e^{i\vec{q}\cdot\vec{b}} \int \psi_f^*(\vec{r}_1^3 \ldots \vec{r}_A^3) d^3\vec{r}_1 \ldots d^3\vec{r}_A$$

$$x\ \Gamma_{tot}(\vec{b}, \vec{s}_1, \ldots \vec{s}_A)\ \psi_i(\vec{r}_1^3 \ldots \vec{r}_A^3)$$

$$\delta^3\left(\frac{1}{A} \sum_{j=1}^{A} \vec{r}_j\right) d^2\vec{b} \quad . \tag{2-10}$$

in which the delta function in the nuclear center-of-mass variable expresses the fact that the final nuclear state has a well defined momentum.[13] Using expressions (2-5) and (2-8) one can rewrite Equation (2-10) as

$$F_{fi}(\vec{q}) = \frac{ik}{2\pi} \int e^{i\vec{q}\cdot\vec{b}} \int \psi_f^*(\vec{r}_1^3 \ldots \vec{r}_A^3) d^3\vec{r}_1 \ldots d^3\vec{r}_A$$

$$x\{1 - \prod_{\ell=1}^{A} [1 - \Gamma_\ell(\vec{b} - \vec{s}_\ell)]\}\ x\ \psi_i(\vec{r}_1^3 \ldots \vec{r}_A^3)$$

$$x\delta\left(A^{-1} \sum_{j=1}^{A} \vec{r}_j\right) d^2\vec{b} \quad . \tag{2-11}$$

One can further express the scattering amplitude for the nucleus in terms of individual scattering amplitudes by using expression (2-4). This leads to the expression

$$F_{fi}(\vec{q}) = \frac{ik}{2\pi} \int e^{i\vec{q}\cdot\vec{b}} \int d^3\vec{r}_1 \ldots d^3\vec{r}_A \; \psi_f^*(\vec{r}_1^3 \ldots \vec{r}_A^3) \; \delta^3\left(\frac{1}{A} \sum_{j=1}^{A} \vec{r}_j\right)$$

$$\times \left\{1 - \prod_{j=1}^{A} \left[1 - \frac{1}{2\pi ik} \int e^{i\vec{q}_j\cdot(\vec{b}-\vec{s}_j)} f_j(\vec{q}_j) \, d^2\vec{q}_j\right]\right\}$$

$$\times \psi_i(\vec{r}_1^3 \ldots \vec{r}_A^3) \, d^2\vec{b} \qquad (2\text{-}12)$$

for the general nuclear scattering amplitude. If one expands the product in the integrand in Equation (2-12) one finds that the nuclear scattering amplitude F can be expressed by a polynomial in the nucleon amplitude f. This can be interpreted as a multiple scattering expansion. (An elaborate general sort of expansion can be found in the references on multiple scattering theory[15,16,17,18].) It is worth noting that the order of the polynomial is A, and that the lowest order term corresponds to the single scattering process and the second order term corresponds to the double scattering process, etc.

To evaluate the scattering amplitude F_{fi} in expression (2-12), one has to specify the structure of the initial and final state wave functions.

B. GLAUBER'S APPROXIMATION FOR DEUTERON SCATTERING

Let $\vec{r}_n$ and $\vec{r}_p$ be the coordinates of the neutron and proton in the deuteron. Then the relative internal coordinate

is $\vec{r} = \vec{r}_p - \vec{r}_n$.

In the case of elastic scattering of an incident particle on a deuteron ψ_i and ψ_f are the same, and the incident particle transfers momentum $\hbar\vec{q} = \hbar(\vec{k} - \vec{k}')$ to the deuteron. If one introduces the form factor

$$S(q) = \int e^{i\vec{q}\cdot\vec{r}} \left|\psi_i(\vec{r})\right|^2 d\vec{r} \qquad (2\text{-}13)$$

for the deuteron ground state, then the amplitude, Equation (2-12), for elastic scattering by a deuteron can be reduced to

$$F_{ii}(\vec{q}) = f_p(\vec{q})S(\tfrac{1}{2}q) + f_n(\vec{q})S(\tfrac{1}{2}q) + \frac{i}{2\pi k}\int S(q')f_p(\tfrac{1}{2}\vec{q} + \vec{q}')$$

$$\times f_n(\tfrac{1}{2}\vec{q} - \vec{q}')\, d^2\vec{q}' \quad . \qquad (2\text{-}14)$$

It is worth noting that the recoil effects of the deuteron are included. The elastic scattering differential cross-section is the square of $F_{ii}(\vec{q})$ and may be written in the form

$$\frac{d\sigma}{d\Omega} = \Big| S(\tfrac{1}{2}q)[f_n(\vec{q}) + f_p(\vec{q})]$$

$$+ \frac{i}{2\pi k}\int S(q')f_p(\tfrac{1}{2}\vec{q} + \vec{q}')f_n(\tfrac{1}{2}\vec{q} - \vec{q}')\, d^2\vec{q}'\Big|^2$$

$$= S^2(\tfrac{1}{2}q)[\,|f_p(\vec{q})|^2 + |f_n(\vec{q})|^2 + 2\,\mathrm{Re}\, f_p(\vec{q})f_n^*(\vec{q})]$$

$$- \frac{1}{\pi k} S(\tfrac{1}{2}q)\,\mathrm{Im}[(f_n^*(\vec{q}) + f_p(\vec{q}))\int S(q')f_p(\tfrac{1}{2}\vec{q} + \vec{q}')$$

$$\times f_n(\tfrac{1}{2}\vec{q} - \vec{q}')d^2\vec{q}'$$

$$+ \frac{1}{(2\pi k)^2}\left|\int S(q')f_p(\tfrac{1}{2}\vec{q} + \vec{q}')f_n(\tfrac{1}{2}\vec{q} - \vec{q}')\,d^2\vec{q}'\right|^2 \qquad (2\text{-}15)$$

In this expression the first term represents single scattering from the individual nucleons, the third term corresponds to pure double scattering , and the second term is the interference between the single and double scattering.

In the case of inelastic scattering one can write the inelastic scattering amplitude for a deuteron as

$$F_{fi}(\vec{q}) = \langle f|F(\vec{q},\vec{s})|i\rangle \qquad (2\text{-}16)$$

where

$$F(\vec{q},\vec{s}) = \exp(\tfrac{1}{2}i\vec{q}\cdot\vec{s})f_n(\vec{q}) + \exp(-\tfrac{1}{2}i\vec{q}\cdot\vec{s})f_p(\vec{q})$$

$$+ \frac{i}{2\pi k}\int \exp(i\vec{q}'\cdot\vec{s})f_p(\vec{q}' + \tfrac{1}{2}\vec{q}) \times f_n(-\vec{q}' + \tfrac{1}{2}\vec{q})\,d^2\vec{q}' \quad .$$

(2-17)

C. THE DIAGRAMATIC FORMULATION OF GLAUBER THEORY

The semi-classical optical model of Glauber is a simple and intuitively appealing approximation to the scattering of a fast particle by a deuteron or a more complicated nucleus. In order to illustrate the approximations that were made in the previous sections and in the hope of improving upon them, it is instructive to consider the diagramatic derivation of the theory.

One may start by considering the impulse approximation to pion-deuteron elastic scattering. The deuteron virtually dissociates into a neutron-proton pair, the pion interacts with proton and the deuteron is reformed. The impulse approximation corresponds to Figure 1 together with the same diagram with the neutron and proton interchanged. Figure 1 is a Feynman graph; in a certain approximation one can show that it leads to Glauber's formulation. Following reference 19, we write the pion-deuteron scattering amplitude as a four dimensional Feynman integral. By applying Glauber's approximation that while the pion and proton are interacting, the neutron is completely unaffected, the neutron propagator associated with Figure 1 can be replaced by a delta function. If all the nucleon spins are ignored, this leads to an amplitude

$$F_{\pi d}(\vec{q}) = \int d^3\vec{q}' \; f_{\pi p}(\vec{q}) \; \psi^*(\vec{q}' - \vec{q}/4) \; \psi(\vec{q}' + \vec{q}/4) \quad (2\text{-}18)$$

where $\vec{q}'$ is the Fermi momentum of the neutron and ψ is the deuteron wave function in momentum space. The off-the-mass shell correction is neglected and the physical pion-proton amplitude is fed into Equation (2-18). However, this amplitude is required at an energy which is a function of both the incident pion momentum and the Fermi momentum $\vec{q}'$. If one considers that the target nucleons are frozen in their positions during the projectile's passage in the preceding sections then $f_{\pi p}(\vec{q})$ can be taken out of the integration at an energy corresponding to $\vec{q}' = 0$.

$$F_{\pi d}(\vec{q}) = f_{\pi p}(\vec{q}) \int d^3\vec{q}' \; \psi^*(\vec{q}' - \vec{q}/4) \; \psi(\vec{q}' + \vec{q}/4)$$

$$\equiv f_{\pi p}(\vec{q}) \; S(q/2) \qquad (2\text{-}19)$$

where S is the deuteron form factor. This is the same result obtained using conventional Glauber theory (c.f., Equation (2-14)). An identical computation with n,p interchanged gives the second term of Equation (2-14). The approximation of neglecting the Fermi motion can be very misleading if there is a resonance in the direct channel[20], e.g., for pion-deuteron scattering below 2 BeV/c.

A graphical diagram also gives the rescattering corrections. The Glauber method envisages a two-stage process in which the pion first scatters off the neutron and then off the proton, before the deuteron reforms; see Figure 2. As

before, while one nucleon is interacting with the incident pion the other one is unaffected. The approximation is made by assuming that in between the two scatterings, the fast pion is also on its mass shell. This assumption would be justified if the proton and neutron were far apart compared to the high energy pion-nucleon force, a situation which is better approximated by light nuclei than the heavier ones. The same method is used, replacing the three propagators by delta functions and neglecting the Fermi motion; and Equation (2-14) is obtained.

Figure 3 shows a diagram in which both nucleon scattering amplitudes involve charge exchange and which was ignored in the simple derivation in the previous sections. The amplitude associated with Figure 3 is simply related to Figure 2 by isospin considerations. If the amplitude associated with Figure 2 is proportional to $f_{\pi n}^{el} f_{\pi p}^{el}$, then the amplitude associated with Figure 3 is proportional to $-(f_{pn}^{c.e.})^2$; the minus sign arises because a neutron-proton pair are interchanged at a deuteron vertex, where the wave function is antisymmetric. The charge exchange amplitude is expressible in terms of elastic amplitudes

$$f_{pn}^{c.e.} = (2)^{-1/2}(f_{\pi p} - f_{\pi n}) \quad . \qquad (2\text{-}20)$$

A simple method to take account of isospin is to make the following replacement in the double scattering amplitude

$$f_{\pi p} f_{\pi n} \rightarrow f_{\pi p} f_{\pi n} - \frac{1}{2} [f_{pn}^{c.e.}]^2$$

$$\equiv f_{\pi p} f_{\pi n} - \frac{1}{4} [f_{\pi p} - f_{\pi n}]^2 \quad . \qquad (2\text{-}21)$$

The correction here is proportional to a charge exchange amplitude squared. The charge exchange amplitude is not large at high energies and can be neglected entirely above about 2 BeV/c. A calculation of the differential cross-section for $\pi^+ d$ elastic scattering with and without the charge exchange correction will be given later, in Chapter IV.

The correction due to double spin flip can also be considered in a similar way; however, at high energies one has little knowledge of the spin structure of the pion-nucleon amplitude, therefore no simple expression like Equation (2-19) can be written down.

The main purpose of this section was to give a clarification of the Glauber approach, especially with regard to charge and spin variables. There are also a series of cautions about the use of the Glauber theory especially away from the forward direction, $t = 0$, and the justification of neglecting the off-the-mass correction[20]. Albers et al.[19] point out that in a Regge pole model the shadow term calculated by Glauber's method should decrease rapidly with increasing energy. This decrease could be somewhat compensated by an increasing contribution from terms due to

inelastic intermediate states, but the effect due to the intermediate states is small.

These problems will be neglected in the application of Glauber's formulation in this thesis. They should, however, be borne in mind in assessing the value of any results obtained.

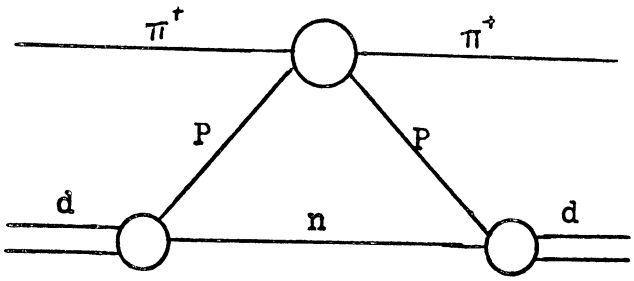

Figure 1. Feynman diagram for the impulse approximation to elastic pion-deuteron scattering.

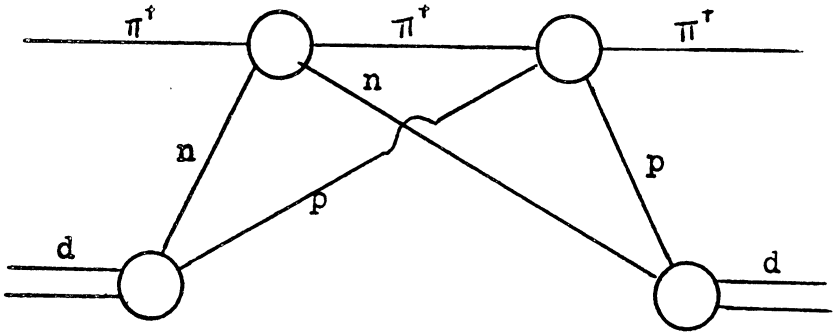

Figure 2. Feynman diagram for the elastic double scattering contribution to elastic pion-deuteron scattering.

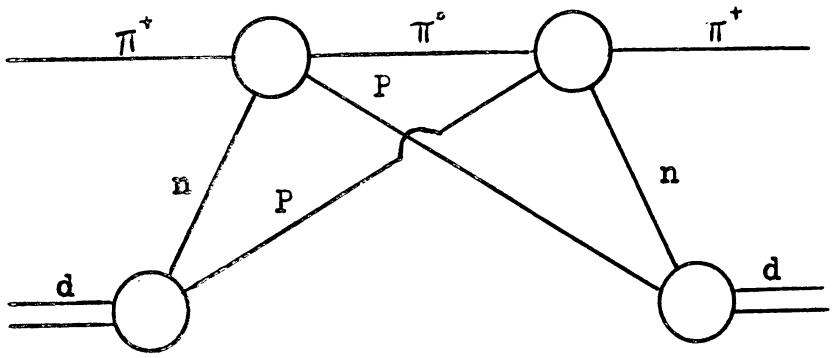

Figure 3. Feynman diagram for the double charge-exchange contribution to elastic pion-deuteron scattering.

CHAPTER III

EXPERIMENTAL PROCEDURES

A. THE BEAM

The 3.65 BeV/c π^+ beam used in this experiment was designed and constructed at the Brookhaven Alternating Gradient Synchrotron during 1960 and 1961. It has been used in conjunction with the 20-inch liquid hydrogen-deuterium bubble chamber. Only the essential features of the beam will be presented in this thesis. A detailed description may be found in the literature[21]. Figure 4 shows the beam layout at the AGS.

The beam consisted of four main sections, the transport section, two similar velocity separator stages, and a beam shaping section. The total length of the beam was 270 feet. The beam was taken off an aluminum target in the F-10 straight section at an angle 8 degrees with respect to the internal circulating proton beam. Eight degrees was the smallest angle at which the beam was able to clear the AGS fringe field. The purpose of the transport section was twofold. The major purpose was to transport the beam from the internal aluminum target to a focused point on slit 2. The other purpose of the transport section was a rough momentum selection. This was achieved mainly by the large bending magnet and also by the dispersive focus at slit 2 of the first two quadrupoles. Slit 1 positioned before the quadrupoles restricted

the angular acceptance of the beam to 40 x 10^{-6} steradian.

The two separator stages were similar. Each contained a pair of quadrupole magnets before and after the velocity separator. These quadrupoles were operated symmetrically in a manner such that the beam particles traversed the separator parallel to the separator plates and widely spreaded horizontally and thus produced maximum separation. Two beam separators consisting of crossed electric and magnetic fields served as a velocity spectrometer to effect mass separation. Precise momentum definitions were achieved through the large bending magnet located between the two separation stages. The shaping section defocused the beam vertically and focused it horizontally in order to properly fill the bubble chamber. When the beam operated as a selector of 3.65 BeV/c π^+ each separator stage provided adequate proton rejection individually. The beam was tuned in such a way that when the first separator was adjusted so that a maximum number of π^+ particles were passed through slit 3, no appreciable amount of protons entered the second separator. Thus when the second separator was swept through a velocity selection no proton peak was found when the beam was swept past the final mass slit. We thus estimated that the proton contamination of the beam was negligible.

The chief contamination of π^+ beam arose from μ^+ decay of the π^+ beam itself. No direct experimental determination of the μ^+ contamination at the 20-inch bubble chamber was

known. However, a detailed description of the estimation of μ^+ contamination at 3.65 BeV/c can be found in reference 22. The estimation was based upon assuming all μ^+ of the momentum and angle resulting from the decay of π^+ arrived in the chamber as contamination. The calculation of the contamination was the approximate integral over the total length of the beam of the probability that a beam π^+ decayed into a μ^+ within the momentum and angular acceptance of the beam. The contamination of μ^+ at the chamber was estimated to be $5 \pm 3\%$.

The π^+ beam entering the bubble chamber had a momentum dispersion, $\Delta p/p$, of $\pm$ 1%.

B. THE CHAMBER

The Brookhaven National Laboratory Shutt 20-inch bubble chamber filled with deuterium was used as the device for exposures for this experiment. The chamber was 20 inches long, 9 inches wide, and 10 inches deep with the beam entering from the 9" x 10" side. Two 1.25-inch thick tempered glass windows sealed with Berkeley-type indium seals were placed on both 20" x 9" sides. Fiducial markings etched on the surface of the front and back glass provided reference points on the film for spatial reconstruction of interactions in the chamber. There were four fiducial markings on the front window and seven fiducial markings on the rear window. All glass surfaces were coated to minimize light reflection.

Photographs, demagnified about 9 times, were taken on 35 mm. film with four cameras arranged on a 9-inch square about 40 inches from the chamber's center with their optical axes perpendicular to the glass window. Figure 5 shows the dimensions of the bubble chamber and the camera positions in space. The chamber was illuminated from the rear by an arc lamp. The light from the arc lamp was filtered, diffused, and then focused by means of a lens system to a point midway between the cameras. In this way only light scattered by bubbles reached the cameras. The illuminated volume in this chamber was about 19 inches in the beam direction, by 8 inches in height, by 9 inches in depth.

A piston located at the end of the wide chamber neck expanded the chamber. The expansion-compression cycle was adjustable down to a minimum of 10 ms. A magnet containing 3.5 tons of copper and 20 tons of iron provided a field of 17,000 gauss. The field was uniform within 3% throughout the chamber. A detailed description of the chamber can be found elsewhere.[23,24]

During the run the chamber was filled with liquid deuterium. The chamber was operated at a temperature 30.9 ± 0.2°K throughout the exposure. The operating pressures of the liquid deuterium were 77 lb/in.^{2} and 5.3 lb/in.^{2} before and after expansion.

The arc light was flashed 150 μ second after the arrival of the beam in order to produce optimum bubble size.

A total of 256,500 pictures were taken in 1964 of which 222,000 pictures were analyzed for this experiment. Each picture contained on the average fifteen incident pions.

C. DATA REDUCTION

C.1 The Scanning

Pictures were scanned on machines which project the film image onto a vertical green translucent screen. Three of the four scanning machines magnify the image approximately 1.3 times of the life size and the fourth one approximately 1.1 times. All four machines are able to project two views simultaneously onto the screen. Superposition of one view on the other can be easily achieved. With this facility one can easily distinguish tracks which stop in the chamber from those which leave the chamber through glass windows.

Camera views 1 and 4 of the chamber were used for scanning. Events were accepted only if they satisfied the following criteria:

a) the beam track which interacts be parallel to the other beam tracks;

b) the vertex lies within or on the boundary defining the fiducial volume;

c) the number of beam tracks entering the bottom of the fiducial volume be less than 40; and

d) tracks leaving the chamber or with secondary scatters have a measurable projected length of at least 2.1 cm.

Since the purpose of this experiment is to measure the pion deuteron elastic scattering differential cross section, scanning personnel were instructed to scan for pion scatterings with a visible recoil track (two pronged events) and to eliminate events which did not belong to the elastic scattering process as follows:

a) Two prong events (two non-decaying outgoing tracks) with either one track or both tracks identified as a proton or protons by positive identification were not recorded. (Curvature templates were used to give ionization-momentum relations for positive identification of different particles); and

b) All two prong events with the interacting vertex connected with any V's or θ's were not recorded.

A more detailed description of the scanning rules for this experiment may be found in reference 25.

From the appearance of the tracks it is difficult to distinguish a π^+ from a proton if the momentum of the particle is greater than 1700 MeV/c[26], and difficult to distinguish a deuteron from a proton if the momentum of the particle is less than 350 MeV/c. With these restrictions there were cases in which the events were ambiguous. The scanners were instructed to record all the ambiguous events.

All pictures used for this experiment were scanned twice by two different scanners. Every disagreement of the two scanners was checked and resolved by experienced professional

scanners. Scanning efficiency for the events used in this experiment was estimated to be 96% (for events with slow outgoing tracks longer than 0.58 cm in the chamber and appropriate azimuthal angle cuts).

C.2 The Measuring

Events were measured on three conventional "B" type measuring machines. These machines have both low and high magnification, the low magnification gives an overall view of the film and the high magnification with a magnification of 2.6 times life size gives a view of a portion of the film. All measuring is performed at high magnification.

The film is carried by a moving stage which is digitized in two orthogonal directions (x and y coordinates). Two machines used Moire-fringe counting devices which give a least count of 1/10,000 inch. The third machine used a disc encoder with a least count of 1/8,000 inch.

The operator measured points on a track by moving the stage until the cross hair attached to the screen and the point on the track to be measured coincided. The operator then initiated the automatic punch device to record the values of x and y digitizers on IBM cards.

Special points such as fiducial marks and the interaction vertex were also measured in a similar manner. In addition to the coordinate points, the cards also contained the frame number, view number, charges of the tracks, etc. Two views were used for the measurements.

The punched cards were fed into a computer program

CHECK[27]. The program carried out simple checks on the data in order to detect any possible format errors on the punched cards. After all errors were corrected CHECK wrote a magnetic tape in the format acceptable to the track reconstruction program.

C.3 Spatial Reconstruction

The geometry program used for this experiment was the TRED reconstruction program.[28] TRED was originally developed by Brookhaven National Laboratory. This program is designed to reconstruct events into three dimensional space from measurements in two stereo film views. TRED uses the coordinates furnished by measurements to determine the momentum and orientation for each track and estimates for the uncertainties of these quantities.

The reconstruction program can be divided into two steps, first the geometric reconstruction of points along the track, and second the fitting of the geometrically reconstructed points into a curve. The geometric reconstruction program is based on the fact that if the film position of a given bubble on a track is known in two views, then tracing the light ray from the two views back through the optics into the bubble chamber produces an intersection of the two rays at the position of the bubble. In actual practice, measurements are not made at corresponding points in two different views, therefore it is necessary to generate an

artificial point in some view by interpolating between two measured points. The interpolation process is simple in the case of an ideal lens system but in an actual case it is quite involved. Effects which must be considered are lens distortion, film shrinkage, a thick glass window, and the index of refraction of the liquid in the bubble chamber. The corresponding point is found by iterating. A detailed description of the iteration process is given in references 28 and 29.

The same procedure is applied to all points measured on one view to yield the space coordinates of a sequence of points that lie along a track. A curve is then fitted to these points, and uncertainties for the fitted variable are estimated.

For a stopping track range-energy relationships are used to calculate the momentum. For a non-stopping track TRED determines momentum from curvature at the midpoint of the measured portion of the track and then computes the momentum at the vertex point by means of range-energy relationships. Since the range-energy relation depends on the mass of the particle TRED computes momentum for five different particles: electron, pion, kaon, proton, and deuteron. TRED program also computes the bubble density of each track for five different mass hypotheses.

The geometrical reconstruction program was not always successful in the reconstruction process. The average fail-

ure rate for events submitted to TRED was 10%. Most of the events which failed TRED program were due to poor measurements. That is the measured points were too far from the fitted curve. All the events which failed TRED were remeasured. The failure rate for the remeasured events submitted to TRED was 25%. No more than two measurements were attempted. Hence 2.5% of the events found were considered unmeasurable.

C.4 Kinematic Analysis

TRED reconstruction is not connected with the properties of the events as a whole but rather with the data of each track separately. Therefore the estimated momenta and angles of all the tracks at an interaction vertex are not generally consistent with conservation of energy and momentum for a given assumption about the interaction taking place at the vertex. The kinematic analysis program examines the vertex based on a set of hypotheses and adjusts track variables subject to two conditions. First, the energy and momentum must be conserved for the interaction assumed at a vertex, and second, track variables should be modified as little as possible. The second condition can be expressed more precisely in terms of χ^2. The adjustment is restricted to rather limited changes in the variables by requiring χ^2 to be smaller than a certain value. χ^2 is defined as

$$\chi^2 = \sum_{i,j=1}^{n} (X_i - X_i^m)\, G_{ij}^{-1}\, (X_j - X_j^m)$$

where n = number of measured variable for vertex

X_i = adjusted value of i^{th} variable

X_i^m = original measured value of i^{th} variable

$G_{ij} = \delta X_i^m \, \delta X_j^m$, a product of the measured errors in X_i and X_j .

The CERN kinematics program, GRIND, written by Böck[30], was used for the kinematic analysis for this experiment.

In this experiment all events were tested by GRIND with the hypotheses

$$\pi^+ + D \rightarrow \pi^+ + D \quad , \qquad \text{(A)}$$

$$\pi^+ + D \rightarrow \pi^+ + p + n \quad , \qquad \text{(B)}$$

$$\pi^+ + D \rightarrow p + p + \pi^\circ \quad , \qquad \text{(C)}$$

and $$\pi^+ + D \rightarrow \pi^+ + D + \pi^\circ \quad . \qquad \text{(D)}$$

χ^2 for Reaction (A) was minimized subject to four constraint equations (4C fit), one for each of the three momentum components and one for the energy. For Reactions (B), (C), and (D) energy conservation is the only constraint (1C fit) since three of the four equations were used to calculate the momentum components of the missing neutral particle. A χ^2 value smaller than 5.4 or 11.6 was considered as giving a good fit

for 1C or 4C fits respectively. Both the χ^2 values correspond to a χ^2 probability of 2%. The relationship between χ^2 and χ^2 probability is as follows:

$$\chi^2 \text{ probability} = \int_{\chi^2}^{\infty} dp(\chi^2)$$

and

$$p(\chi^2) = \frac{\exp(-\frac{\chi^2}{2})(\chi^2)^{(\frac{n}{2}-1)}}{2^{n/2}\,\Gamma(\frac{n}{2})}$$

where n is the number of constraints.

Another feature of GRIND is its capacity to distinguish automatically between different precisions of input variables. GRIND classifies measurements as Well Measured, Badly Measured, Unknown, and Fixed. This feature avoids great mathematical difficulties during the manipulation of matrices in the fitting procedure. In GRIND the beam momentum was set at 3.65 BeV/c with an error of 37 MeV/c at the entrance point.

C.5 Event Identification

After passing through the fitting program GRIND a large fraction of the events were classified as ambiguous events. These were the events which fitted more than one hypothesis. In some cases one can resolve the ambiguity by means of bubble density checking. That is, one compared the observed

and predicted bubble density (from TRED) for each possible fit.

Bubble density is defined as the number of bubbles per unit length of track normalized to a minimum ionizing track. In this experiment we arbitrarily chose the bubble density of the beam as unity. It can be easily shown that the bubble density of a track is approximately proportional to $1/\beta^2$, and β is the ratio of the velocity of the particle to the velocity of light.[31] Figure 6 shows the approximate dependence of bubble density on momentum for pions, protons, and deuterons. It can be easily seen that fast protons are not distinguishable from π^+ ($\sim$ 1700 MeV/c) and slow protons can not be distinguished from deuterons ($<$ 350 MeV/c). With these restrictions bubble density check usually does not suffice to resolve the ambiguity. However for $-t > 0.3$ (BeV/c)^2 ($-t$ is the four-momentum transfer squared), the deuterons do not stop in the chamber but they can be easily distinguished from protons by plotting bubble density versus curvature.

Table I summarizes the event classification. All events were carefully examined by means of bubble density checking except events classified as Reaction (C). The later analysis of these fitted events was performed by using POLISH. The program POLISH reads the GRIND output tape and calculates for each event all the physically interesting variables that one may want written onto magnetic tapes, papers, or cards.

TABLE I

EVENT CLASSIFICATION

(After bubble density checking except for $pp\pi^\circ$ unambiguous events.)

Category		Number of Events
π^+d	Unambiguous	405
π^+pn	"	2190
$\pi^+d\pi^\circ$	"	1067
$pp\pi^\circ$	"	545
π^+d / π^+pn	Ambiguous	2001
π^+d / $\pi^+d\pi^\circ$	Ambiguous	84
π^+pn / $pp\pi^\circ$	Ambiguous	3991
π^+pn / $\pi^+d\pi^\circ$	Ambiguous	1950
$pp\pi^\circ$ / $\pi^+d\pi^\circ$	Ambiguous	629
π^+d / π^+pn / $pp\pi^\circ$	Ambiguous	2540
π^+pn / $pp\pi^\circ$ / $\pi^+d\pi^\circ$	Ambiguous	1470
π^+d / π^+pn / $pp\pi^\circ$ / $\pi^+d\pi^\circ$	Ambiguous	20

This program was written at Michigan by B. P. Roe and C. Arnold. In the analysis for this experiment IBM cards or tapes containing x, y, and z components of the momentum for each track of an event were obtained through POLISH. These were then analyzed with a program SCATTERGRAM which displayed on paper any desired scattergram.

D. EXPERIMENTAL RESULTS

D.1 Elastic Scattering Cross Section

In order to fit Reaction (B), (C), and (D) an event need only satisfy one constraint of energy conservation, whereas to fit Reaction (A) each event must satisfy the four constraints of energy and momentum conservation. Thus a fit for Reaction (A) is not easily faked. Therefore events which were ambiguous between (A) and either of the others were classified as Reaction (A). A total of 5050 events corresponding to the elastic process were found.

We can get some estimates of the purity of the elastic sample by looking at the kinematics of the events.

We take all the events (from a sample of the film) which fit Reaction (B) only and plot in Figure 7 the proton-neutron effective mass. Figure 8 is a plot of proton-neutron effective mass determined by the one-constraint fit to Reaction (B) for ambiguous events which fit (A)-(B) and (A)-(B)-(C). In Figure 8 we have a narrow peak around the deuteron mass. This is strong evidence that the ambiguous

events were elastic events. In particular for $-t > 0.3$ $(BeV/c)^2$ deuterons do not stop inside the bubble chamber as we mentioned in the previous section, and they have been positively identified by plotting bubble density versus curvature. Thus the contamination in the elastic scattering data was considered negligible.

There is a serious scanning bias in the analysis of the very small angle region. This difficulty arose because of the short recoil-deuteron tracks when the plane of the scattering is parallel to the camera axis. This effect was seen in this experiment and has been seen elsewhere[32].

A study of the expected bias in right-left as opposed to up-down scattering of the recoil deuterons in the elastic events indicated severe losses at small momentum transfer region. Figure 9 shows the distribution of events in the azimuthal angle φ about the beam direction as polar axis, as a function of cosine of the center-of-mass scattering angle ($\cos \theta_{cm}$) where $\varphi = 0$ is defined by a plane perpendicular to the camera axis. The distributions have been folded into one quadrant. At very small angles ($\cos \theta_{cm} \geq 0.990$) the losses in the region $60° \leq \varphi < 90°$ are almost complete. In order to avoid scanning losses we have decided to restrict the data presented to $\cos \theta_{cm} \leq 0.992$, this corresponds to $-t \geq 0.043$ and the deuteron range of 0.58 cm in the chamber. Moreover, for $0.043 \leq -t < 0.225$ we restrict to $|\varphi| \leq 30°$, and for $-t \geq 0.225$, to $|\varphi| \leq 60°$. The deuteron range energy

relation is shown in Figure 10, and the relation of cos θ_{cm} to -t is presented in Figure 11.

The differential cross section of elastically scattered π^+ at 3.65 BeV/c from deuterons is tabulated in Table II and shown in Figure 12.

The cross section per event which was used in this section is 0.524 μb. The normalization of this cross section was obtained from the scanned path length and has an overall uncertainty of ±6%. The method of normalization of cross section is given in Appendix C.

Approximately one year after the completion of the experimental part of this investigation, Chase et al.[33] reported their preliminary result of π^--d elastic scattering at 3.75 BeV/c for $0.2 < -t \leqslant 0.9$. The π^-d data are in good agreement with this experiment. The comparison of these two sets of data is shown in Figure 13.

TABLE II

DIFFERENTIAL CROSS SECTION OF $\pi^+ d$ ELASTIC SCATTERING AT 3.65 BEV/C

-t Range $(BeV/c)^2$	Midpoint of -t	$\frac{d\sigma}{dt}$ $(mb/(BeV/c)^2)$
0.043 - 0.075	0.059	29.2 ± 3.0
0.075 - 0.1	0.0875	13.6 ± 1.77
0.1 - 0.125	0.1125	7.41 ± 1.12
0.125 - 0.15	0.1375	5.14 ± 0.87
0.15 - 0.175	0.1625	2.39 ± 0.52
0.175 - 0.2	0.1875	1.84 ± 0.44
0.2 - 0.225	0.2125	1.04 ± 0.31
0.225 - 0.025	0.2375	0.428 ± 0.140
0.25 - 0.275	0.2625	0.214 ± 0.093
0.275 - 0.30	0.2875	0.183 ± 0.086
0.30 - 0.40	0.35	0.0535 ± 0.0234
0.40 - 0.50	0.45	0.0535 ± 0.0234
0.50 - 0.60	0.55	0.0230 ± 0.015
0.60 - 0.80	0.70	0.008 ± 0.0055
0.80 - 1.00	0.90	0.012 ± 0.0074

D.2 Deuteron Break Up Reaction Cross Section

In this section the experimental cross section of the deuteron break up reaction will be presented. For the break up reaction the target deuteron breaks up into two

components, namely proton and neutron. A total of 9,601 events were obtained for this process, among them 2,190 events that fit Reaction (B) alone, and 7,411 events that were ambiguous with Reaction (C) or (D) (c.f., Table I). The maximum contamination in this sample was estimated to be 15.8% by a method given in Appendix D.

The purpose of this experiment was to determine the elastic scattering cross section, therefore the scanning rules were set to eliminate events when the scanners were able to identify the slow outgoing particles as protons. However, due to the difficulties in distinguishing a slow proton from a slow neutron, events for Reaction (B) were recorded for proton momentum less than 350 MeV/c.

Due to scanning losses for small angle regions we only present data for $-t \geq 0.0625$ $(\text{BeV/c})^2$, and our scanning rules were not able to allow us to pick up events for Reaction (B) for $-t > 0.30$ $(\text{BeV/c})^2$. Therefore we only present data in the range $0.0625 \leq -t < 0.30$. Again for reasons similar to the elastic case we only used events with $0° < |\varphi| \leq 30°$.

The cross section $\frac{d\sigma}{dt}$ for the deuteron break up reaction as a function of $-t$ is tabulated in Table III and shown in Figure 14.

TABLE III

MEASURED DIFFERENTIAL CROSS SECTION FOR
THE DEUTERON BREAK UP REACTION

(Errors are statistical.)

-t Range $(BeV/c)^2$	Midpoint of -t	$\frac{d\sigma}{dt}$ $(mb/(BeV/c)^2)$
0.0625 - 0.08	0.073	25.18 ± 1.38
0.08 - 0.12	0.10	19.68 ± 0.86
0.12 - 0.16	0.14	17.74 ± 0.85
0.16 - 0.20	0.18	11.95 ± 0.69
0.20 - 0.24	0.22	9.92 ± 0.63
0.24 - 0.28	0.26	6.54 ± 0.52
0.28 - 0.30	0.29	5.60 ± 1.30

The cross section of the break up reaction with events selected for a symmetrical configuration of final state is tabulated in Table IV and shown in Figure 15. For the symmetrical configuration the energy of the proton is equal to the energy of the neutron. This configuration is of theoretical interest and we will discuss it in Chapter V. Experimentally one can not select events with proton and neutron energies exactly equal. We have included all events with $|E_p - E_n| \leq 2$ MeV.

TABLE IV

MEASURED DIFFERENTIAL CROSS SECTION FOR THE DEUTERON BREAK UP REACTION FOR EVENTS $|E_p - E_n| \leq 2$ MEV

(Errors are statistical.)

-t Range $(BeV/c)^2$	Midpoint of -t	$\frac{d\sigma}{dt}$ $(mb/(BeV/c)^2)$
0.0625 - 0.08	0.0733	3.64 ± 0.54
0.08 - 0.12	0.10	0.93 ± 0.19
0.12 - 0.16	0.14	0.31 ± 0.065
0.16 - 0.20	0.18	0.11 ± 0.396
0.20 - 0.24	0.22	0.094 ± 0.038
0.24 - 0.30	0.27	0.0267 ± 0.016

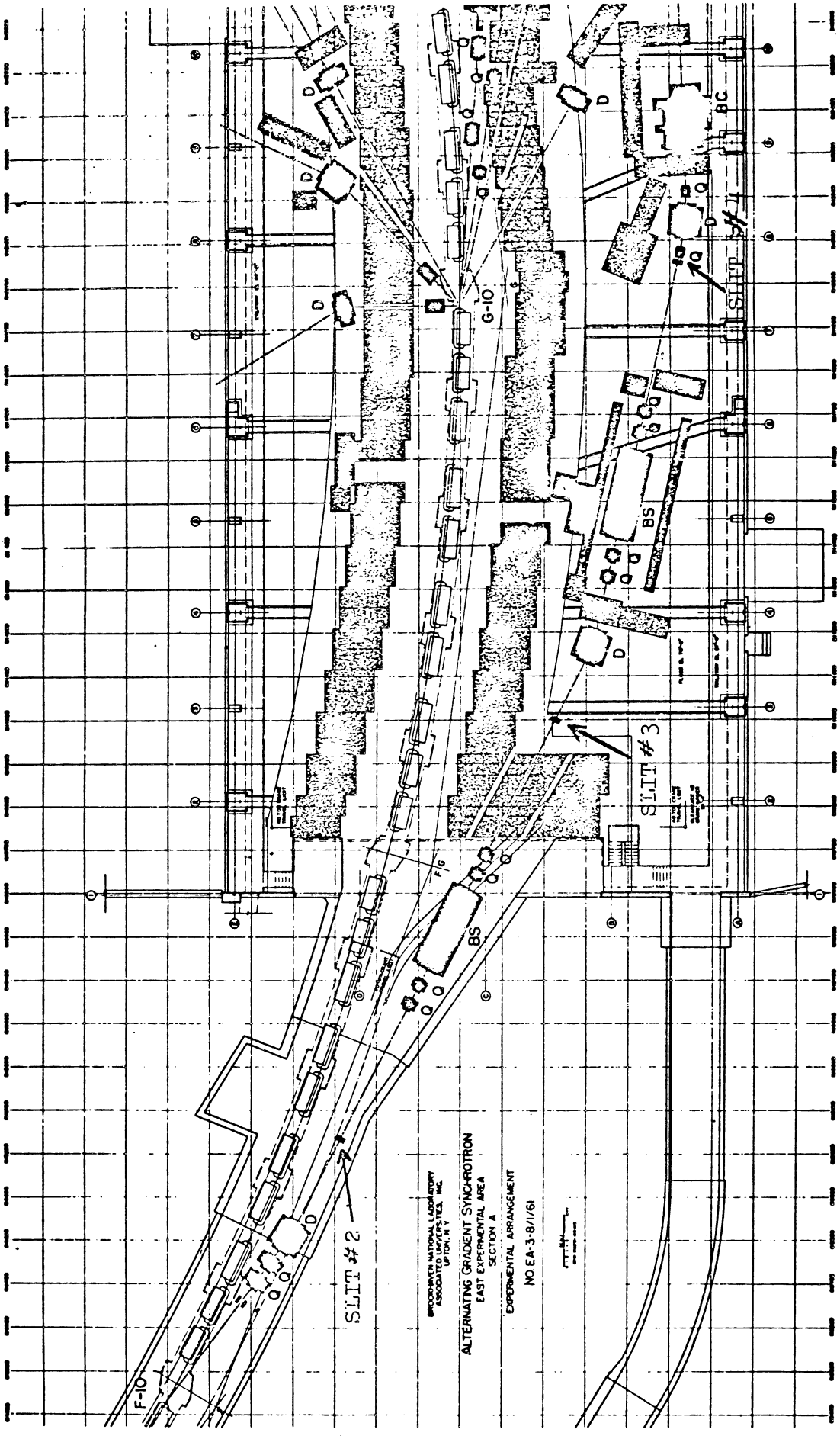

Figure 4. Beam layout at the AGS building.

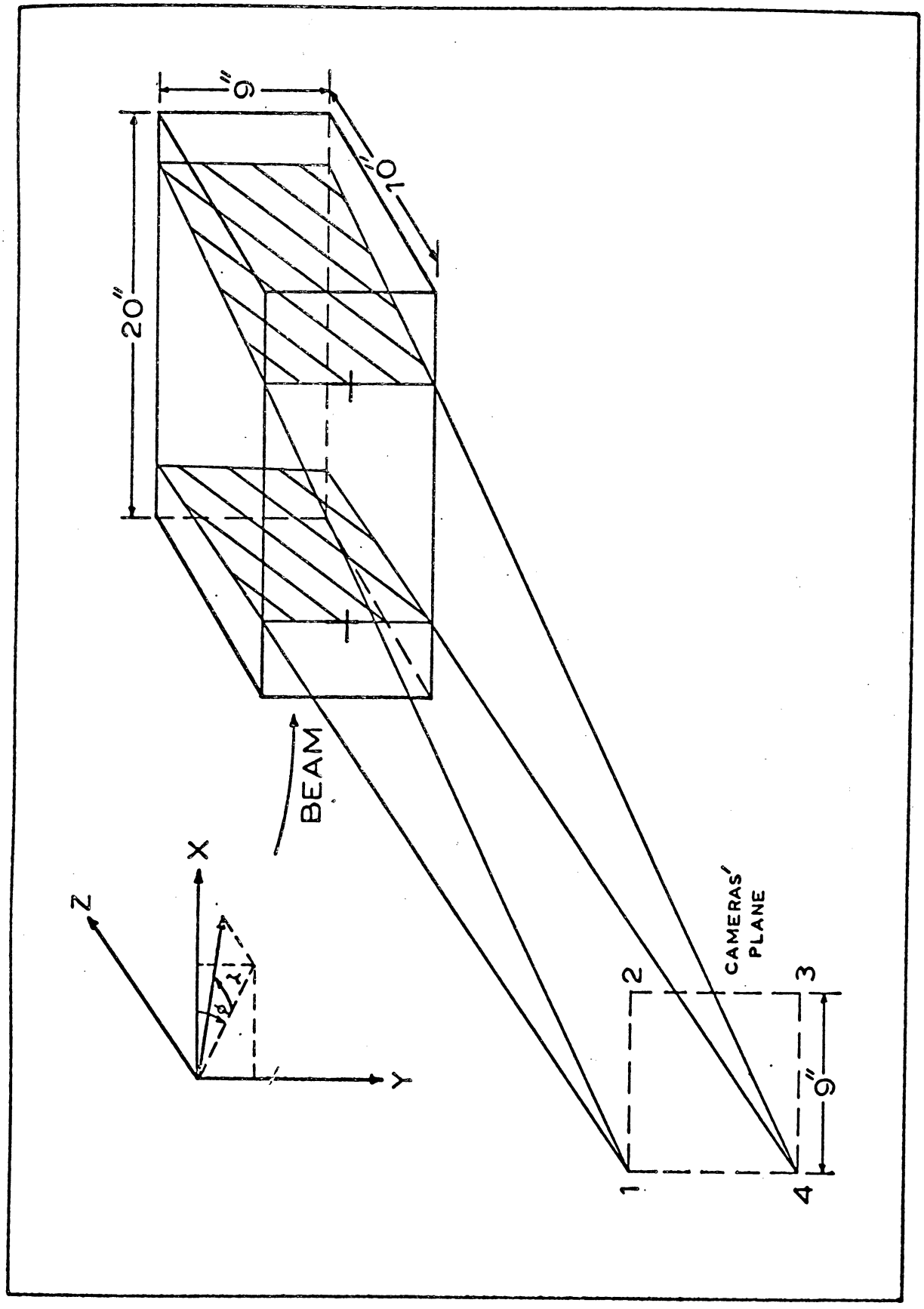

Figure 5. Dimensions of the bubble chamber and camera positions.

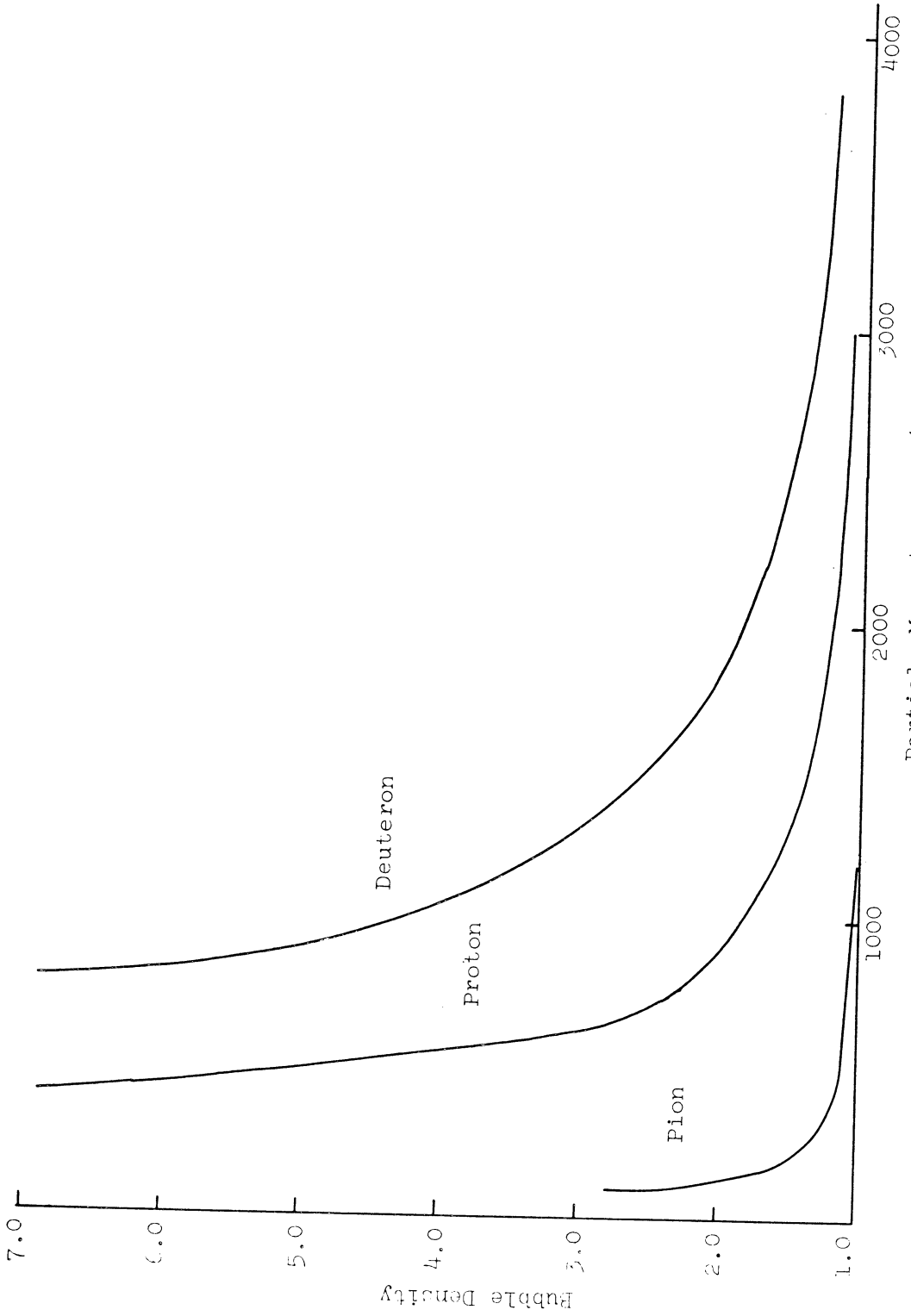

Figure 6. Relation of bubble density vs particle momentum in deuterium.

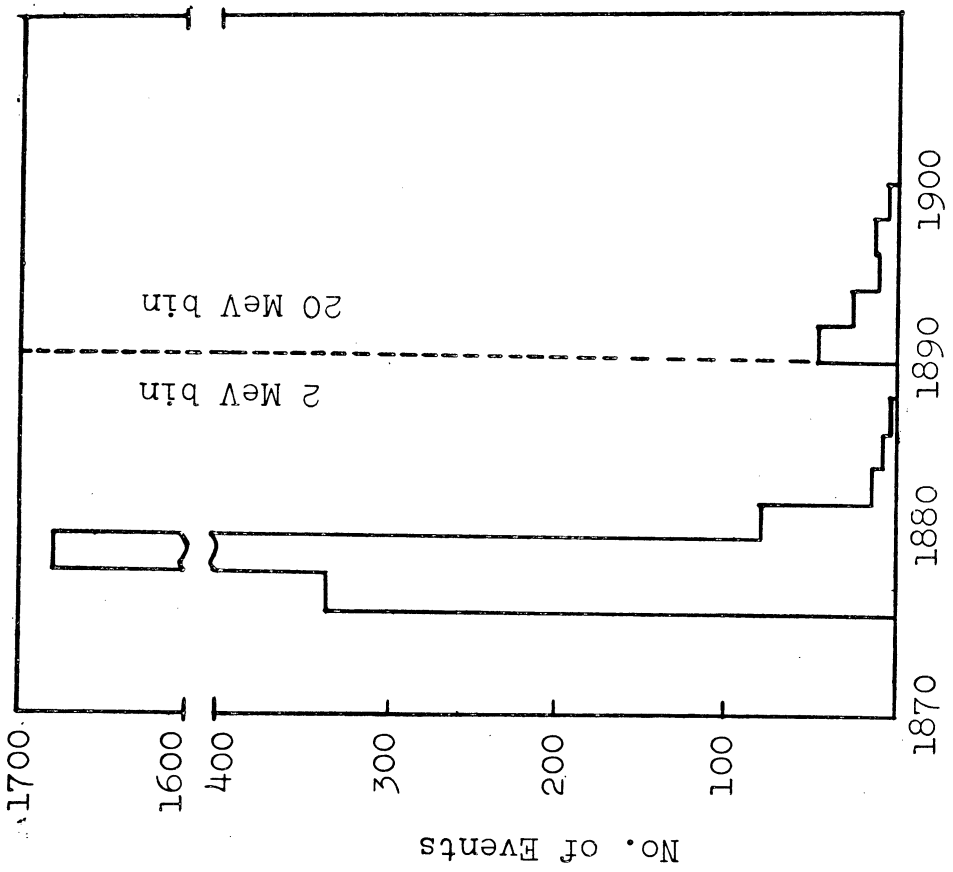

Figure 8. Effective-mass spectrum of proton-neutron system for events that fit (A) and (B), and (A), (B) and (C).

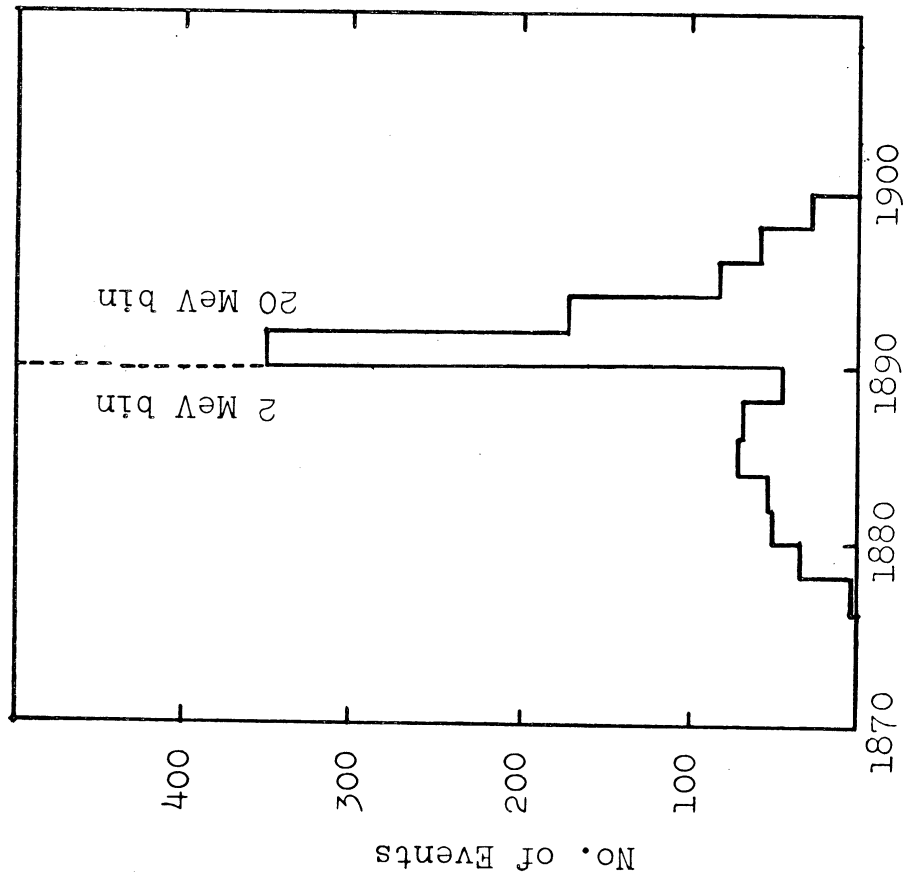

Figure 7. Effective-mass spectrum of proton-neutron system for events that fit Reaction (B).

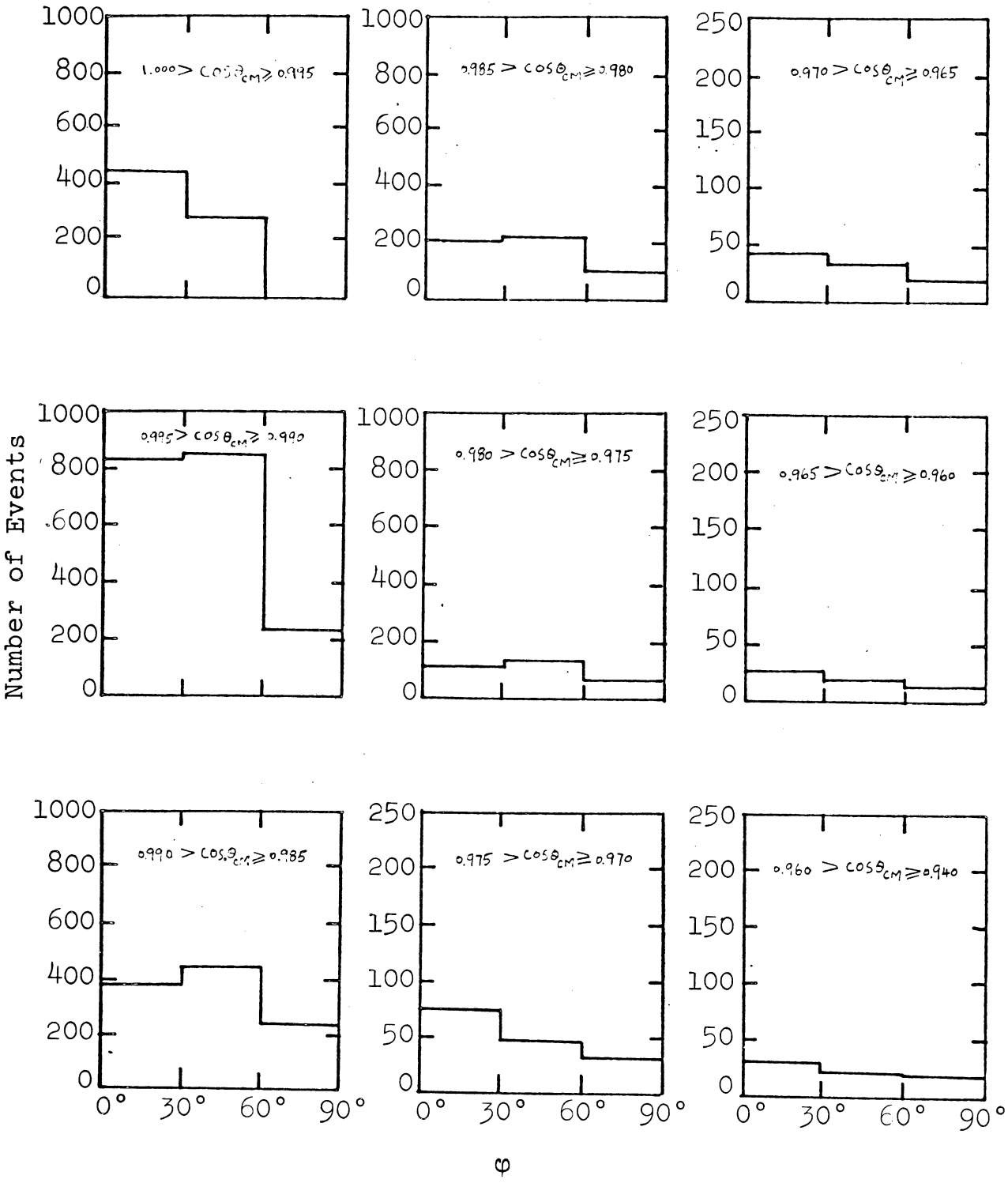

Figure 9. Azimuthal distribution of the outgoing deuteron about the incoming pion direction as a function of cos θ_{cm}.

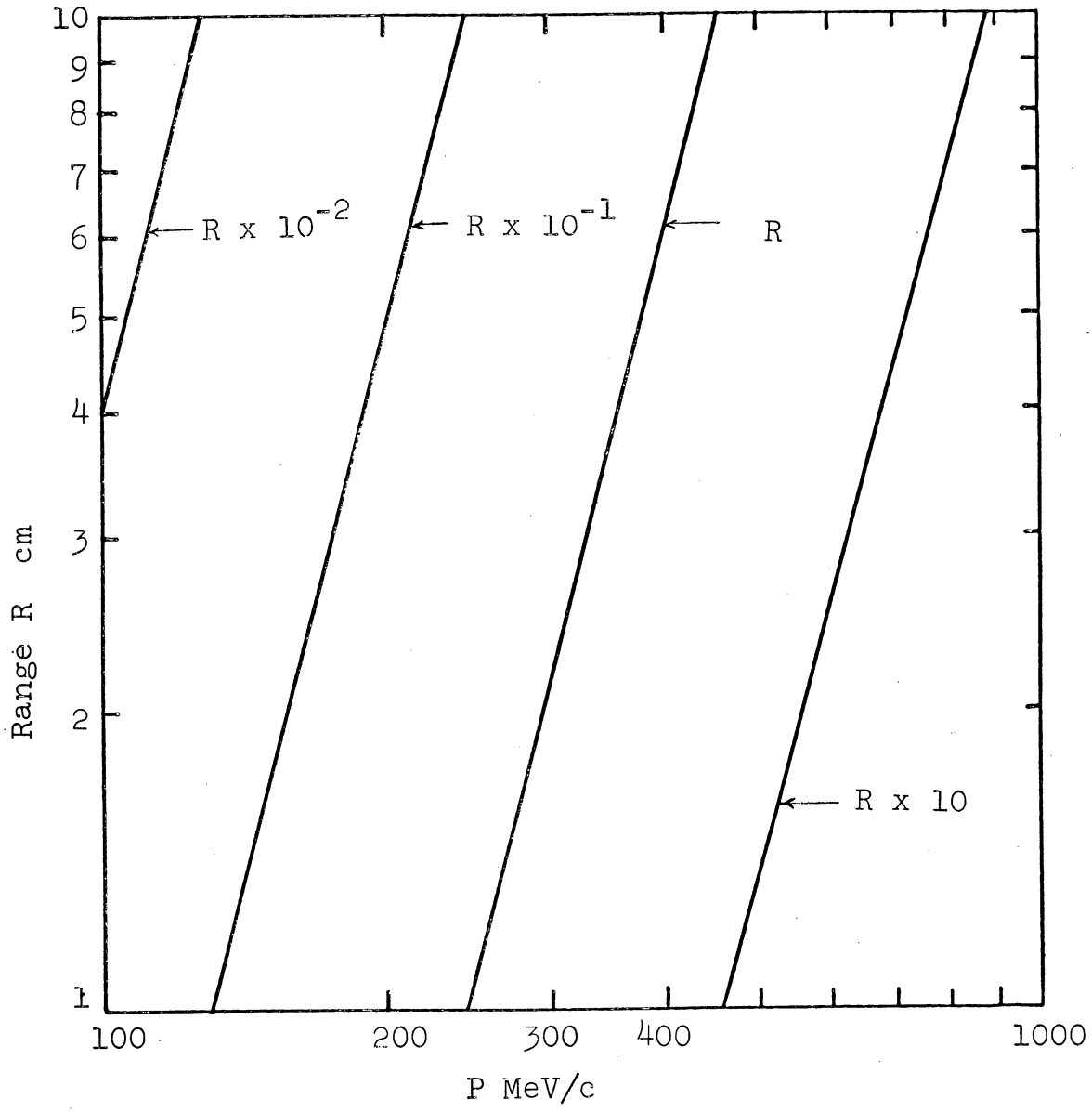

Figure 10. Deuteron range energy relation in deuterium.

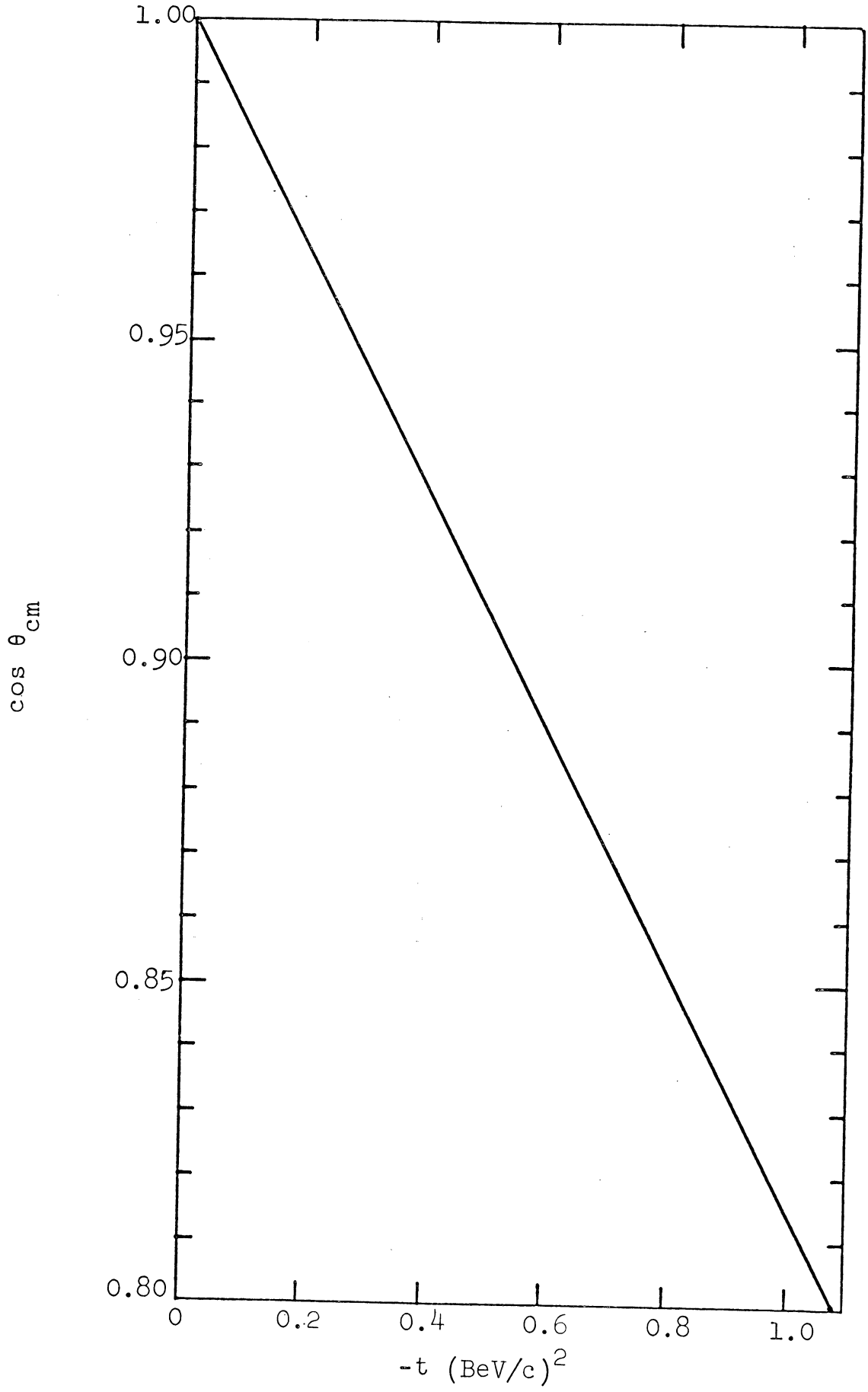

Figure 11. Relation of cosine of center-of-mass scattering angle and -t (four momentum transfer squared).

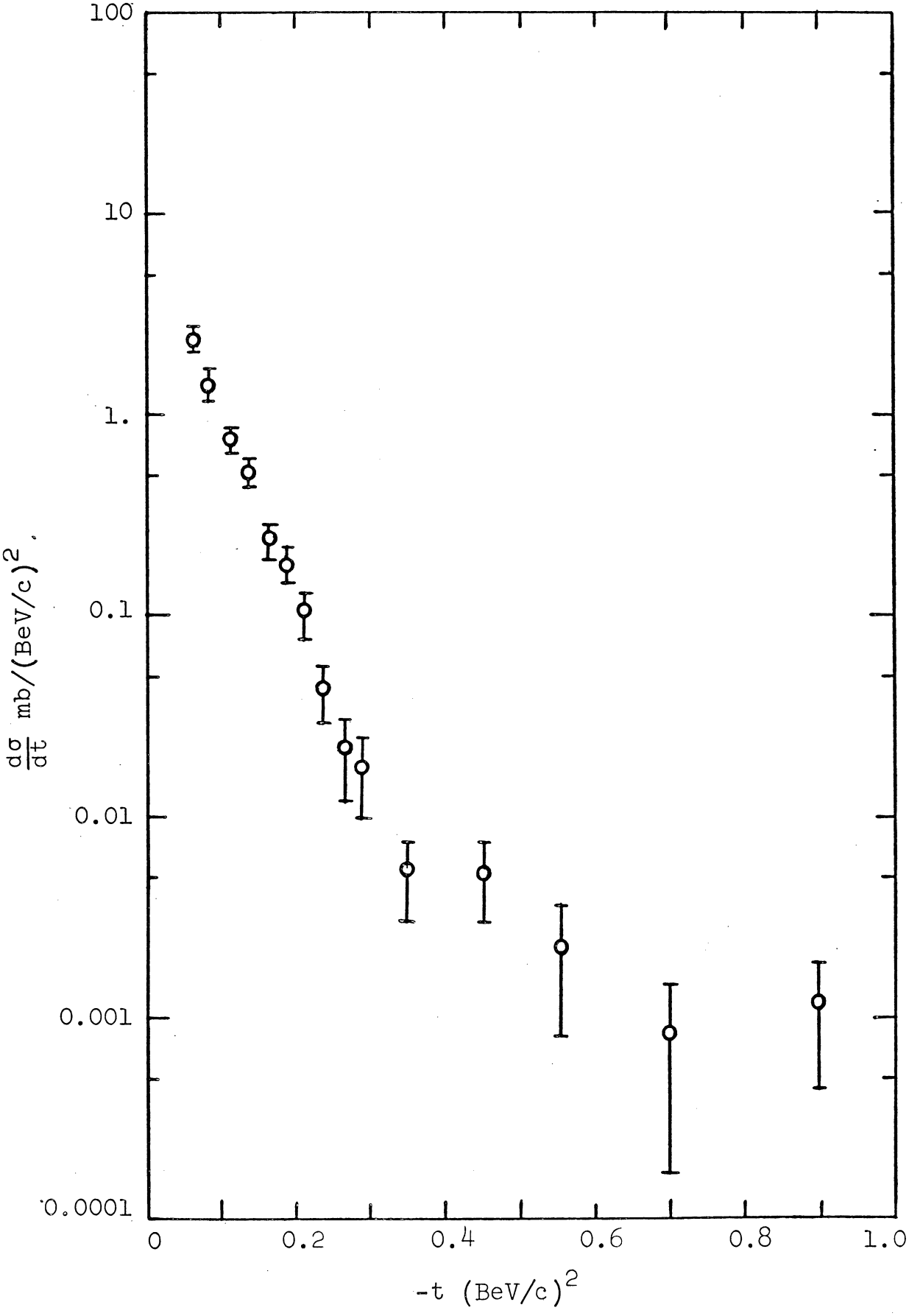

Figure 12. Measured differential cross section of elastically scattered π^+ at 3.65 BeV/c from deuterons.

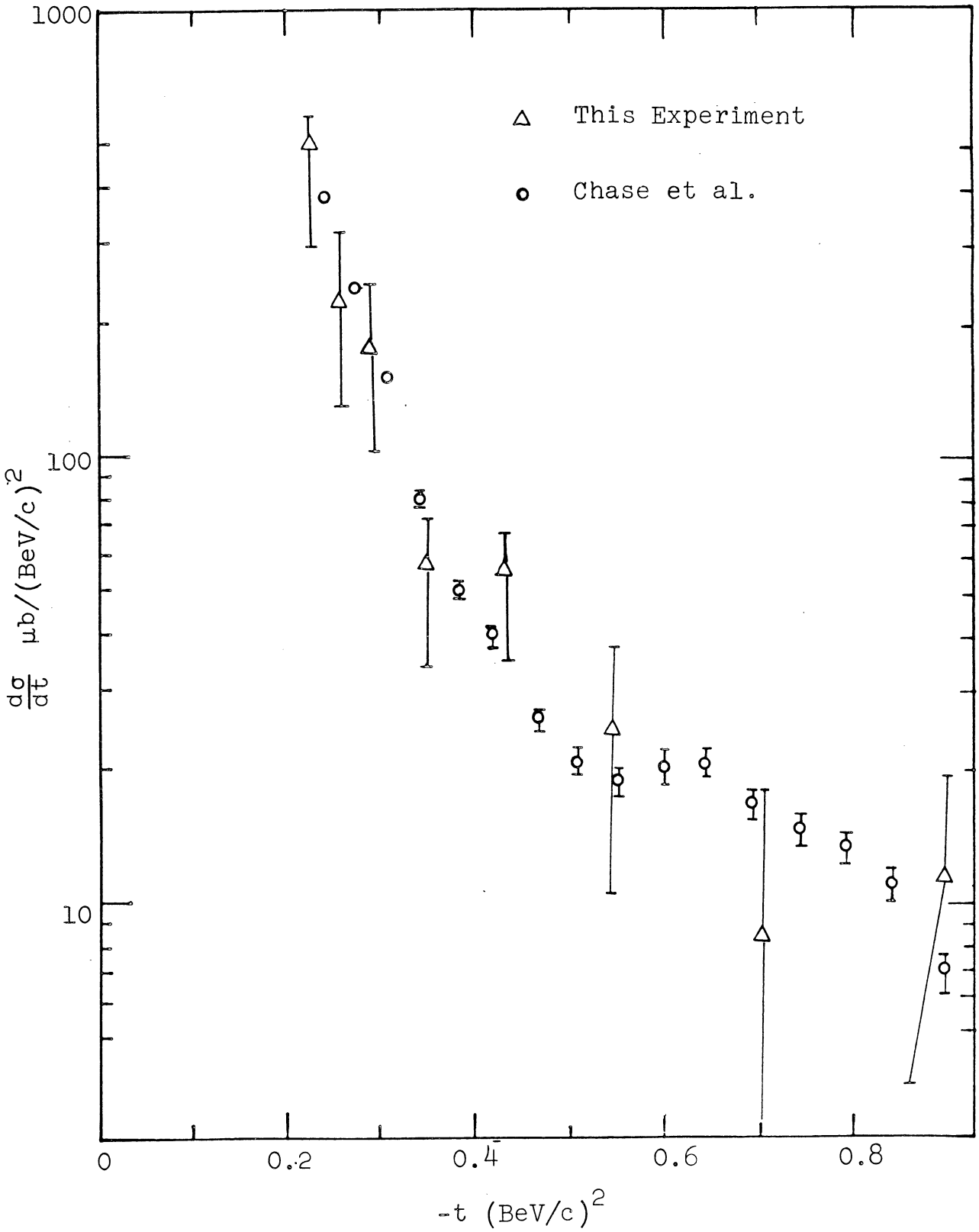

Figure 13. Comparison of π^-d elastic scattering differential cross section at 3.75 BeV/c (data are from Chase et al.) with this experiment.

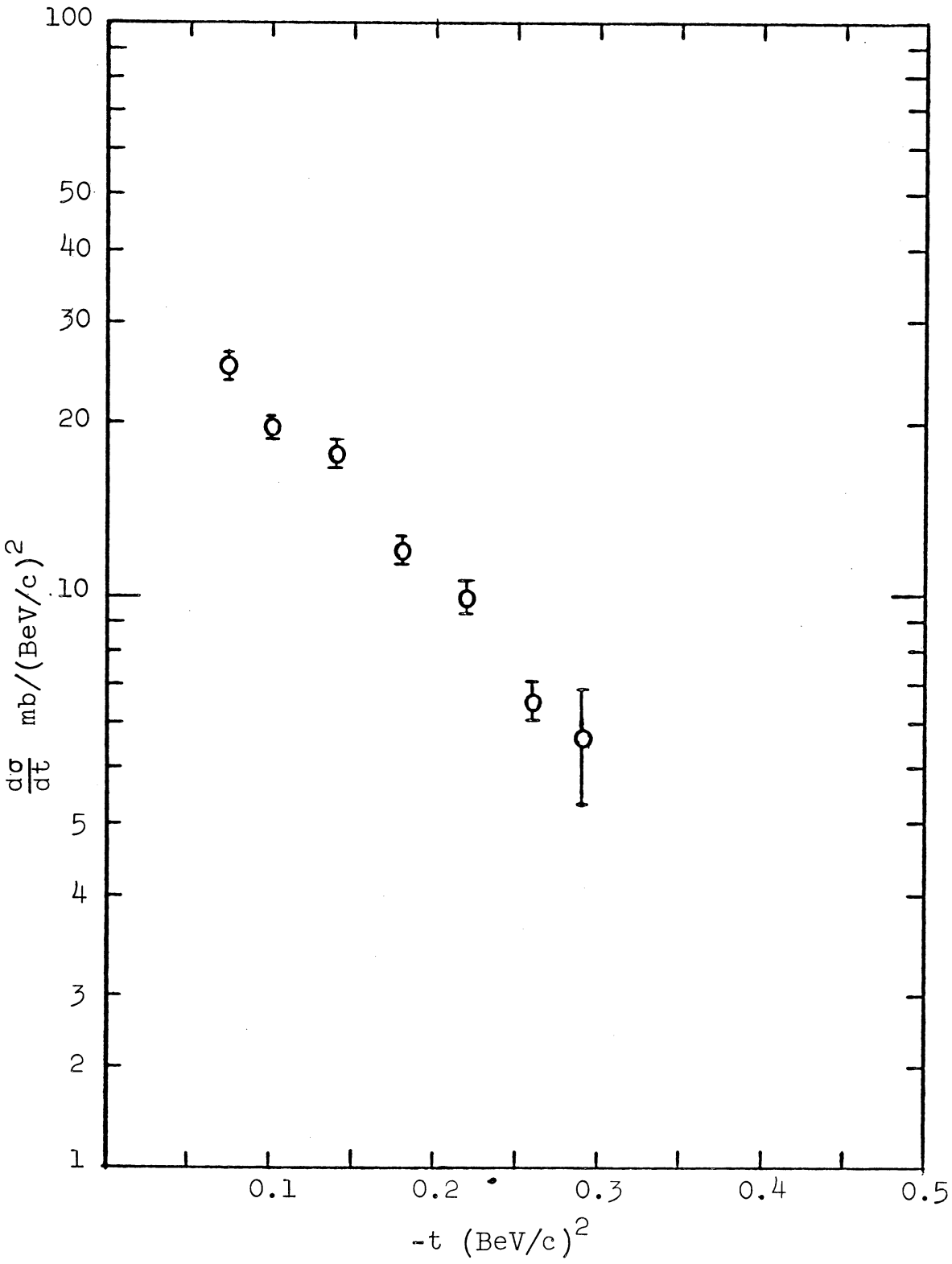

Figure 14. Measured differential cross section for the deuteron break up reaction (errors are statistical).

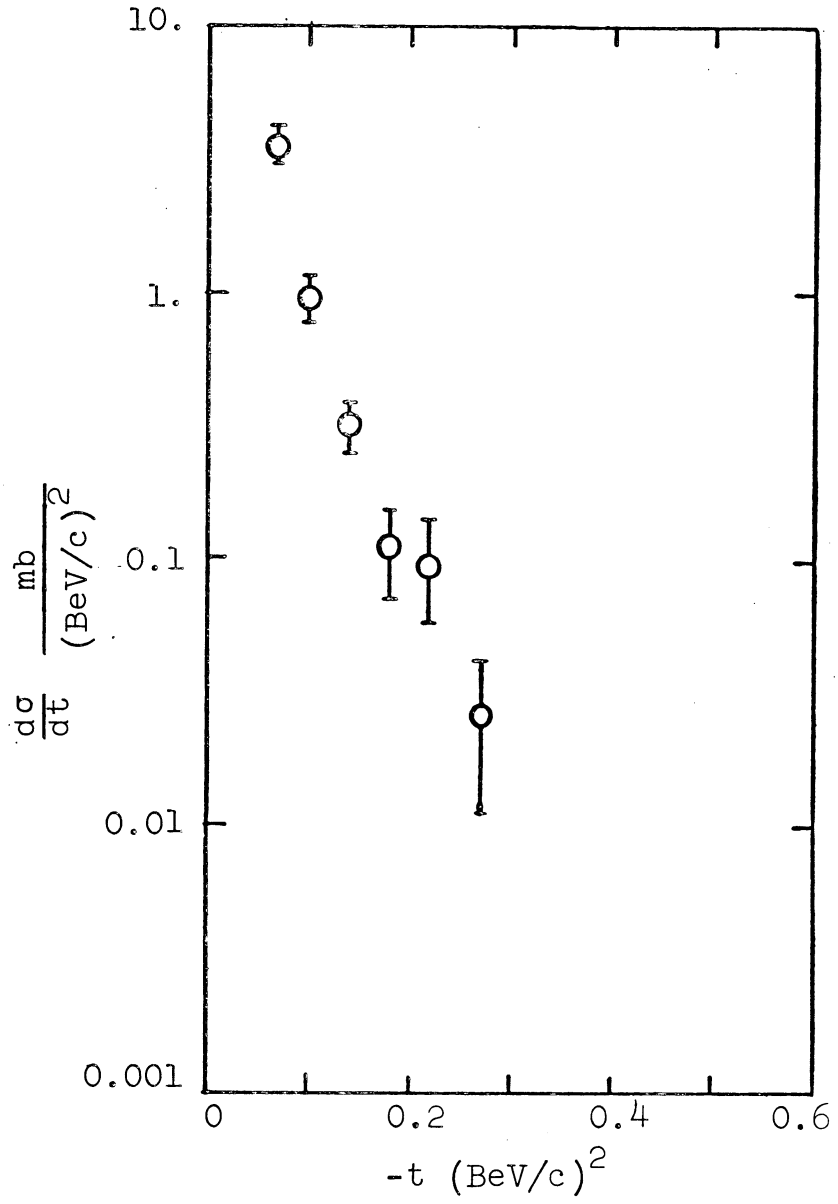

Figure 15. Measured differential cross section for the deuteron break up reaction for events $|E_p - E_n| \leq$ 2 MeV. (Errors are statistical.)

CHAPTER IV

COMPARISON OF EXPERIMENTAL ELASTIC CROSS SECTION WITH THE GLAUBER THEORY

A. CALCULATION OF THE CONSTANT-PHASE CROSS SECTION USING $^3S_1$ STATE DEUTERON WAVE FUNCTION

To evaluate the differential cross section by Equation (2-15) an expression must be found for the scattering amplitudes $f_p(\vec{q})$ and $f_n(\vec{q})$. For the calculation of pion deuteron elastic scattering the pion nucleon amplitudes can be represented by

$$f_p(\vec{q}) = (i + \alpha_p)\left(\frac{k\sigma_p}{4\pi}\right) \exp(-A_p\, q^2/2)$$

$$f_n(\vec{q}) = (i + \alpha_n)\left(\frac{k\sigma_n}{4\pi}\right) \exp(-A_n\, q^2/2)$$

(for the t range of our interest) (4-1)

where σ_p is the total pion-proton cross section, σ_n is the total pion-neutron cross section, α_p is the ratio of the real to the imaginary part of the pion-proton scattering amplitude, α_n is the ratio of the real to the imaginary part of the pion-neutron scattering amplitude, A_p is the slope of the pion-proton elastic differential cross section, and A_n is the slope of the pion-neutron elastic differential cross section.

Substituting Equation (4-1) into Equation (2-15) yields

$$\frac{d\sigma}{d\Omega} = S^2(\tfrac{1}{2}q)\left(\frac{k}{4\pi}\right)^2 \Big[(1+\alpha_n^2)\,\sigma_n^2\, e^{-A_n q^2} + (1+\alpha_p^2)\,\sigma_p^2\, e^{-A_p q^2} + (2+2\alpha_p\alpha_n)\,\sigma_p\sigma_n\, e^{-\frac{1}{2}(A_n+A_p)q^2}\Big]$$

$$- \frac{k^2\sigma_n\sigma_p}{64\,\pi^4} S(\tfrac{q}{2}) \Big[(1+\alpha_n^2)\,\sigma_n\, e^{-\frac{1}{2}A_n q^2} + (1+\alpha_p^2)\,\sigma_p \times e^{-\frac{1}{2}A_p q^2}\Big] e^{-(A_n+A_p)q^2/8}\, I(q)$$

$$+ \frac{k^2\sigma_n\sigma_p}{1024\,\pi^6}(1+\alpha_n^2+\alpha_p^2+\alpha_n^2\alpha_p^2)\, e^{-\frac{1}{4}(A_n+A_p)q^2}\, I^2(q) \qquad (4\text{-}2)$$

where

$$I(q) = \int S(q') \exp[-\tfrac{1}{2}(A_n - A_p)\,\vec{q}\cdot\vec{q}'] \exp[-\tfrac{1}{2}(A_n + A_p)\,q'^2]\, d\vec{q}' \quad . \qquad (4\text{-}3)$$

As input for the calculations we have used the quantities $\alpha_p = -0.286$, $\sigma_p = 28.1$ mb, and $A_p = 6.64$ $(\text{BeV/c})^{-2}$ from Sauly and Hohler et al.,[34,35] and $\alpha_n = -0.187$, $\sigma_n = 31.5$ mb, and $A_n = 7.34$ $(\text{BeV/c})^{-2}$ from correspondence with π-nucleon values assuming $\sigma_{\pi^+ n} = \sigma_{\pi^- p}$ by charge symmetry.[35] The

ground state deuteron form factor, S(q), was calculated from the analytical expression for the Gartenhaus deuteron wave function given as "Approximation III" by Moravcsik[36]

$$\psi(r) = \frac{N}{r}(e^{-\alpha r} - e^{-dr})(1 - e^{-cr})(1 - e^{-gr}) \qquad (4\text{-}4)$$

in which the parameter α may be regarded as the reciprocal of the radius of the deuteron, and is given in terms of the deuteron binding energy, E_d, by $\alpha = (2\mu\hbar E_d)^{1/2}$, where μ is the reduced mass of the proton and neutron. The numerical value of α is 0.232 Fermi^{-1}; the other constants in Equation (4-4) have numerical values $d = 8.19\ \alpha$, $c = 6.853\ \alpha$, $g = 10.766\ \alpha$, and N is the normalization constant. This wave function contains the $^3S_1$ state component only. The effect of $^3D_1$ state component in the deuteron wave function will be discussed in the next section. Using Equations (4-4) and (2-13) one obtains

$$S(q/2) = \frac{8\pi N^2}{q}\left[\tan^{-1}\frac{q}{4\alpha} + \tan^{-1}\frac{q}{4d} + \tan^{-1}\frac{q}{4\alpha + 4c}\right.$$

$$+ \tan^{-1}\frac{q}{4\alpha + 4g} + \tan^{-1}\frac{q}{4(\alpha + c + g)}$$

$$+ \tan^{-1}\frac{q}{4c + 4d} + \tan^{-1}\frac{q}{4d + 4g}$$

$$\left. + \tan^{-1}\frac{q}{4(c + d + g)} - 2\tan^{-1}\frac{q}{2\alpha + 2d}\right.$$

$$- 2 \tan^{-1} \frac{q}{4\alpha + 2c} - 2 \tan^{-1} \frac{q}{4\alpha + 2g}$$

$$+ 4 \tan^{-1} \frac{q}{4\alpha + 2c + 2g} + 4 \tan^{-1} \frac{q}{2(\alpha + c + d)}$$

$$+ 4 \tan^{-1} \frac{q}{2(\alpha + d + g)} - 8 \tan^{-1} \frac{q}{2(\alpha + c + d + g)}$$

$$- 2 \tan^{-1} \frac{q}{2(c + 2d)} - 2 \tan^{-1} \frac{q}{2(2d + g)}$$

$$+ 4 \tan^{-1} \frac{q}{2(c + 2d + g)} - 2 \tan^{-1} \frac{q}{2(2\alpha + 2c + g)}$$

$$- 2 \tan^{-1} \frac{q}{2(\alpha + 2c + d)} + 4 \tan^{-1} \frac{q}{2(\alpha + 2c + d + g)}$$

$$- 2 \tan^{-1} \frac{q}{2(2\alpha + c + 2g)} - 2 \tan^{-1} \frac{q}{2(\alpha + d + 2g)}$$

$$+ 4 \tan^{-1} \frac{q}{2(\alpha + c + d + 2g)} - 2 \tan^{-1} \frac{q}{2(\alpha + 2c + d + 2g)}$$

$$- 2 \tan^{-1} \frac{q}{2(2c + 2d + g)} - 2 \tan^{-1} \frac{q}{2(c + 2d + 2g)}$$

(4-5)

One may see that the form factor $S(q/2)$ is a function of the deuteron configuration only. It approaches zero for very weak binding and unity for very strong binding. It is always unity for zero momentum transfer. From Equation (2-13) one

observes that it decreases monotonically with increasing magnitudes of momentum transfer. In Figure 16, S(q/2) is plotted as a function of -t, using the approximation, $-t = q^2$. I(q) was calculated in a simplified manner. Because of the near equality of A_n and A_p, and the oscillatory nature of $\vec{q}\cdot\vec{q}'$, I(q) has neglible q dependence. Little error is introduced by taking $I(q) \equiv I(0) \equiv I$. This I can be calculated by numerical integration and has a value of $I = 0.173\ mb^{-1}$ for the parameters we used. The value of I can also be checked experimentally from its relation to the defect in the total cross section

$$\delta\sigma = \sigma_p + \sigma_n - \sigma_d$$

by evaluating Equation (2-14) at q = 0. One obtains

$$I = \frac{8\pi^2 \delta\sigma}{\sigma_p \sigma_n (1 - \alpha_p \alpha_n)} \quad . \qquad (4\text{-}6)$$

Using[37] $\delta\sigma = (1.5 \pm 0.5)$ mb one gets $I = (0.14 \pm 0.05)\ mb^{-1}$, in good agreement with the calculated value.

A plot of the predicted differential cross section calculated on the basis of Equation (4-2) is shown (solid curve) in Figure 17 along with the experimental data (the normalization of both data and theory is absolute). The agreement of the theoretical curve with the experimental

points is good, except in the region of the dip (-t = 0.3 - 0.5). A similar disagreement has been observed in proton deuteron scattering at 1 BeV[38] and 2 BeV[12] incident proton kinetic energies. The theoretical dip occurs at a point where the first and third terms of expression (4-2) are nearly equal and are almost canceled by the second term. Figure 18 shows the magnitudes of the three different terms in Equation (4-2) as a function of -t. The single scattering term (1st term) is overwhelming in the forward direction and goes down with -t with a law which is mainly governed by the form factor of the deuteron. The double scattering term (3rd term), which is small at -t = 0, goes down with -t with a much smaller slope. Double scattering therefore overwhelms single scattering at large -t. However, there exists an interval of -t, around -t = 0.40, in which the single and double scattering amplitudes are of the same order of magnitude, and therefore they interfere appreciably and cause a dip in the differential cross section.

The dip region is particularly sensitive to the ratio of the real to imaginary part of the pion-nucleon forward scattering amplitudes if the D-state component of the deuteron wave function is ignored. If the free-nucleon amplitudes are purely imaginary, then the cancellation will be complete. The values used in the calculations in this section for f_p and f_n were based on known pion-nucleon differential cross sections and were taken to have a phase independent of

scattering angles and equal to the values established for forward scattering ($-t = 0$). The effect of the real parts of the free pion-nucleon amplitudes on the pion-deuteron differential cross section is shown in Figure 19.

The increase of the α_N (N is for proton or neutron) changes the magnitude of the pion-nucleon amplitude slightly. One can renormalize the amplitude easily for the optical point and to keep σ_N constant by multiplying it with a factor $\sqrt{\frac{1+\alpha_N^2}{1+\alpha_N'^2}}$, where α_N' is the new value used in the amplitude. However, in this calculation only the size of the dip is significant.

The double charge exchange is a small effect at high energy. The contribution it makes is indicated explicitly in Figure 20.

B. EFFECT OF D-WAVE IN THE CROSS SECTION CALCULATION

Figure 17 shows that the agreement between theory and experiment in general is very good, except in the region $0.3 < -t < 0.5$ where the theory predicted a dip which is inconsistent with the experiment. Similar disagreement was also found in proton deuteron scattering.[38,12]

In this section we will show that the large dip calculated in the previous section was mainly the consequence of ignoring the $^3D_1$ state of the deuteron wave function.[39,40,41] The inclusion of a small D-state component in the deuteron

wave function allows large S-D transition in the interference region and the dip is then transformed to a shoulder-like region when the differential cross sections are summed over the deuteron spin states.

According to the Glauber approximation, the differential cross section for pion-deuteron scattering for momentum transfer $\vec{q}$, summed and averaged over final and initial deuteron spins, is given by

$$\frac{d\sigma}{d\Omega} = \frac{1}{3} \sum_{MM'} \left| T_{MM'}(\vec{q}) \right|^2 \qquad (4\text{-}7)$$

where $T_{MM'}$ is the scattering amplitude from a deuteron of spin projection M (in the direction of the momentum transfer $\vec{q}$) to M', and $T_{MM'}$ can be written as

$$T_{MM'}(\vec{q}) = \int d^3\vec{r}\ \psi^*_{M'}(\vec{r})\ T(\vec{q}\ ,\ \vec{r})\ \psi_M(\vec{r}) \qquad (4\text{-}8)$$

and $T(\vec{q}\ ,\ \vec{r})$ is related to the pion-nucleon scattering amplitude $f(\vec{q})$ by

$$T(\vec{q}\ ,\ \vec{r}) = f_n(\vec{q}) \exp(-\tfrac{1}{2} i\vec{q} \cdot \vec{r}) + f_p(\vec{q}) \exp(-\tfrac{1}{2} i\vec{q} \cdot \vec{r})$$

$$+ \frac{i}{2\pi k} \int f_n(\vec{q}' + \tfrac{1}{2}\vec{q})\ e^{(-i\vec{q}'\cdot\vec{r})}\ f_p(\tfrac{1}{2}\vec{q} - \vec{q}')\ d^2\vec{q}' \quad . \qquad (4\text{-}9)$$

The deuteron wave function, $\psi_M(\vec{r})$ can be expressed in terms of radial wave functions and spin-one spinors χ_M as follows[42]

$$\psi_M(\vec{r}) = \frac{1}{4\pi r}\left[u(r) + \frac{1}{\sqrt{8}} S_{12}(\vec{r})\, w(r)\right] \chi_M \qquad (4\text{-}10)$$

where u(r) and w(r) are the radial S and D wave functions,

$$S_{12}(\vec{r}) = 3(\vec{\sigma}_1 \cdot \hat{r})(\vec{\sigma}_2 \cdot \hat{r}) - \vec{\sigma}_1 \cdot \vec{\sigma}_2 \qquad (4\text{-}11)$$

is a tensor operator, and the σ's are the Pauli spin matrices.

The nine scattering amplitudes for $T_{MM'}$ can be shown to be:

$$T_{11} = [f_p(\vec{q}) + f_n(\vec{q})][S_0(\tfrac{1}{2}q) - S_2(q/2)/\sqrt{2}]$$

$$+ \frac{i}{2\pi k}\int q'dq'd\alpha\, f_p(\frac{\vec{q}}{2} + \vec{q}')\, f_n(\frac{\vec{q}}{2} - q')$$

$$\times[S_0(q') - S_2(q')(3\cos^2\alpha - 1)/2\sqrt{2}] \quad ,$$

$$T_{-1-1} = T_{11} \quad ,$$

$$T_{00} = [f_p(\vec{q}) + f_n(\vec{q})][S_0(\tfrac{q}{2}) + \sqrt{2}\, S_2(\tfrac{q}{2})]$$

$$+ \frac{i}{2\pi k} \int q'dq'd\alpha \; f_p(\frac{\vec{q}}{2} + \vec{q}') \; f_n(\frac{\vec{q}}{2} - \vec{q}')$$

$$\times [S_0(q') + \frac{\sqrt{2}}{2} S_2(q')(3 \cos^2 \alpha - 1)] \quad ,$$

$$T_{1-1} = - \frac{i}{2\pi k} \int q'dq'd\alpha \; f_p(\frac{\vec{q}}{2} + \vec{q}') \; f_n(\frac{\vec{q}}{2} - \vec{q}')$$

$$\times \frac{3}{2\sqrt{2}} S_2(q') \sin^2 \alpha \quad ,$$

$$T_{-11} = T_{1-1} \quad ,$$

$$T_{10} = 0 \quad ,$$

$$T_{01} = 0 \quad ,$$

$$T_{0-1} = 0 \quad ,$$

and

$$T_{-10} = 0 \quad . \qquad (4\text{-}12)$$

The functions S_0 and S_2 are deuteron "spherical" and "quadrupole" form factors, respectively,

$$S_0(q) = \int_0^\infty dr[u^2(r) + w^2(r)]\, j_0(qr) \quad , \qquad (4\text{-}13)$$

$$S_2(q) = \int_0^\infty dr\ 2w(r)[u(r) - \frac{1}{\sqrt{8}}\, w(r)]\, j_2(qr) \quad . \qquad (4\text{-}14)$$

A detailed derivation of Equation (4-12) can be found in Appendix E.

From Equations (4-7) and (4-12) we find

$$\frac{d\sigma}{d\Omega} = \frac{1}{3}\left[2|T_{11}|^2 + |T_{00}|^2 + 2|T_{1-1}|^2\right] \qquad (4\text{-}15)$$

where

$$|T_{11}|^2 = [f_p(\vec{q}) + f_n(\vec{q})]^2[S_0(\tfrac{q}{2}) - S_2\,(q/2)/\sqrt{2}]^2$$

$$- \frac{i}{\pi k}\left[S_0(\tfrac{q}{2}) - \frac{S_2(\frac{q}{2})}{\sqrt{2}}\right] \mathrm{Im}\left\{[f_p^*(\vec{q}) + f_n^*(\vec{q})]\right.$$

$$\int q'dq'd\alpha\ f_p(\tfrac{\vec{q}}{2} + \vec{q})\ f_n(\tfrac{\vec{q}}{2} - \vec{q}')[S_0(q') - S_2(q')$$

$$\left.(3\cos^2\alpha - 1)/2\sqrt{2}]\right\}$$

$$+ \frac{1}{(2\pi k)^2}\left|\int q'dq'd\alpha\ f_p(\tfrac{\vec{q}}{2} + \vec{q}')\ f_n(\tfrac{\vec{q}}{2} - \vec{q}')\right.$$

$$\left.[S_0(q') - S_2(q')\ (3\cos^2\alpha - 1)/2\sqrt{2}]\right|^2 \quad ,$$

$$\left| T_{00} \right|^2 = [f_p(\vec{q}) + f_n(\vec{q})]^2 [S_0(\tfrac{q}{2}) + \sqrt{2}\, S_2(\tfrac{q}{2})]^2$$

$$- \frac{i}{\pi k} [S_0(\tfrac{q}{2}) + \sqrt{2}\, S_2(\tfrac{q}{2})]\, \mathrm{Im} \Big\{ [f_p^*(\vec{q}) + f_n^*(\vec{q})]$$

$$\times \int q'dq'd\alpha\, f_p(\tfrac{\vec{q}}{2} + \vec{q}')\, f_n(\tfrac{\vec{q}}{2} - \vec{q}') \Big[S_0(q') - \tfrac{\sqrt{2}}{2} S_2(q')$$

$$\times (3\cos^2\alpha - 1) \Big] \Big\}$$

$$+ \frac{1}{(2\pi k)^2} \left| \int q'dq'd\alpha\, f_p(\tfrac{\vec{q}}{2} + \vec{q}')\, f_n(\tfrac{\vec{q}}{2} - \vec{q}') \right.$$

$$\left. \times \Big[S_0(q') + \tfrac{\sqrt{2}}{2} S_2(q')\, (3\cos^2\alpha - 1) \Big] \right|^2 \quad \text{and}$$

$$\left| T_{1-1} \right|^2 = \frac{1}{2(2\pi k)^2} \left| \int q'dq'd\alpha\, f_p(\tfrac{\vec{q}}{2} + \vec{q}')\, f_n(\tfrac{\vec{q}}{2} - \vec{q}') \right.$$

$$\left. \Big[\tfrac{3}{2\sqrt{2}} S_2(q') \sin^2\alpha \Big] \right|^2 .$$

Equation (4-15) can be simplified by integrating over the variable α. Then, it follows,

$$\frac{d\sigma}{d\Omega} = \frac{1}{3} \Big\{ 2(f_p(\vec{q}) + f_n(\vec{q}))^2 \Big[S_0(\tfrac{1}{2} q) - \frac{S_2(\frac{1}{2} q)}{\sqrt{2}} \Big]^2$$

$$- \frac{2i}{\pi k} \Big[\Big(S_0(\tfrac{1}{2} q) - \frac{S_2(\frac{1}{2} q)}{\sqrt{2}} \Big)\, \mathrm{Im}(f_p^*(\vec{q}) + f_n^*(\vec{q})) \Big)$$

$$x\left(I_0 - \frac{I_2}{4\sqrt{2}}\right)\Big] + \frac{2}{(2\pi k)^2}\left(I_0 - \frac{I_2}{4\sqrt{2}}\right)^2 + (f_p(\vec{q}) + f_n(\vec{q}))^2$$

$$\times[S_0(\tfrac{1}{2}q) + \sqrt{2}\,S_2(\tfrac{1}{2}q)]^2 - \frac{i}{\pi k}\Big[(S_0(\tfrac{1}{2}q) + \sqrt{2}\,S_2(\tfrac{1}{2}q)$$

$$\mathrm{Im}(f_p^*(\vec{q}) + f_n^*(\vec{q}))\left(I_0 + \frac{I_2}{2\sqrt{2}}\right)\Big] + \frac{1}{(2\pi k)^2}\left(I_0 + \frac{I_2}{2\sqrt{2}}\right)^2$$

$$+ \frac{2}{(2\pi k)^2}\left(\frac{3}{\sqrt{8}}\,\frac{I_2}{2}\right)^2\Bigg\}$$

or we may write the above equation as

$$\frac{d\sigma}{d\Omega} = \left(\frac{d\sigma}{d\Omega}\right)_0 + \left(\frac{d\sigma}{d\Omega}\right)_2 \qquad (4\text{-}16)$$

where

$$\left(\frac{d\sigma}{d\Omega}\right)_0 = \left|[f_p(\vec{q}) + f_n(\vec{q})]\,S_0(\tfrac{1}{2}q) + \frac{i}{2\pi k}\,I_0\right|^2$$

$$\left(\frac{d\sigma}{d\Omega}\right)_2 = \frac{3}{4}\left|\left[(f_p(\vec{q}) + f_n(\vec{q})\right]S_2(\tfrac{1}{2}q)\right|^2$$

$$+ \frac{1}{4}\left|\left[f_p(\vec{q}) + f_n(\vec{q})\right]S_2(\tfrac{1}{2}q) + \frac{i}{2\pi k}\;I_2\right|^2 .$$

$$I_0 = \int 2\pi q'dq'\; f_p(\tfrac{1}{2}\vec{q} + \vec{q}')\,f_n(\tfrac{1}{2}\vec{q} - \vec{q}')\,S_0(q') \quad ,$$

and

$$I_2 = \int 2\pi q' dq' \; f_p(\tfrac{1}{2}\vec{q} + \vec{q}') \; f_n(\tfrac{1}{2}\vec{q} - \vec{q}') \; S_2(q') \quad .$$

The first term, $\left(\frac{d\sigma}{d\Omega}\right)_0$, in Equation (4-16) is the differential cross section if the D-wave component of the deuteron is ignored except for the small w^2 term in $S_0(\frac{1}{2}q)$. The contribution of $\left(\frac{d\sigma}{d\Omega}\right)_2$ to the cross section is small compared with $\left(\frac{d\sigma}{d\Omega}\right)_0$ except in the dip region where the single and double scattering contribution to $\left(\frac{d\sigma}{d\Omega}\right)_0$ interfere destructively and tend to cancel.

We have made numerical calculations with scattering amplitudes of pion nucleon represented by Equation (4-1) and the input quantities are known pion-nucleon values. The qunatities used for free pion-nucleon amplitude are as follows:

$$\alpha_p(t) = \alpha_p(0) = -0.187$$

$$\alpha_n(t) = \alpha_n(0) = -0.286$$

$$\sigma_p = 28.1 \text{ mb}$$

$$\sigma_n = 31.5 \text{ mb}$$

$$A_p = 6.64 \text{ (BeV/c)}^{-2}$$

$$A_n = 7.31 \text{ (BeV/c)}^{-2} \quad .$$

The "spherical" and "quadrupole" deuteron form factors $S_0(\frac{q}{2})$

and $S_2(\frac{q}{2})$ are taken from the "potential No. 3" table of Glendenning and Kramer[43] and their values are plotted in Figure 21 as a function of -t, the four momentum transfer squared. This wave function calculated by using "potential No. 3" of Glendenning and Kramer has a D-state probability of 5.97%.

The theoretical predictions calculated according to Equation (4-16) along with the experimental data of positive pion elastic scattering on deuterons are shown in Figure 22. The dashed curve is the contribution of $\left(\frac{d\sigma}{d\Omega}\right)_0$, the dash dot (—·—·—·—) curve is the contribution of $\left(\frac{d\sigma}{d\Omega}\right)_2$ and the solid curve is their sum. All calculations were performed in the laboratory frame and then transformed to $\frac{d\sigma}{dt}$.

The original dip region has been raised by a factor of seventeen (17) and thus the dip has been filled in quite neatly. The inclusion of the D-state produces modifications to render a smooth transition from the slope of the diffraction peak to a slope of approximately half of its value. The theoretical predictions are slightly higher than the experimental data in the region between -t = 0.25 and -t = 0.80. It does not seem to be due to statistical errors since the deviations are all one-sided in this region. Improvement was made by renormalizing the "Potential No. 3 Glendenning and Kramer" wave function (5.97% D-state probability) we used before to 4% and 2% D-state probabilities and recalculating the differential cross section using Equation (4-16). The

effect of changing D-state probability is significant in the transition region. It can be seen from Figure 23 that the height of the curve in the dip region is essentially proportional to the D-state probability. The experimental data are in favor of the wave function with 4% D-state probability.

Further improvement was achieved by multiplying the double scattering amplitude with a parameter $\lambda(q^2)$ and thus, the modified I_0 and I_2 in Equation (4-16) are expressed as follows:

$$I_0 = \lambda(q^2) \int 2\pi q' dq' \; f_p(\tfrac{1}{2}\vec{q} + \vec{q}') \; f_n(\tfrac{1}{2}\vec{q} - \vec{q}') \; S_0(q') \quad ,$$

and

$$I_2 = \lambda(q^2) \int 2\pi q' dq' \; f_p(\tfrac{1}{2}\vec{q} + \vec{q}') \; f_n(\tfrac{1}{2}\vec{q} - \vec{q}') \; S_2(q') \quad .$$

Figure 24 shows the calculated result for $\lambda(q^2) = \lambda(0) = 0.7$, 0.9, and 1.0 along with the experimental data. In this calculation a D-state probability of 4% for the "Potential No. 3 Glendenning and Kramer" deuteron wave function was used. A significant change was observed in the region where the double scattering contribution dominates. A similar calculation was performed by using a varying $\lambda(q^2)$:

$$\lambda(q^2) = 1 - \frac{q^2}{3} \quad .$$

The result is shown in Figure 25. The agreement between the calculation and the experimental data is very good.

C. CALCULATION OF CROSS SECTION WITH VARYING PHASE PION-NUCLEON SCATTERING AMPLITUDES

Without considering D-state component of the deuteron wave function the depth of the dip, i.e., the extent of the cancellation which occurs appears to be quite sensitive to the values of the phase in the scattering amplitude[37]. However, in this section we will show that with the inclusion of the D-state of the deuteron wave function the cross section predicted in the dip region is not sensitive to a phase variation of the pion-nucleon scattering amplitudes.

Instead of using a Gaussian form of free pion-nucleon amplitudes we use a phase varying pion-nucleon amplitudes parameterized as:

$$f_p(\vec{q}) = \frac{\sigma_p k}{4\pi} [(i + \alpha_p) \exp(-A_p q^2/2) + b_p q^2]$$

$$f_n(\vec{q}) = \frac{\sigma_n k}{4\pi} [(i + \alpha_n) \exp(-A_n q^2/2) + b_n q^2] \qquad (4\text{-}17)$$

where b_p and b_n are constants.

We rewrite Equation (4-16) in the form:

$$\frac{d\sigma}{d\Omega} = \{A_0 + B_0 + C_0\} + \frac{3}{4} A_2 + \frac{1}{4}\{A_2 + B_2 + C_2\} \qquad (4\text{-}18)$$

where

$$A_0 = S_0^2(\tfrac{1}{2}\,q)[\,|f_p(\vec{q})|^2 + |f_n(\vec{q})|^2 + 2\,\mathrm{Re}\, f_p(\vec{q})f_n^*(\vec{q})]\ , \tag{4-18a}$$

$$B_0 = \frac{1}{\pi k} S_0(\tfrac{1}{2}\,q)\ \mathrm{Im}[(f_n^*(\vec{q}) + f_p^*(\vec{q}))\int S_0(q') \times f_n(\tfrac{1}{2}\,\vec{q} + q')\ f_p(\tfrac{1}{2}\,\vec{q} - q')\ d\vec{q}'] \tag{4-18b}$$

$$C_0 = \frac{1}{(2\pi k)^2}\left|\int S_0(q')\ f_n(\tfrac{1}{2}\,\vec{q} + \vec{q}')\ f_p(\tfrac{1}{2}\,\vec{q} - \vec{q}')\ d\vec{q}'\right|^2 \tag{4-18c}$$

$$A_2 = S_2^2(\tfrac{1}{2}\,q)[\,|f_p(\vec{q})|^2 + |f_n(\vec{q})|^2 + \mathrm{Re}\, f_p(\vec{q})\ f_n^*(\vec{q})] \tag{4-18d}$$

$$B_2 = \frac{1}{\pi k} S_2(\tfrac{1}{2}\,q)\ \mathrm{Im}[(f_n^*(\vec{q}) + f_p^*(q))\int S_2(q') \times f_n(\tfrac{1}{2}\,\vec{q} + \vec{q}')\ f_p(\tfrac{1}{2}\,\vec{q} - \vec{q}')\ d\vec{q}'] \tag{4-18e}$$

and

$$C_2 = \frac{1}{(2\pi k)^2}\left|\int S_2(q')\ f_n(\tfrac{1}{2}\,\vec{q} + \vec{q}')\ f_p(\tfrac{1}{2}\,\vec{q} - \vec{q}')\ d\vec{q}'\right|^2 \tag{4-18f}$$

Substituting Equation (4-17) into Equation (4-18) we obtain:

$$A_0 = \frac{S_0^2(\frac{1}{2}q)k^2}{16\pi^2}\Big[\Big(\sigma_p e^{-\frac{A_p q^2}{2}} + \sigma_n e^{-\frac{A_n q^2}{2}}\Big)^2$$

$$+\Big(\sigma_p\alpha_p e^{-\frac{A_p q^2}{2}} + \sigma_p b_p q^2 + \sigma_n\alpha_n e^{-\frac{A_n q^2}{2}}$$

$$+ \sigma_n b_n q^2\Big)^2\Big]$$

$$B_0 = \frac{S_0(\frac{1}{2}q)k^2\sigma_p\sigma_n}{64\pi^4}\Big\{\Big[(-1+\alpha_p\alpha_n)\, e^{-(\frac{A_p+A_n}{2})\frac{q^2}{4}} K_1$$

$$+\Big(\alpha_n b_p e^{-\frac{A_n q^2}{8}} + \alpha_p b_n e^{-\frac{A_p q^2}{8}}\Big)$$

$$\times\Big(\frac{q^2}{4}K_2 + K_3\Big)\Big] \times \Big(\sigma_p e^{-\frac{A_p q^2}{2}} + \sigma_n e^{-\frac{A_n q^2}{2}}\Big)$$

$$-\Big[(\alpha_p+\alpha_n)\, e^{-(A_p+A_n)\frac{q^2}{8}} K_1$$

$$+\Big(b_p e^{-\frac{A_n q^2}{8}} + b_n e^{-\frac{A_p q^2}{8}}\Big)\Big(\frac{q^2}{4}K_2 + K_3\Big)\Big]$$

$$x\left(\sigma_p\alpha_p\, e^{-\frac{A_p q^2}{2}} + \sigma_n\alpha_n\, e^{-\frac{A_n q^2}{2}} + \sigma_p b_p q^2 + \sigma_n b_n q^2\right)\Bigg\}$$

$$C_0 = \frac{k^2\sigma_p^2\sigma_n^2}{1024\pi^6}\left\{\left[(-1+\alpha_p\alpha_n)\, e^{-(A_p+A_n)\frac{q^2}{8}} K_1 + \left(\alpha_n b_p\, e^{-\frac{A_n q^2}{8}} + \alpha_p b_n\, e^{-\frac{A_p q^2}{8}}\right) x\left(\frac{q^2}{4}K_2 + K_3\right)\right]^2\right.$$

$$\left. + \left[(\alpha_p+\alpha_n)\, e^{-(A_p+A_n)\frac{q^2}{8}} + \left(b_p\, e^{-\frac{A_n q^2}{8}} + b_n\, e^{-\frac{A_p q^2}{8}}\right)\left(\frac{q^2}{4}K_2 + K_3\right)\right]^2\right\}$$

$$A_2 = \frac{S_2^2(\frac{1}{2}q)k^2}{16\pi^2}\left[\left(\sigma_p\, e^{-\frac{A_p q^2}{2}} + \sigma_n\, e^{-\frac{A_n q^2}{2}}\right)^2 + \left(\sigma_p\alpha_p\, e^{-\frac{A_p q^2}{2}} + \sigma_n\alpha_n\, e^{-\frac{A_n q^2}{2}} + \sigma_p b_p q^2 + \sigma_n\alpha_n q^2\right)^2\right]$$

$$B_2 = \frac{S_2(\frac{1}{2}q)k^2\sigma_p\sigma_n}{64\pi^4}\left\{\left[(-1+\alpha_p\alpha_n)\,e^{-\frac{(A_p+A_n)}{2}\frac{q^2}{4}}L_1\right.\right.$$

$$+\left(\alpha_n b_p\, e^{-\frac{A_n q^2}{8}} + \alpha_p b_n\, e^{-\frac{A_p q^2}{8}}\right)$$

$$\left.\left.\times\left(\frac{q^2}{4}L_2 + L_3\right)\right] \times \left(\sigma_p\, e^{-\frac{A_p q^2}{2}} + \sigma_n\, e^{-\frac{A_n q^2}{2}}\right)\right.$$

$$-\left[(\alpha_p+\alpha_n)\,e^{-(A_p+A_n)\frac{q^2}{8}}L_1\right.$$

$$\left.+\left(b_p\, e^{-\frac{A_n q^2}{8}} + b_n\, e^{-A_p q^2}\right)\left(\frac{q^2}{4}L_2 + L_3\right)\right]$$

$$\times\left(\sigma_p\alpha_p\, e^{-\frac{A_p q^2}{2}} + \sigma_n\alpha_n\, e^{-\frac{A_n q^2}{2}}\right.$$

$$\left.\left.+\,\sigma_p b_p q^2 + \sigma_n b_n q^2\right)\right\}$$

$$C_2 = \frac{k^2\sigma_p^2\sigma_n^2}{1024\pi^6}\left\{\left[(-1+\alpha_p\alpha_n)\,e^{-(A_p+A_n)\frac{q^2}{8}}L_1 + \left(\alpha_n b_p\, e^{-\frac{A_n q^2}{8}}\right.\right.\right.$$

$$\left.\left.\left.+\,\alpha_p b_n\, e^{-\frac{A_p q^2}{8}}\right)\times\left(\frac{q^2}{4}L_2 + L_3\right)\right]^2\right.$$

$$+\left[(\alpha_p+\alpha_n)\,e^{-(A_p+A_n)\frac{q^2}{8}}+\left(b_p\,e^{-\frac{A_nq^2}{8}}+b_n\,e^{-\frac{A_pq^2}{8}}\right)\left(\frac{q^2}{4}L_2+L_3\right)\right]^2\Bigg\}$$

where $$K_1=\int S_0(q')\,e^{-\frac{(A_n+A_p)}{2}q'^2}\,d\vec{q}'$$

$$K_2=\int S_0(q')\,e^{-\frac{A}{2}q'^2}\,d\vec{q}'$$

$$K_3=\int S_0(q')\,q'^2\,e^{-\frac{A}{2}q'^2}\,d\vec{q}'$$

$$L_1=\int S_2(q')\,e^{-\frac{(A_n+A_p)}{2}q'^2}\,d\vec{q}'$$

$$L_2=\int S_2(q')\,e^{-\frac{A}{2}q'^2}\,d\vec{q}'$$

and $$L_3=\int S_2(q')\,q'^2\,e^{-\frac{A}{2}q'^2}\,d\vec{q}'\quad .$$

Due to the fact the A_n and A_p are almost equal, we make the assumption $A_p = A_n = A = 7.0\ (\text{BeV/c})^{-2}$ in evaluating K_2, K_3, L_2, and L_3.

In evaluating A_0 through C_2, some negligibly small terms were dropped, e.g., terms containing $b_p b_n q^4$ and $\int S(q')q'^4 e^{-\frac{A}{2}q'^2} d\vec{q}'$. b_p and b_n may be different for proton and neutron but we assume them to be the same in the calculation to make the calculation simpler. Thus $b_p = b_n = b$. The differential cross section calculated with varying phase amplitudes parameterized by Equation (4-17) is shown in Figure 26 with various b values. Again, in the calculation we used the values S_0 and S_2 from the "potential No. 3" table of Glendenning and Kramer. It is easy to see from Figure 26 that the effect of phase of the pion-nucleon amplitudes is indeed very small. One can calculate the phase, $\theta_{ph}(q^2)$, as a function of q^2 approximately by assuming $A_p = A_n = A$, $\alpha_p = \alpha_n = \alpha$, and writing

$$\theta_{ph}(q^2) = \cot^{-1}\alpha'(q^2)$$

where

$$\alpha'(q^2) = \frac{\alpha\, e^{-\frac{A}{2}q^2} + bq^2}{e^{-\frac{Aq^2}{2}}}$$

or

$$\alpha'(q^2) = \alpha + bq^2 \, e^{\frac{Aq^2}{2}} \quad .$$

For $b = 0.15$, $q^2 = 0.5$ $(\mathrm{BeV/c})^2$, $\alpha = -0.24$, $A = 7.0$, one finds

$$\theta_{ph}(0.5) = 79^\circ \quad ,$$

and for $q^2 = 0$

$$\theta_{ph}(0) = 103^\circ \quad .$$

The change of phase between $q^2 = 0$ and $q^2 = 0.5$ for $b = 0.15$ is thus quite large.

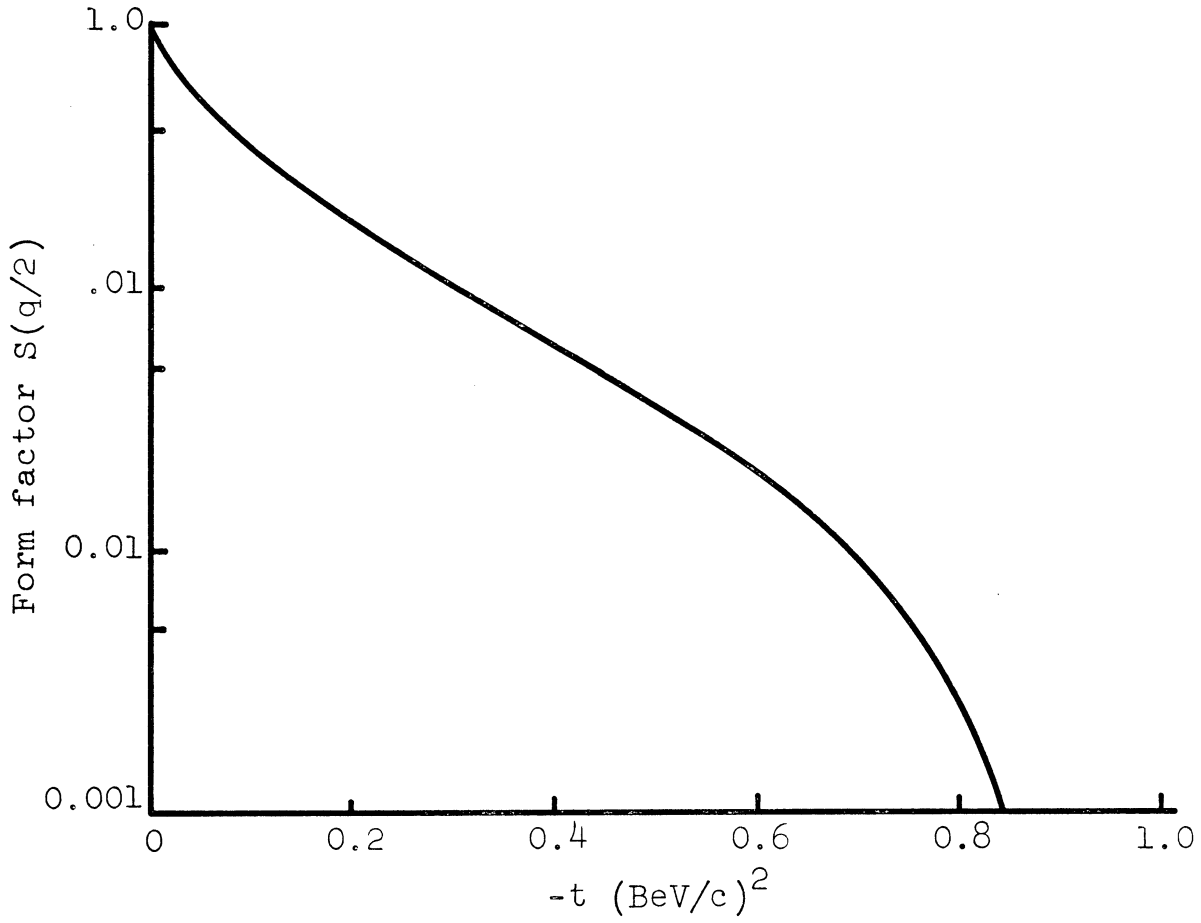

Figure 16. The form factor S(q/2) as a function of -t, the four momentum transfer squared. Moravcsik III fit to Gartenhaus wave function was used.

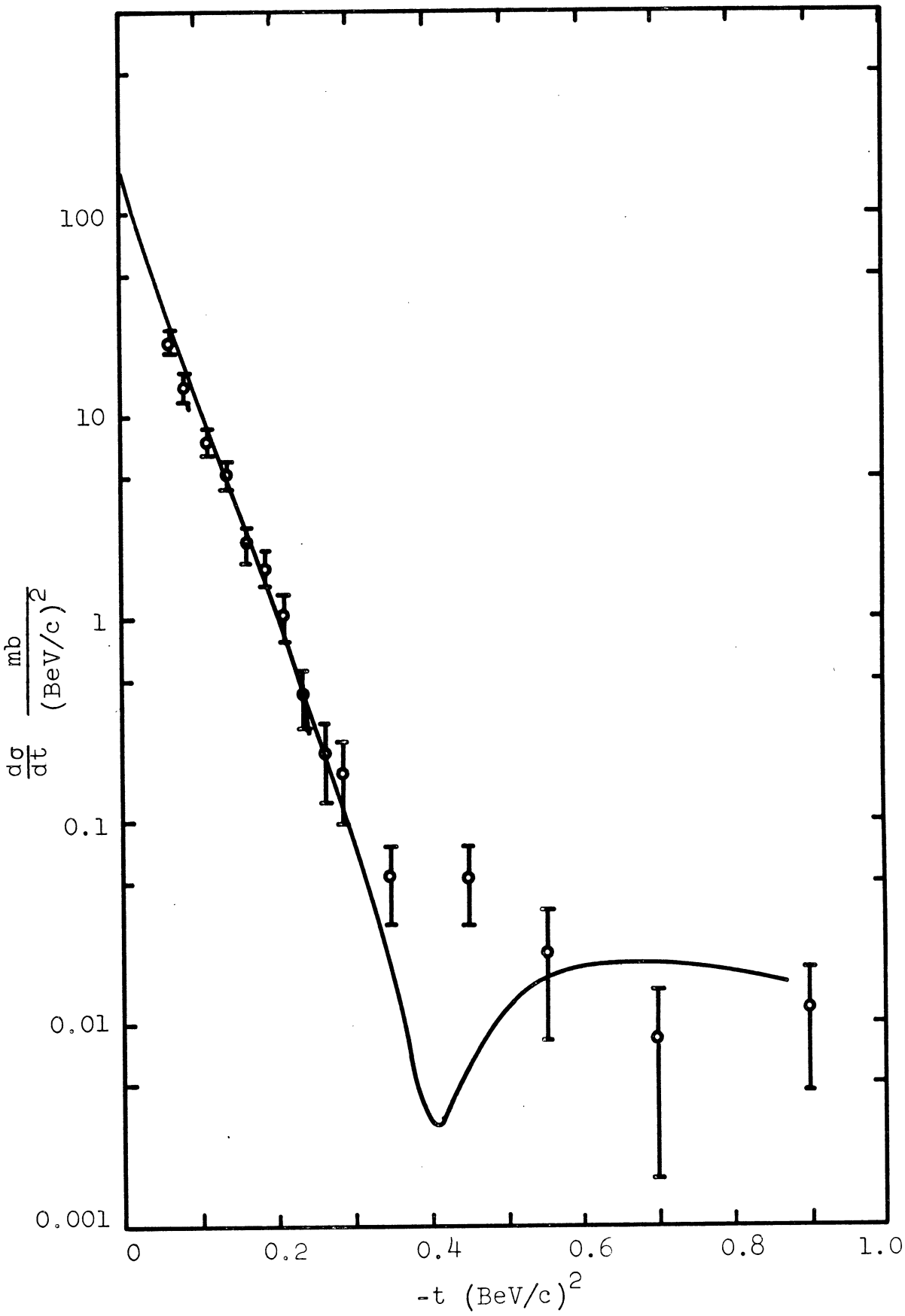

Figure 17. Theoretical π^+-d elastic differential cross section calculated with constant phase amplitudes, $^3S_1$ state deuteron wave function was utilized, along with experimental data.

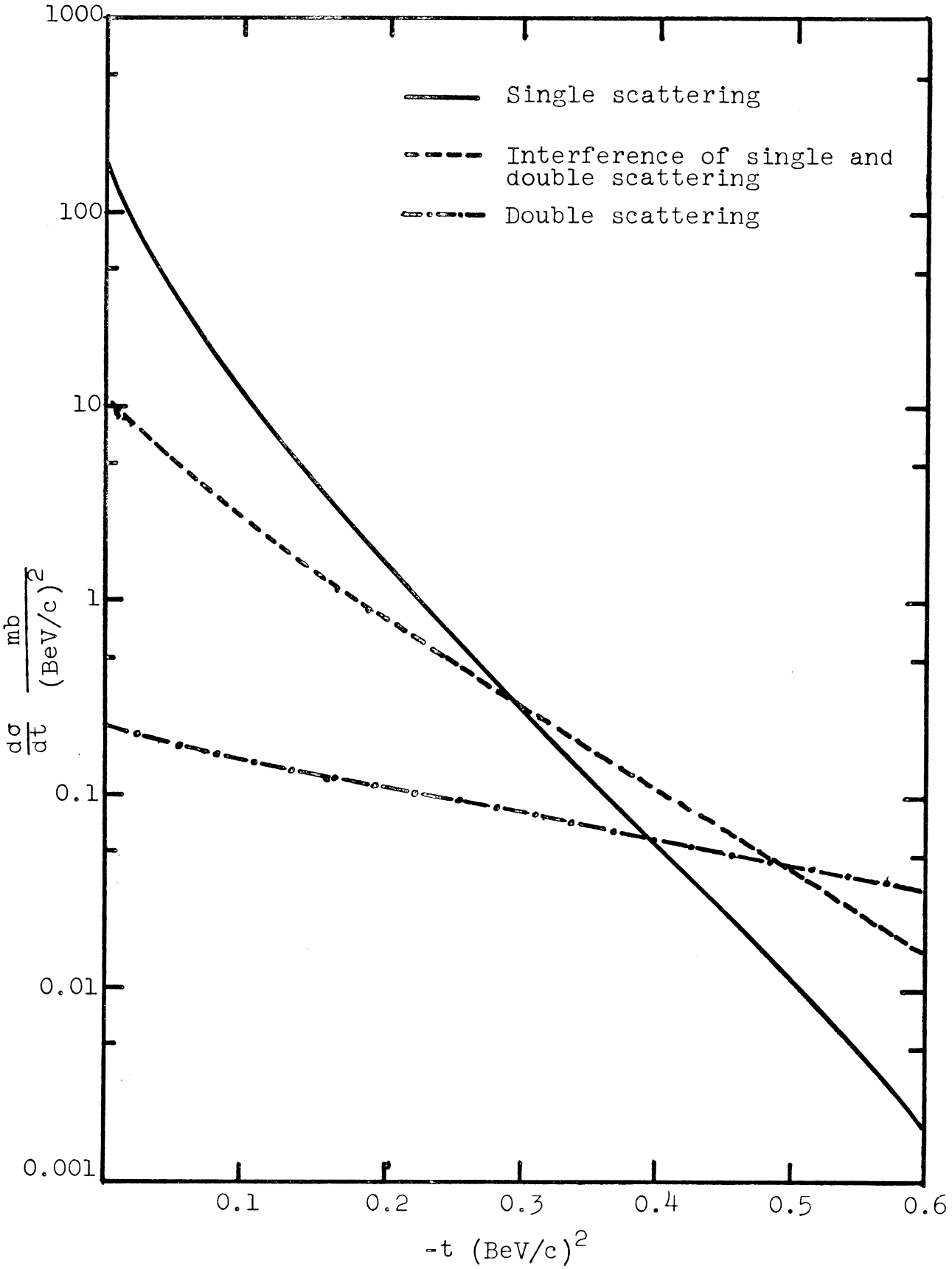

Figure 18. Comparison of magnitudes of single scattering, double scattering and the interference of single and double scattering.

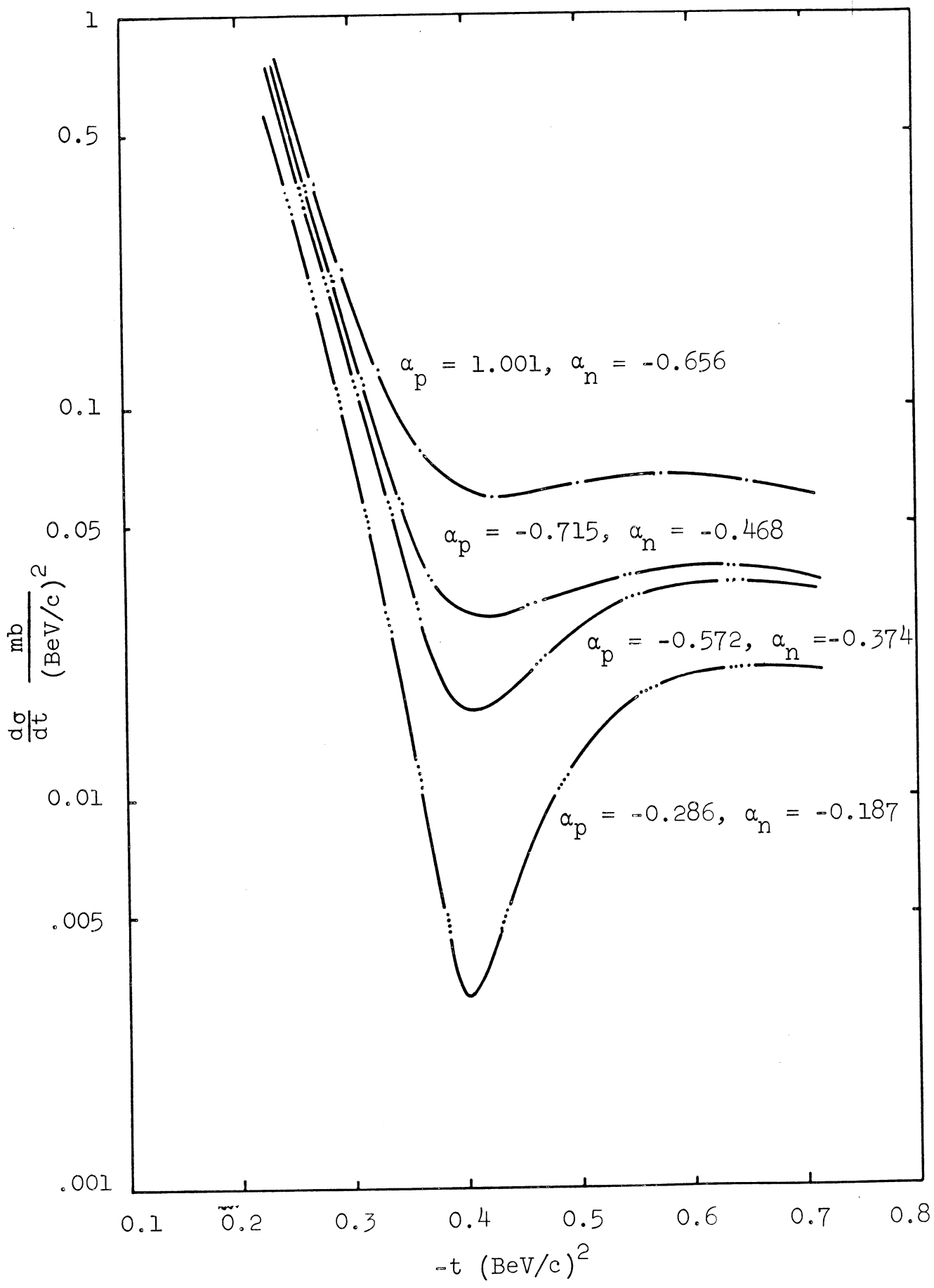

Figure 19. Effect of real parts of the free pion-nucleon scattering amplitudes on the pion-deuteron cross section.

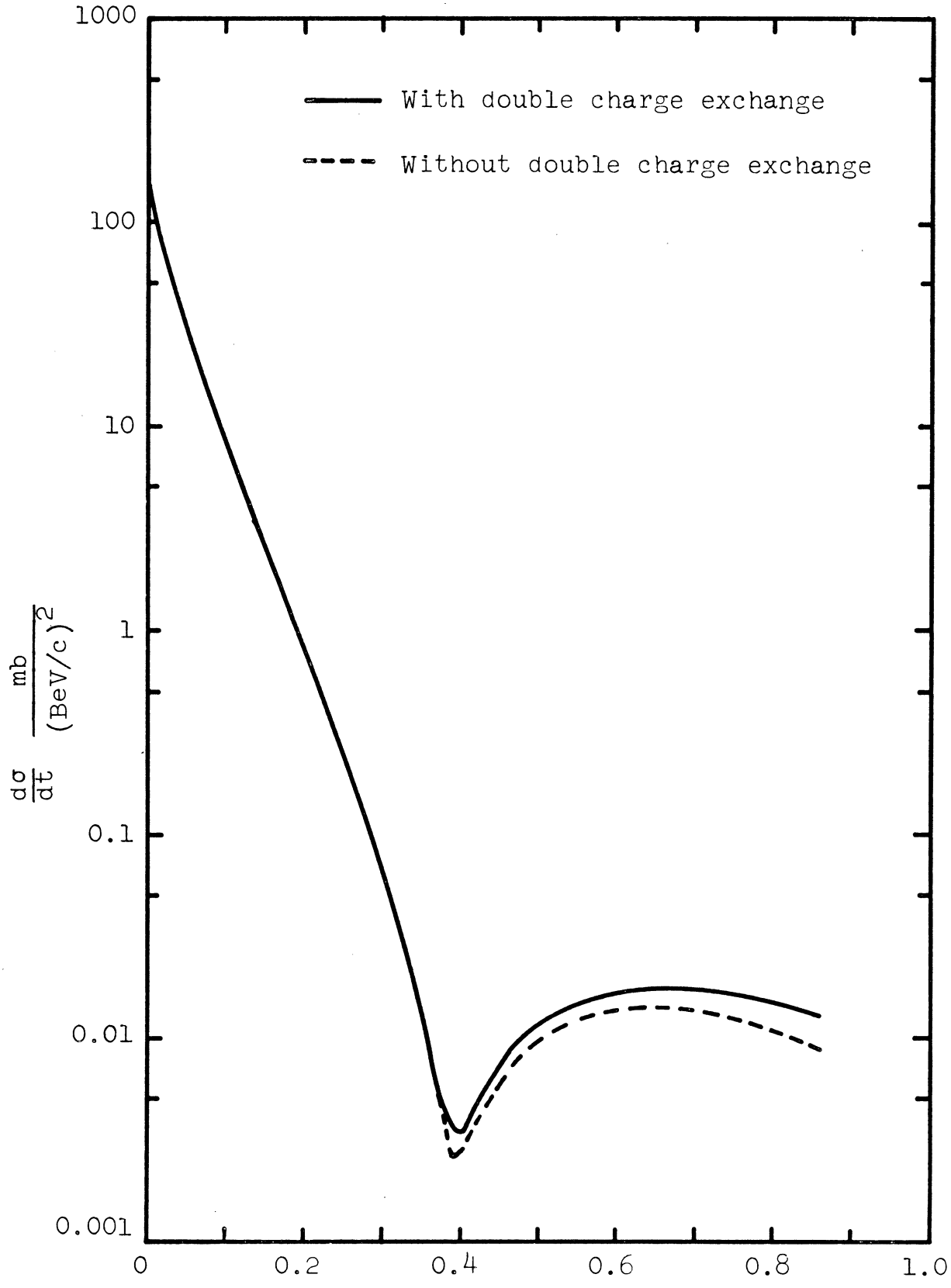

Figure 20. The π^+-d elastic differential cross section shown with and without the contribution of double charge exchange collisions.

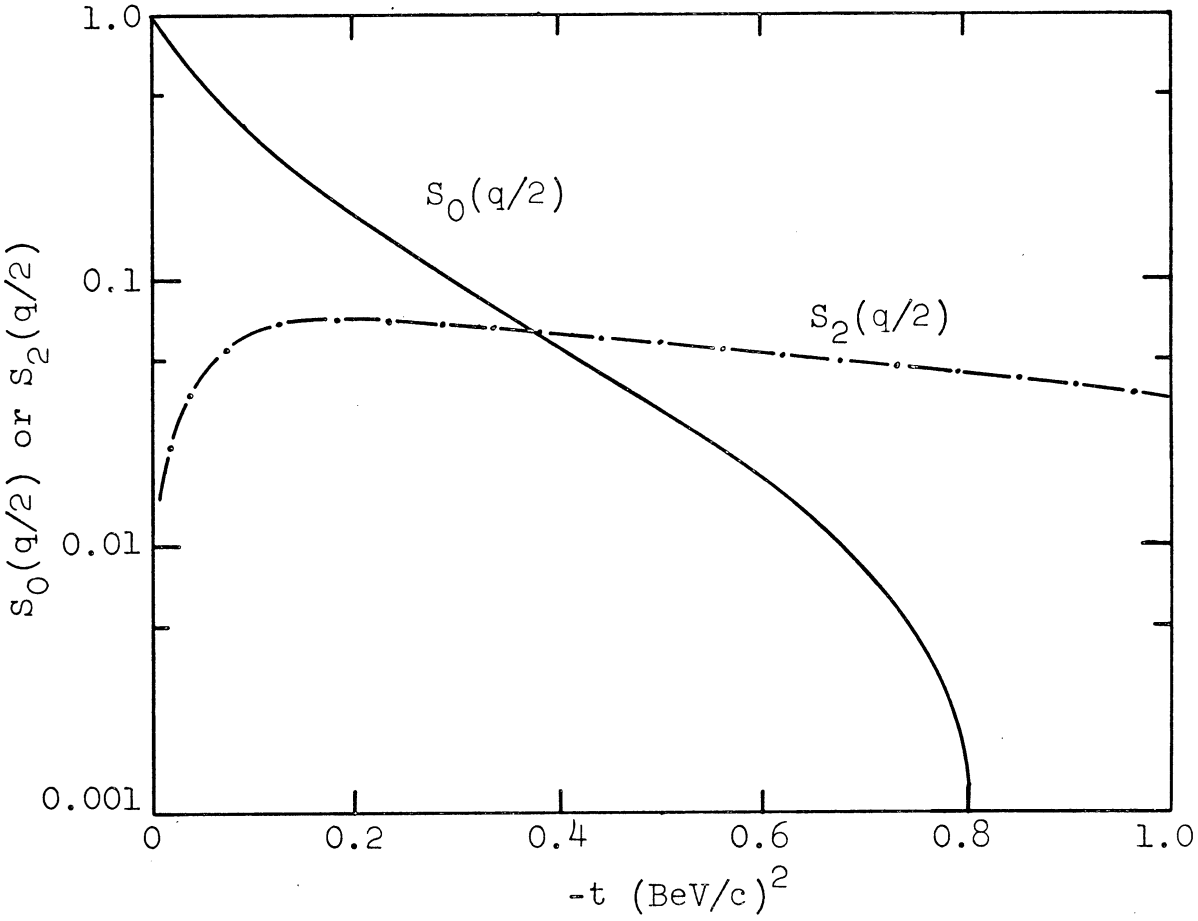

Figure 21. "Spherical" and "quadrupole" form factors, $S_0(q/2)$ and $S_2(q/2)$, as a function of -t. Values taken from the "potential No. 3" table of Glendenning and Kramer.

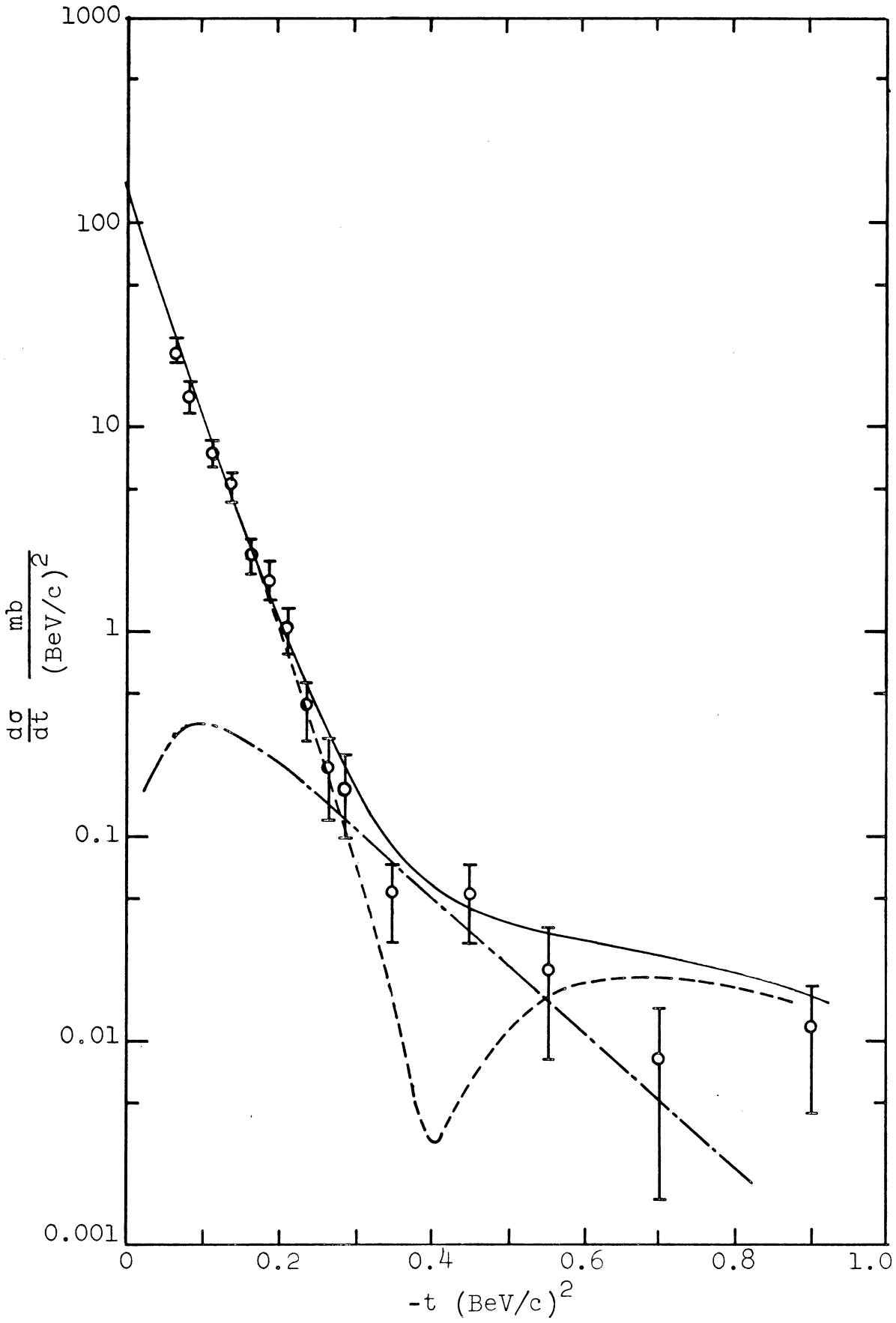

Figure 22. The theoretical predictions along with experimental data of 3.65 BeV/c pion-deuteron elastic scattering. The dashed curve is the contribution of $(\frac{d\sigma}{dt})_0$, the dash dot (—·—·—·—) curve is the contribution of $(\frac{d\sigma}{dt})_2$ and the solid curve is their sum.

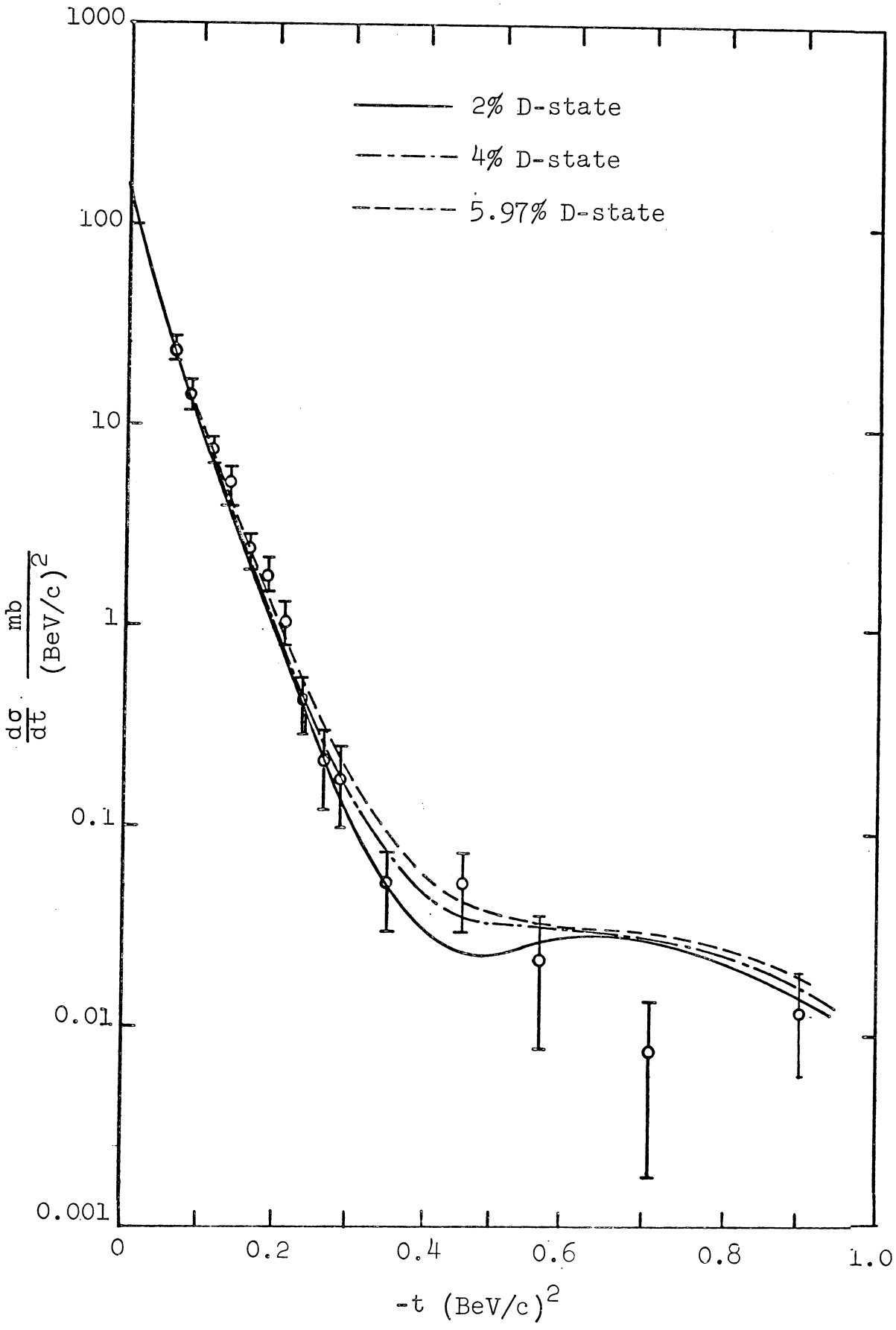

Figure 23. Effect of the D-state probability of the deuteron wave function to the π^+-d elastic scattering cross section, along with experimental data.

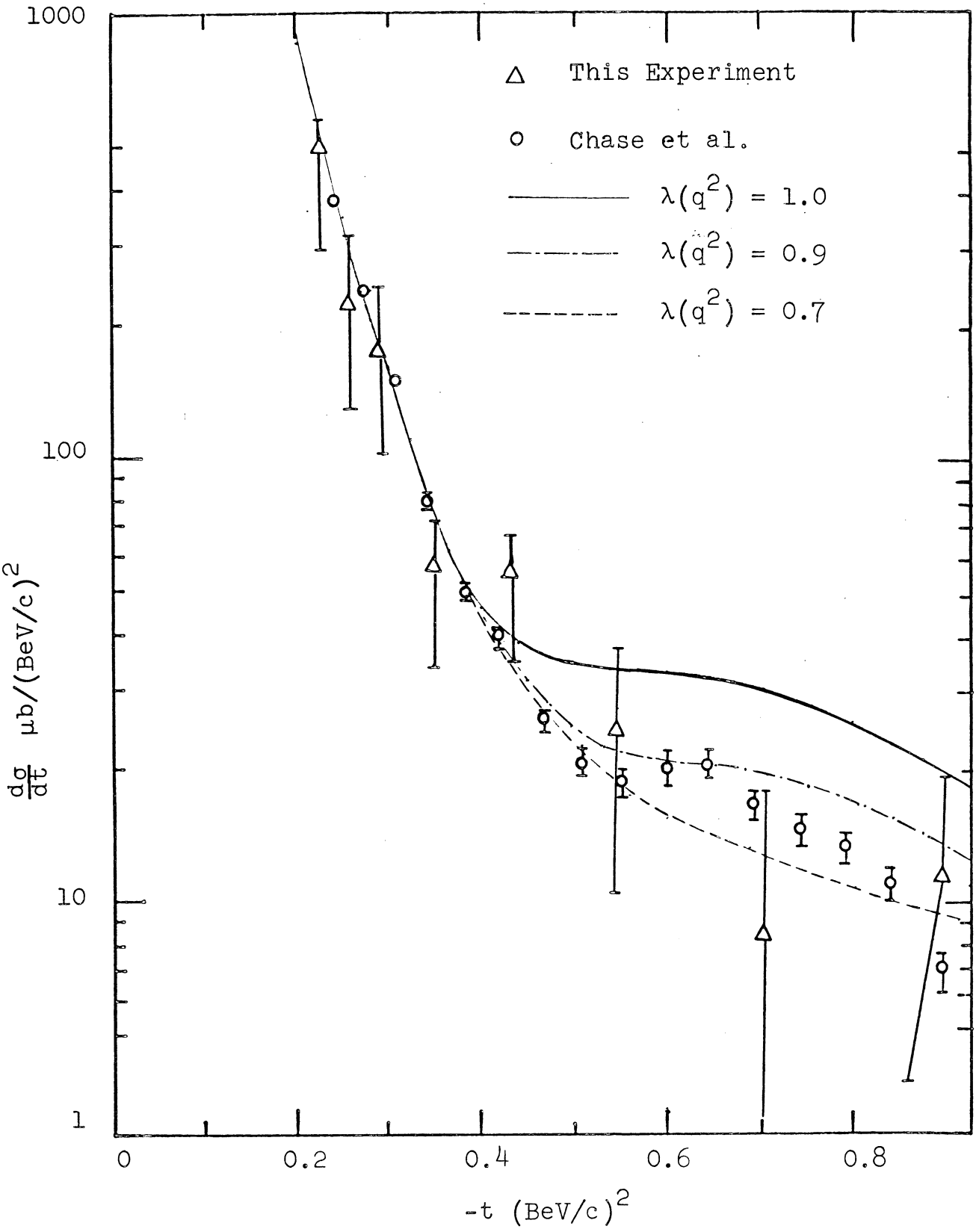

Figure 24. Effect of the parameter $\lambda(q^2)$ to the π -d elastic scattering along with experimental data.

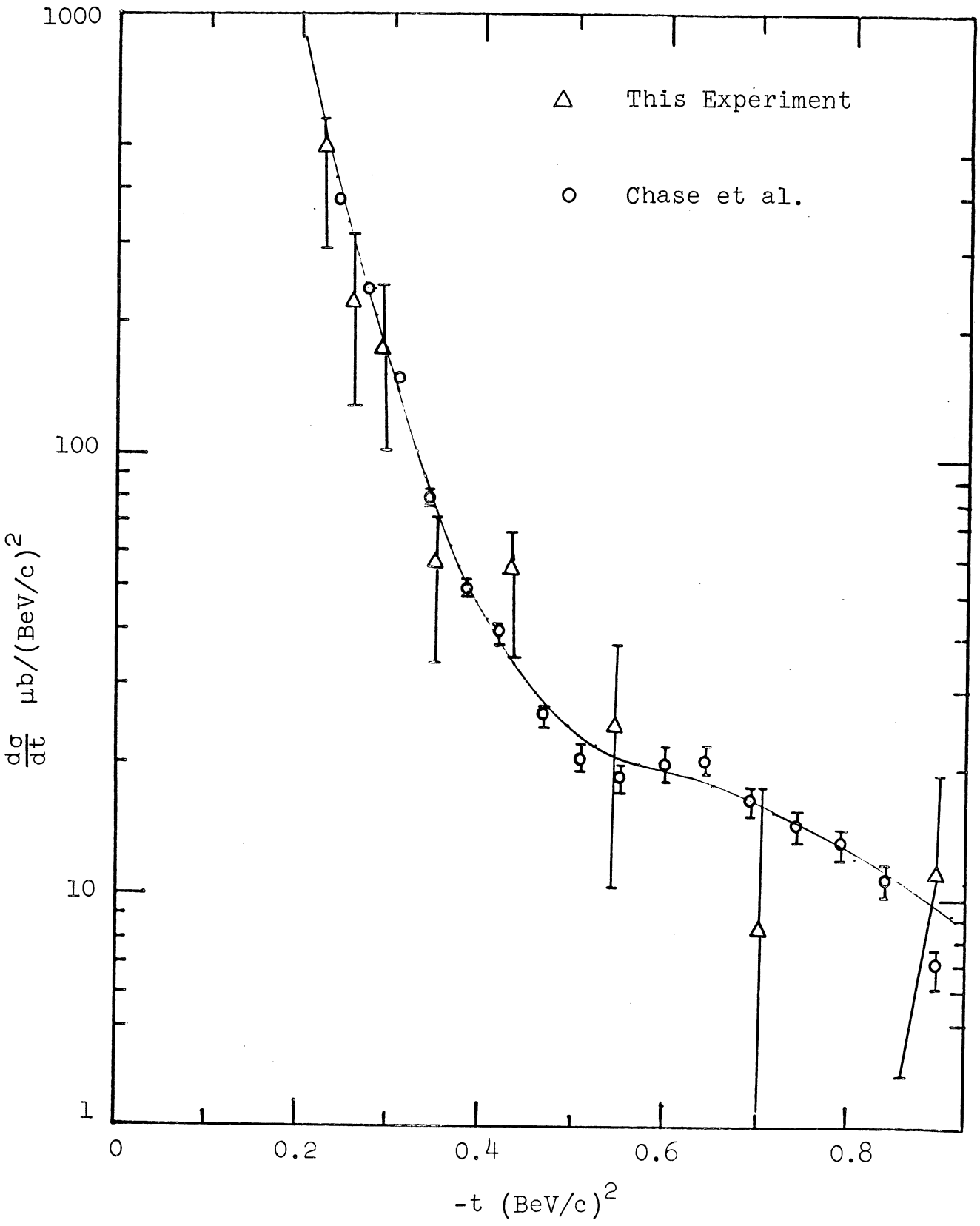

Figure 25. Theoretical prediction of π-d elastic scattering cross section calculated with modified double scattering amplitude with $\lambda(q^2) = 1 - q^2/3$. The "Glendenning and Kramer potential No. 3" wave function renormalized to D-state probability of 4% was utilized. Data are from this experiment and Chase et al.

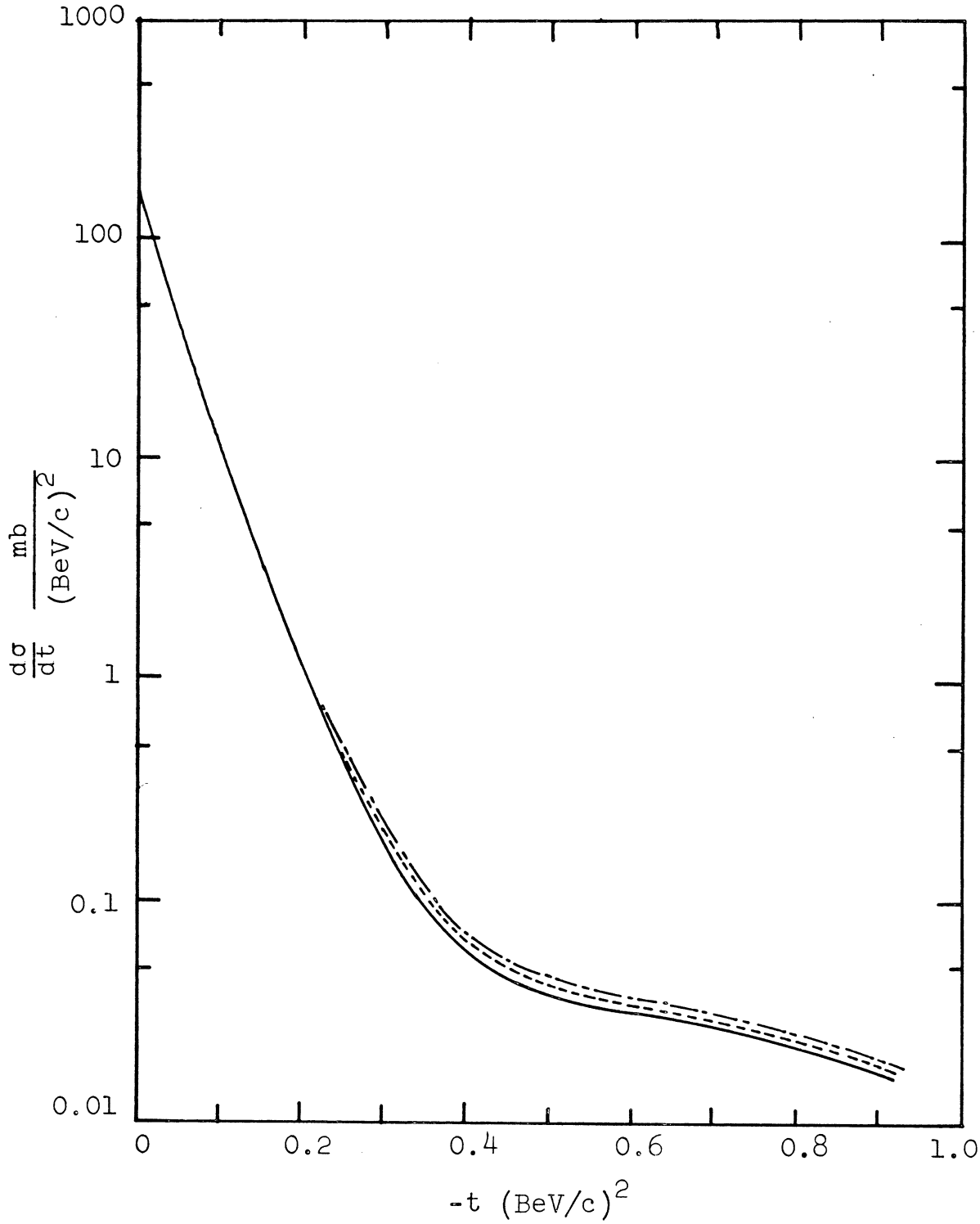

Figure 26. Effect of phase variation to the elastic scattering cross section calculated with amplitudes parameterized as Equation (4-17). The solid curve is for b = 0, the dashed curve is for b = 0.1 and the dash dot curve is for b = 0.15.

CHAPTER V

COMPARISON OF THE EXPERIMENTAL RESULT WITH THE THEORETICAL PREDICTION FOR THE DEUTERON BREAK UP REACTION

The interference between single and double scattering amplitudes which produces the theoretical dip in the differential cross section is not limited to elastic scattering process, but occurs also in the deuteron break up reaction, if all the independent variables in the final configuration are specified.

For our interest, we will only discuss the case of the deuteron break up reaction with incident π^+,

$$\pi^+ + d \rightarrow \pi^+ + p + n \quad , \qquad (5\text{-}1)$$

for one particular final state configuration.

The method used to calculate the theoretical prediction for the deuteron break up reaction developed by Bertocchi[44] will be discussed briefly in this chapter. A detailed report may be found in reference 44. In treating this problem, we will neglect all the complication with the spin variables and other effects stated in Section C, Chapter II.

For the break up reaction four independent variables are needed to describe the final state of the system (the total energy being fixed). We choose four independent variables in the laboratory system of the deuteron (c.f. Figure 27) namely:

$$(p_\pi - p_{\pi'})^2 = q^2 \; ; \; k_{ll}^2 \; ; \; k_\perp^2 \; ; \text{ and } \vec{k}_\perp \cdot \vec{q} \qquad (5\text{-}2)$$

(3 vectors squared)

where $\vec{p}_\pi$ and $\vec{p}'_\pi$ are the momenta of the incoming and outgoing π^+, $\vec{k}_{ll}$ and $\vec{k}_\perp$ are the projections of $\vec{k}_B = (\vec{k}_p - \vec{k}_n)/2$ along the beam direction and in the plane perpendicular to the beam. Note $\vec{k}_B$ is different from $\vec{k}$ defined in previous chapters.

In the high energy limit, but small momentum transfer ($p_\pi^2 \to \infty$, but $-t$, k_p^2, $k_n^2 \ll m$ (m = nucleon mass)), energy and momentum conservation give the following constraints

$$\begin{aligned}
&t \equiv (E_\pi - E'_\pi)^2 - q^2 \simeq -q^2 \\
&\vec{k}_p + \vec{k}_n = +\vec{q} \\
&\vec{q} \cdot \vec{p}_\pi = 0 \\
&k_p^2 + k_n^2 = 2k_B^2 + \frac{q^2}{2} \\
&k_p^2 - k_n^2 = +2\vec{k}_B \cdot \vec{q} \\
&(k_B)_{ll} = (k_p)_{ll} = -(k_n)_{ll}
\end{aligned} \qquad (5\text{-}3)$$

The scattering amplitude for the break up reaction can be expressed with Equation (2-16), and the cross section is the square of the amplitude. For the final state $\langle f|$ we use plane waves for the wave functions of the proton and neutron and neglect the effect of final state interactions. This leads to

$$\frac{d^4\sigma}{dtd^3k_B} = \frac{1}{8\pi^2 p_\pi^2} \Big| f_n(t)\ \psi(\vec{k}_p) + f_p(t)\ \psi(\vec{k}_n)$$

$$+ \frac{i}{2\pi p_\pi} \int d^{(2)}\vec{q}'\ \psi(\vec{q}' - \vec{k}_B)\ f_p(-\vec{q}' + \frac{\vec{q}}{2})$$

$$\times f_n(\vec{q}' - \frac{\vec{q}}{2})\Big|^2 \qquad (5\text{-}4)$$

where $\vec{q}'$ is the impact parameter, on the plane orthogonal to the beam, $\psi(\vec{k})$ is the Fourier transform of the deuteron wave function. Only the dependence upon the momentum transfer is explicitly indicated in Equation (5-4). Equation (5-4) includes single and double scattering processes corresponding to the diagrams given in Figure 27.

We can show the -t dependence of the differential cross section by keeping all the remaining three variables fixed. We can easily show that the maximum contribution to the double scattering with a net momentum transfer, -t, arises from two individual scatterings each with a partial momentum transfer square $-t/4$; that is, the best configuration for a large double scattering contribution is a symmetrical one, in which $|E_p - E_n| = 0$, and therefore $\vec{k}_B \cdot \vec{q} = 0$.

Figure 28 shows a plot of the differential cross section as a function of -t for the symmetrical configuration calculated with f_p and f_n indicated in Equation (4-1) and all the appropriate values for the input as follow:

$$\alpha_p(t) = \alpha_p(0) = -0.187$$

$$\alpha_n(t) = \alpha_n(0) = -0.286$$

$$\sigma_p = 28.1 \text{ mb}$$

$$\sigma_n = 31.5 \text{ mb}$$

$$A_p = 6.64 \text{ (BeV/c)}^{-2}$$

$$A_n = 7.31 \text{ (BeV/c)}^{-2} \quad .$$

In the computation the Moravcsik III fit to the Gartenhaus wave function for the deuteron without D-state component was used. The dip is at $-t = 0.28 \text{ (BeV/c)}^2$.

A comparison of the theoretical prediction with the experimental data shows good agreement except in the dip region. The disagreement in the dip region is perhaps due to the $^3D_1$ state of the deuteron which was ignored in the calculation.

The experimental data in Figure 28 were obtained by selecting events with $|E_p - E_n| \leq 2$ MeV.

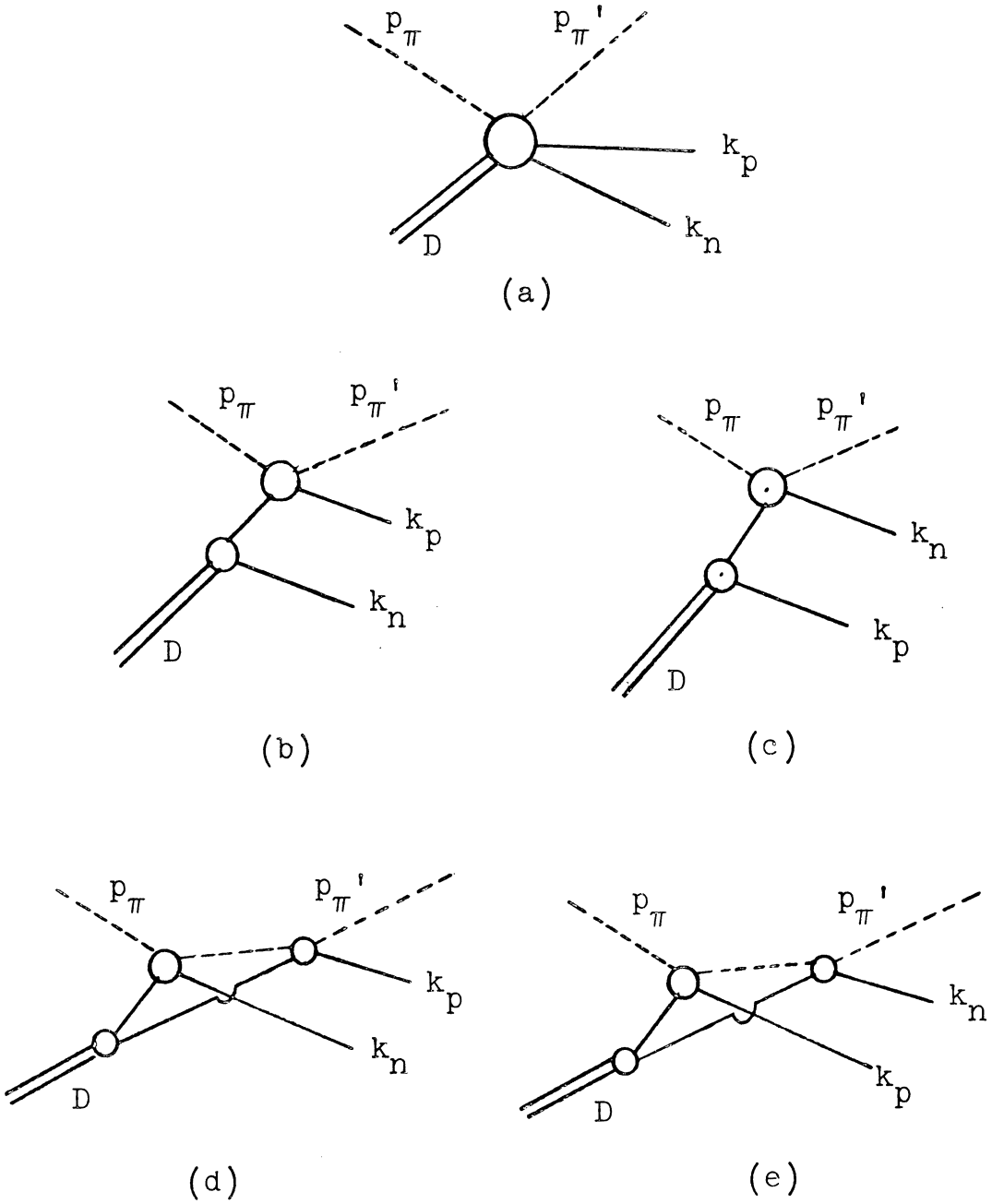

Figure 27. Single and double scattering diagrams of the deuteron break up.

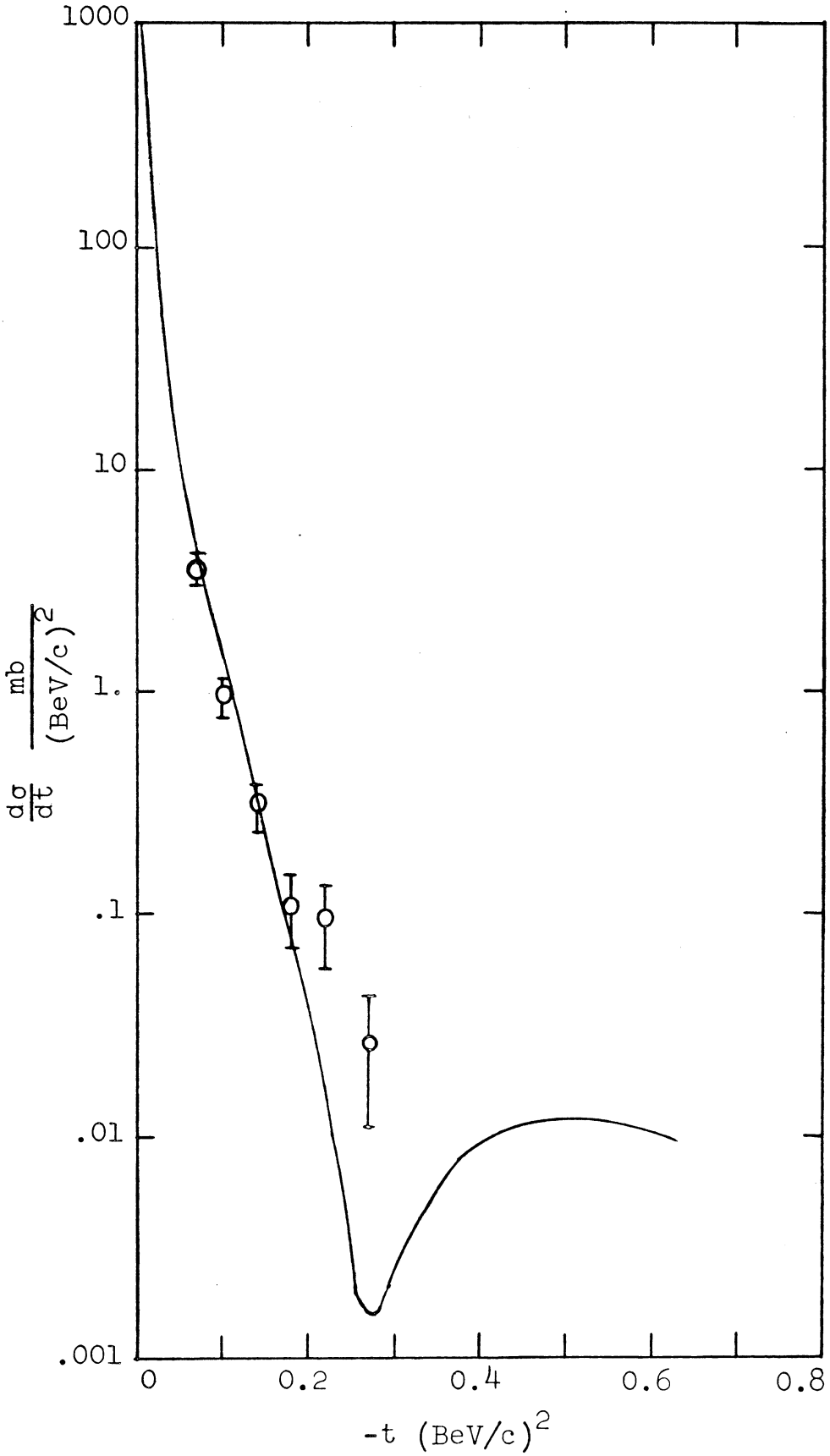

Figure 28. Theoretical predictions of the deuteron break up with the condition $E_p = E_n$ along with the experimental data selected for events $|E_p - E_n| \leq$ 2 MeV.

APPENDIX A

HIGH ENERGY SCATTERING AMPLITUDE FOR ASYMMETRIC INTERACTIONS

At large distances the wave function of the incident particle from the target particle is the sum of an incoming plane wave and an outgoing spherical wave with the elastic-scattering amplitude

$$f(\theta,\varphi) = \exp(i\vec{k} \cdot \vec{r}) + (e^{ikr}/r)\, f(\theta,\varphi)$$

where $\vec{k}$ is the propagation vector of the incident plane wave and $\vec{r}$ is the position vector measured from a point in the target particle, θ is the scattering angle measured with respect to the direction of the beam (positive z direction) and φ is the azimuthal scattering angle measured with respect to the positive x axis. $f(\theta,\varphi)$ can be expanded in a series of spherical harmonics as

$$f(\theta,\varphi) = \sum_{\ell=0}^{\infty} \sum_{m=-\ell}^{\ell} f_{\ell m}(\theta,\varphi) \qquad \text{(A-1)}$$

where

$$f_{\ell m}(\theta,\varphi) = \frac{1}{2ik}\,(2\ell+1)(C_{\ell m} - \delta_{mo})e^{im\varphi}\, p_{\ell}^{m}(\cos\theta) \qquad \text{(A-2)}$$

and the coefficients $C_{\ell m}$ are determined by the scattering

interactions. For an azimuthally symmetrical potential, $C_{\ell m}$ may be expressed as

$$C_{\ell m} = \delta_{mo} \exp(2i\delta_{\ell}) \qquad \text{(A-3)}$$

where δ_{ℓ} is the phase shift for the ℓ^{th} partial wave. Near the forward direction p_{ℓ}^{m} may be expressed by the Bessel function

$$p_{\ell}^{m}(\cos\theta) \simeq (-1)^{m}(\ell + 1/2)^{m} J_{m}[(2\ell + 1)\sin(1/2)\theta] \quad . \qquad \text{(A-4)}$$

Furthermore a Bessel function can be expressed by its integral representation

$$J_{m}[(2\ell + 1)\sin(1/2)\theta] = \frac{i^{-m}}{2\pi} \int_{0}^{2\pi} e^{i(2\ell+1)\sin(1/2)\theta \cos\alpha + im\alpha} \, d\alpha \qquad \text{(A-5)}$$

Substituting (A-5) into (A-2) one obtains

$$f(\theta,\varphi) = \frac{1}{2\pi ik} \int_{0}^{2\pi} \sum_{\ell=0}^{\infty} (\ell + 1/2)\, e^{2i(\ell+1/2)\sin(1/2)\theta \cos\alpha}$$

$$\times \left[\sum_{m=-\ell}^{+\ell} i^{-m}(\ell + 1/2)^{m} C_{\ell m}\, e^{im(\alpha+\varphi-\pi)} - 1 \right] d\alpha \qquad \text{(A-6)}$$

or

$$f(\theta,\varphi) = \frac{1}{2\pi ik} \int_0^{2\pi} \sum_{\ell=0}^{\infty} (\ell + \tfrac{1}{2})\, e^{2i(\ell+1/2)\sin\frac{\theta}{2}\cos\alpha}\, d\alpha$$

$$\times\, [A(\ell,\psi) - 1] \qquad \text{(A-7)}$$

where $\psi \equiv \alpha + \varphi - \pi$ (A-8)

and

$$A(\ell,\psi) = \sum_{m=-\ell}^{\ell} i^{-m}(\ell + 1/2)^m\, C_{\ell m}\, e^{im\psi} \quad . \qquad \text{(A-9)}$$

At high energies the wave length of the incident particle is much smaller than the range of interaction, and so the summation over ℓ in the integrand of Equation (A-7) contains many terms and may be approximated by an integral. Defining impact parameter b by the relation $kb = \ell + 1/2$, the integral may be expressed as one carried out over the variable b. One may write Equation (A-7) as

$$f(\theta,\varphi) = \frac{ik}{2\pi} \int_0^{2\pi} \int_0^{\infty} e^{2ikb\,\sin(1/2)\theta\cos\alpha} \left[1 - e^{i\chi(b,\psi)}\right] b\,db\,d\alpha \qquad \text{(A-10)}$$

where $A(\ell,\psi)$ is replaced by $\exp[i\chi(b,\psi)]$ and $\chi(b,\psi)$ is the complex phase shift.

By taking α to be the angle that the impact parameter vector b makes with the positive x direction and using the

small angle approximation

$$(\vec{k} - \vec{k}') \cdot \vec{b} = 2kb \sin(\theta/2)\cos(\alpha - \varphi + \pi) \quad ,$$

one obtains

$$f(\theta,\varphi) = \frac{ik}{2\pi} \int \exp[i(\vec{k} - \vec{k}') \cdot \vec{b}]\{1 - \exp[i\chi(\vec{b})]\}\, d^{(2)}\vec{b} \quad . \tag{A-11}$$

APPENDIX B

TRANSFORMATION OF SCATTERING AMPLITUDE FROM THE CENTER-OF-MASS SYSTEM TO THE LABORATORY SYSTEM

In this Appendix we will demonstrate the fact that the formulas which describe small angle scattering in the laboratory system are of the same form as those which describe it in the center-of-mass system.

Let γ be the ratio of the incident-particle total energy in the laboratory system to its rest energy, and λ be the ratio of the mass of the incident particle to that of the target particle. We define

$$\gamma_1 = (1 + \lambda\gamma)(1 + 2\lambda\gamma + \lambda^2)^{-1/2} \quad ,$$

and

$$\gamma_2 = (\lambda + \gamma)(1 + 2\lambda\gamma + \lambda^2)^{-1/2} \quad ,$$

to be two relativistic factors which will be used in the Lorentz transformation, and use subscripts c and L to indicate quantities associated with the center-of-mass and laboratory systems respectively.

One can write the Lorentz transformation as[45]

$$k_L = (\gamma_1 + \lambda\gamma_2)k_c$$

and

$$f_L(\vec{k}'_L,\vec{k}_L) = [\sin^2 \theta_c + (\gamma_1 \cos \theta_c + \lambda\gamma_2)^2]^{3/4}$$

$$\times (\gamma_1 + \lambda\gamma_2 \cos \theta_c)^{-1/2} \times f_c(\vec{k}'_c,\vec{k}_c) \quad .$$

For small-angle scattering this expression reduces to

$$f_L(\vec{k}'_L,\vec{k}_L) = (\gamma_1 + \lambda\gamma_2) f_c(\vec{k}'_c,\vec{k}_c) \quad .$$

Because $\vec{b}$ is a vector perpendicular to the direction of the incident particle, the Lorentz transformation will not affect transverse components of the momentum. Therefore,

$$(\vec{k}'_L - \vec{k}_L) \cdot \vec{b} = (\vec{k}'_c - \vec{k}_c) \cdot \vec{b}$$

and

$$f_L(\vec{k}'_L,\vec{k}_L)$$

$$= (\gamma_1 + \lambda\gamma_2) \frac{ik_c}{2\pi} \int \exp[i(\vec{k}_c - \vec{k}'_c) \cdot \vec{b}] \Gamma(\vec{b}) \, d^{(2)}\vec{b}$$

$$= \frac{ik_L}{2\pi} \int \exp[i(\vec{k}_L - \vec{k}'_L) \cdot \vec{b}] \Gamma(\vec{b}) \, d^{(2)}\vec{b} \quad .$$

The phase shifts are not affected by the Lorentz transformation[11], therefore Equation (2-1) expresses the scattering

amplitude correctly in the laboratory system as soon as the laboratory $\vec{k}$ and $\vec{k}'$ are used in this expression.

APPENDIX C

THE NORMALIZATION OF CROSS SECTION

In this Appendix the normalization of the absolute cross section will be given. The normalization was obtained from the scanned path length. A detailed method to determine the cross section can be found in reference 22.

The expression of the cross section per event for the elastic process is given[22]

$$\sigma/\text{event} = [\rho L F_1 F_2 F_3 F_4 F_5 F_6]^{-1} \quad ,$$

where ρ = density of liquid deuterium in deuterons/cc

L = track length

F_1 = correction factor for beam contamination

F_2 = correction factor for beam absorption

F_3 = correction factor for interaction loss

F_4 = correction factor for scan loss

F_5 = correction factor for events not measured

F_6 = correction factor for elastic events lost in other reaction channels,

and F_i stands for 1 minus the values listed in Table V.

TABLE V

VALUES USED IN EVALUATING THE CROSS SECTION

	Value	% Error
ρ^*, deuterons/cc	$4.19 \pm 0.08 \times 10^{22}$	2%
L^*, cm	$1.14 \pm 0.04 \times 10^{7}$	4%
F_1^*	$(5 \pm 3)\%$	
F_2^*	$(2.6 \pm 0.1)\%$	
F_3	$(3.6 \pm 1.3)\%$	
F_4	1%	
F_5	2.5%	
F_6	9.8%	
σ/event, μb	2.72 ± 0.16	

*Values taken from reference 22.

The σ/event listed in Table V is based on a portion of the film which is only 19.4% of the total track length. Therefore, the cross section per event for the film we used for this experiment is 0.194 times the cross section given in Table V. The elastic scattering cross section is thus

$$\sigma_{el}/\text{event} = 0.524 \pm 0.031 \ \mu\text{b/event} \quad .$$

F_3, the correction for interaction loss, is obtained from the data given in reference 22 by considering the ratio for

interaction loss between 4 prong events and 2 prong events. Benson[22] concluded the correction for interaction loss for 4 prong events to be (7.3 ± 2.5)%. It is reasonable to approximate the interaction loss for 2 prong events as just half of that for 4 prong events since the ratio of number of outgoing tracks is two to one.

F_4, the correction factor for scanning loss, is calculated from the scan efficiency. The two-prong single scanning efficiency is estimated to be 96% from the double scan (after azimuthal angle cuts). This indicated both scanners missed $(1-96\%)^2$ or < 1% of the total number of elastic events on the film, since the entire film used for this experiment was scanned twice by independent scanners.

F_5, the correction factor for events not measured, given in Table V is based on events failed to pass the geometry program. Our failure rate for first measurement is 10% and 25% for remeasurement. This amounts to (25%)(10%) = 2.5% of the events failed the geometry program after the remeasurement.

The last correction factor, F_6, is an estimation of elastic events lost in reaction channels other than elastic process. Table VI shows the estimation of elastic events lost in other reaction channels.

Quantities in Table VI were obtained in the following manner. For (1) and (2) we assumed all the events fit the hypothesis π^+pn and calculated the proton-neutron effective mass, M(pn), and number of events which are above the smooth

TABLE VI

ELASTIC EVENTS LOST IN VARIOUS REACTION CHANNELS

	Reaction Channels		No. of Events
(1)	π^+pn	Unambiguous	85 events
(2)	$\pi^+pn - pp\pi^\circ$ $\pi^+pn - \pi^+d\pi^\circ - pp\pi^\circ$ $\pi^+pn - \pi^+d\pi^\circ$	Ambiguous	136 events
(3)	$\pi^+d\pi^\circ$	Unambiguous	51 events
(4)	$pp\pi^\circ - \pi^+d\pi^\circ$	Ambiguous	170 events
(5)	No fit		50 events
		Total	492 events

492 events corresponds to 492/5050 = 9.8%, since the total number of elastic events is 5050.

curve of a phase space and have M(p,n) between 1876-1886 MeV were counted for each reaction channel.

For (3), (4), and (5) we assumed all the events in these reaction channels were elastic and the momentum components for each event were obtained from TRED tape with properly assigned particle mass for each track, then the missing energy, E_{miss}, and the missing momentum, P_{miss}, were calculated for each event. Events which satisfied the conditions

$$0 < E_{miss} < 5 \text{ MeV}$$

and

$$0 < P_{miss} < 5 \text{ MeV/c}$$

were considered to be elastic events and were counted for each reaction channel. We assume that these 492 events have the same t dependence as the other elastic events.

The cross section for deuteron break up process was calculated in a similar way except F_6 is 1% instead of 9.8%. Because there is only 1% of break up events which was lost in the elastic scattering channel, this gives

$$\sigma/\text{event} = 0.482 \pm 0.029 \ \mu\text{b/event} \quad .$$

APPENDIX D

ESTIMATION OF THE BACKGROUND IN THE BREAK UP REACTION

In this Appendix a crude estimation of the background the sample of deuteron break up reaction will be given.

a) Background from elastic events.

From Table VI a total of 221 elastic events were contained in the sample retained for the break up reaction (both single fit and ambiguous events).

b) Background from charge exchange reaction,

$\pi^+ d \rightarrow p + p + \pi^\circ$ (D-1).

The total cross section for this reaction is estimated to be 130μb[46]. The estimation was made by considering the proton as a spectator and charge symmetry as valid. A maximum of 270 events due to reaction (D-1) is possible in the sample.

c) Background from reaction,

$\pi^+ d \rightarrow \pi^+ + d + \pi^\circ$ (D-2).

There is no experimental cross section given for this reaction. However, we can estimate the cross section for this reaction by comparing reaction (D-2) with the following reaction

$$K^+ + d \rightarrow K^+ + \pi^\circ + d \quad . \qquad \text{(D-3)}$$

The cross section of reaction (D-3) is 105 ± 21 μb at

4.5 BeV/c[47] and 150 ± 35 μb at 2.3 BeV/c[48]. An estimated cross section for reaction (D-3) at 3.65 BeV/c is 123 μb.

If we consider the diagrams, Figures 29 and 30, for reaction (D-2) and (D-3) on the basis of a peripheral single-meson exchange model, only isoscalar exchange is possible for both cases, and assuming the reaction mechanisms are both through ω exchange for reaction (D-2) and (D-3) and that the SU_3 model is valid, then the ratio of cross section for reactions (D-2) and (D-3) should be 4 to 1[49].

Thus, the cross section for reaction (D-2) is 492 μb. This amounts to a maximum possible of 1040 events in the sample.

Therefore, the upper limit of the background due to (a), (b), and (c) is 1531/9601 = 15.8%.

In fact, the contamination is much lower than 15.8% since we used the total cross sections for both Reactions (D-1) and (D-2) in this calculation.

In this experiment 1067 unambiguous events corresponding to Reaction (D-2) have been found (c.f. Table I), therefore the contamination due to Reaction (D-2) in the sample for the deuteron break up process is probably negligible since we estimated only 1040 (D-2) events could occur. If we ignore the (D-2) background then the background of the break up reaction is approximately (221 + 270)/9601 = 5.1%.

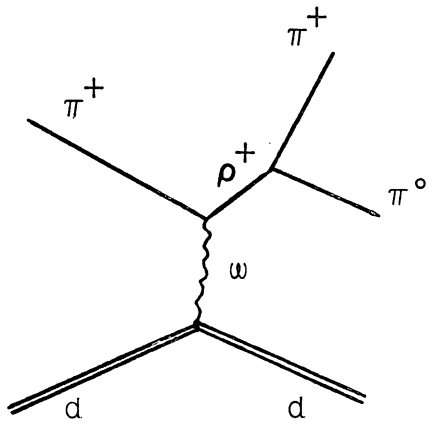

Figure 29. Feynman diagram for Reaction (D-2).

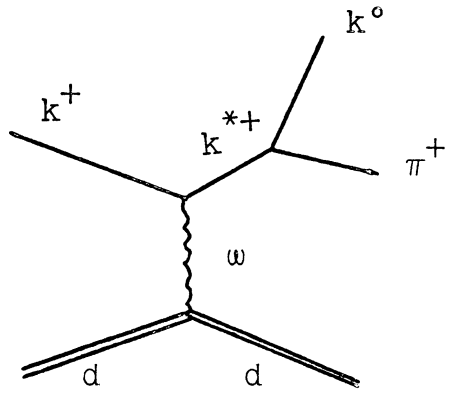

Figure 30. Feynman diagram for Reaction (D-3).

APPENDIX E

EVALUATION OF MATRIX ELEMENTS $T_{MM'}$

The total deuteron wave function can be written as:

$$\psi_M = \frac{1}{4\pi}\frac{1}{r}\left[u(r) + \frac{1}{\sqrt{8}}\, w(r)\, S_{12}\right] \chi_M \,, \quad M = 0, \pm 1 \qquad \text{(E-1)}$$

$$S_{12} = 3(\vec{\sigma}_1 \cdot \hat{r})(\vec{\sigma}_2 \cdot \hat{r}) - (\vec{\sigma}_1 \cdot \vec{\sigma}_2) \,,$$

where χ_M is a triplet spin function.

It is equivalent to write Equation (E-1) as follows:

$$\psi_1 = \frac{1}{r}\, u(r)\, \frac{1}{\sqrt{(4\pi)}}\, \chi_1 + \frac{1}{r}\, w(r)\left[\sqrt{\frac{1}{10}}\, Y_{20}(\theta,\varphi)\, \chi_1 - \sqrt{\frac{3}{10}}\, Y_{21}(\theta,\varphi)\, \chi_0 + \sqrt{\frac{6}{10}}\, Y_{22}(\theta,\varphi)\, \chi_{-1}\right]$$

$$\psi_{-1} = \frac{1}{r}\, u(r)\, \frac{1}{\sqrt{(4\pi)}}\, \chi_{-1} + \frac{1}{r}\, w(r)\left[\sqrt{\frac{6}{10}}\, Y_{2-2}(\theta,\varphi)\, \chi_1 - \sqrt{\frac{3}{10}} \times Y_{2-1}(\theta,\varphi)\, \chi_0 + \sqrt{\frac{1}{10}}\, Y_{20}(\theta,\varphi)\, \chi_{-1}\right]$$

$$\psi_0 = \frac{1}{r}\, u(r)\, \frac{1}{\sqrt{(4\pi)}}\, \chi_0 + \frac{1}{r}\, w(r)\left[\sqrt{\frac{3}{10}}\, Y_{2-1}(\theta,\varphi)\, \chi_1 - \sqrt{\frac{4}{10}}\, Y_{20}(\theta,\varphi) \times \chi_0 + \sqrt{\frac{3}{10}}\, Y_{20}(\theta,\varphi)\, \chi_{-1}\right]$$

where the $Y_{\ell M}$'s are the normalized spherical harmonics, and they are given as:

$$Y_{20} = \frac{1}{\sqrt{(2\pi)}} \frac{\sqrt{10}}{4} (3 \cos^2 \theta - 1)$$

$$Y_{21} = - \frac{1}{\sqrt{(2\pi)}} \frac{\sqrt{15}}{2} \sin \theta \cos \theta \, e^{+i\varphi}$$

$$Y_{22} = \frac{1}{\sqrt{(2\pi)}} \frac{\sqrt{15}}{4} \sin^2 \theta \, e^{2i\varphi}$$

$$Y_{2-1} = \frac{1}{\sqrt{(2\pi)}} \frac{\sqrt{15}}{2} \sin \theta \cos \theta \, e^{-i\varphi}$$

$$Y_{2-2} = \frac{1}{\sqrt{(2\pi)}} \frac{\sqrt{15}}{4} \sin^2 \theta \, e^{-2i\varphi}$$

The coordinate system is chosen in a convenient way as shown in Figure 31, where Y is the beam direction, $\vec{q}'$ is in the XZ plane, $\vec{q}$ is in the Z direction, the angle between q and q' is α, ω is the angle between $\vec{r}$ and $\vec{q}'$, and $\cos \omega = \cos \theta \cos \alpha + \sin \theta \sin \alpha \cos \varphi$.

$T_{MM'}$ in Equation (4-12) is simply $\langle \psi_M | T(\vec{q}, \vec{r}) | \psi_{M'} \rangle$ and may be expressed as follows:

$$T_{MM'} = T_{0,MM'} + T_{2,MM'}$$

where

$$T_{0,MM'} = \left\langle \psi_M \left| f_n(\vec{q}) \exp\left(\frac{-1}{2}\vec{q}\cdot\vec{r}\right) + f_p(\vec{q}) \exp\left(-\frac{1}{2}\vec{q}\cdot\vec{r}\right) \right| \psi_{M'} \right\rangle$$

and

$$T_{2,MM'} = \left\langle \psi_M \left| \frac{i}{2\pi k} \int d^2q' \; f_n\left(\frac{\vec{q}}{2} - \vec{q}'\right) f_p\left(\frac{\vec{q}}{2} + \vec{q}\right) e^{-i\vec{r}\cdot\vec{q}'} \right| \psi_{M'} \right\rangle \quad .$$

For $M = M' = 1$,

$$T_{11} = T_{0,11} + T_{2,11}$$

where $T_{0,11} = \left\langle \psi_1 \left| f_n(\vec{q}) \exp\left(-\frac{1}{2}\vec{q}\cdot\vec{r}\right) + f_p(\vec{q}) \exp\left(-\frac{1}{2}\vec{q}\cdot\vec{r}\right) \right| \psi_1 \right\rangle$

and

$$T_{2,11} = \left\langle \psi_1 \left| \frac{i}{2\pi k} \int d^2\vec{q}' \; f_n\left(\frac{\vec{q}}{2} - \vec{q}'\right) f_p\left(\frac{\vec{q}}{2} + \vec{q}'\right) e^{-i\vec{r}\cdot\vec{q}'} \right| \psi_1 \right\rangle \quad .$$

First, let us evaluate $T_{0,11}$ by writing

$$T_{0,11} = \int d^3\vec{r} \left[\frac{1}{\sqrt{(4\pi)}} \frac{u^*}{r} \chi_1^* + \frac{w^*}{r} \left(\sqrt{\frac{1}{10}} Y_{20}^* \chi_1^* - \sqrt{\frac{3}{10}} Y_{21}^* \chi_0^* \right.\right.$$

$$\left.\left. + \sqrt{\frac{6}{10}} Y_{22}^* \chi_{-1}^* \right) \right] \left(f_n(\vec{q}) + f_p(\vec{q})\right) e^{-(1/2)qr\cos\theta}$$

$$\times \left[\frac{1}{\sqrt{(4\pi)}} \frac{u}{r} \chi_1 + \frac{w}{r} \left(\sqrt{\frac{1}{10}} Y_{20} \chi_1 - \sqrt{\frac{3}{10}} Y_{21} \chi_0 \right.\right.$$

$$\left.\left. + \sqrt{\frac{6}{10}} Y_{22} \chi_{-1} \right) \right] \quad .$$

Using the orthogonality of $\chi^*_M \chi_{M'} = \delta_{MM'}$, $T_{0,11}$ can be simplified as:

$$T_{0,11} = \int dr \sin\theta \, d\theta d\varphi \left\{ \frac{1}{4\pi} u^2 + 2uw\sqrt{\frac{1}{4\pi}}\sqrt{\frac{1}{10}} Y_{20} + w^2 \left[\frac{1}{10} Y^*_{20} Y_{20} + \frac{3}{10} Y^*_{21} Y_{21} + \frac{6}{10} Y^*_{22} Y_{22} \right] \right\} \times (f_n(\vec{q}) + f_p(\vec{q})) \, e^{-\frac{irq\cos\theta}{2}} .$$

Integrating over φ we obtain,

$$T_{0,11} = 2\pi(f_n(\vec{q}) + f_p(\vec{q})) \int dr \sin\theta \, d\theta \left\{ \frac{1}{2\sqrt{2}} (u^2 + w^2) P_{00} + \frac{w(u - 8^{-(1/2)}w)}{\sqrt{(20)}\pi} P_{20} \right\} e^{-\frac{irq}{2}\cos\theta}$$

where $P_{\ell M}$'s are the normalized associated Legendre polynomials. Several $P_{\ell M}$'s used in this appendix are listed as follows:

$$P_{00}(\theta) = \frac{1}{\sqrt{2}}$$

$$P_{10}(\theta) = \sqrt{\frac{3}{2}} \cos\theta$$

$$P_{1\pm1}(\theta) = \mp\sqrt{\frac{3}{4}} \sin\theta$$

$$P_{20}(\theta) = \sqrt{\frac{5}{8}} (3\cos^2\theta - 1)$$

$$P_{2\pm1}(\theta) = \mp\sqrt{\frac{15}{4}} \sin\theta\cos\theta$$

$$P_{2\pm2}(\theta) = \sqrt{\frac{15}{16}} \sin^2\theta \quad .$$

Using the following relationships between spherical harmonics and spherical Bessel functions,

$$\int_0^\pi e^{is\cos\theta} P_0(\cos\theta) \sin\theta \, d\theta = \sqrt{2}\, j_0(s) \quad ,$$

$$\int_0^\pi e^{is\cos\theta} P_2(\cos\theta) \sin\theta \, d\theta = -\sqrt{10}\, j_2(s) \quad ,$$

and the property of spherical Bessel functions

$$j_n(-rq) = (-1)^n j_n(rq) \quad ,$$

$T_{0,11}$ can be simplified as:

$$T_{0,11} = 2\pi(f_p(\vec{q}) + f_n(\vec{q})) \int dr \left\{ \frac{1}{2\pi} (u^2 + w^2)\, j_0(-\frac{rq}{2}) - \frac{w(u - 8^{-(1/2)} w)}{\sqrt{2}\,\pi} j_2(-\frac{qr}{2}) \right\}$$

or

$$T_{0,11} = (f_p(\vec{q}) + f_n(\vec{q}))[S_0(\tfrac{q}{2}) - \tfrac{1}{\sqrt{2}} S_2(\tfrac{q}{2})]$$

where

$$S_0(\tfrac{q}{2}) = \int_0^\infty dr(u^2 + w^2)\, j_0(\tfrac{rq}{2})$$

and

$$S_2(\tfrac{q}{2}) = \int_0^\infty dr\ 2w(u - 8^{-1/2} w)\, j_2(\tfrac{rq}{2}) \quad .$$

Next, $T_{2,11}$ can be written as:

$$T_{2,11} = \left\langle \psi_1 \middle| \frac{i}{2\pi k} \int d^2q'\ f_n(\tfrac{\vec{q}}{2} - \vec{q}')\, f_p(\tfrac{\vec{q}}{2} + \vec{q}')\, e^{-i\vec{q}\cdot\vec{r}} \middle| \psi_1 \right\rangle$$

$$= \frac{i}{2\pi k} \int d^2q'\ f_n(\tfrac{\vec{q}}{2} - \vec{q}')\, f_p(\tfrac{\vec{q}}{2} + \vec{q}')\, I_{11}(q')$$

where

$$I_{11}(q') = \int r^2 dr \sin\theta\, d\theta\, d\varphi \left[\frac{1}{\sqrt{4\pi}} \frac{u^*}{r} \chi_1^* + \frac{w^*}{r} \left(\sqrt{\tfrac{1}{10}}\, Y_{20}^*\, \chi_1^* \right.\right.$$

$$\left.\left. - \sqrt{\tfrac{3}{10}}\, Y_{21}^*\, \chi_0^* + \sqrt{\tfrac{6}{10}}\, Y_{22}^*\, \chi_{-1}^* \right) \right]$$

$$\times e^{-rq'(\cos\theta\cos\alpha + \sin\theta\sin\alpha\cos\varphi)}$$

$$\times \left[\frac{1}{\sqrt{4\pi}} \frac{u}{r} \chi_1 + \frac{w}{r} \left(\sqrt{\tfrac{1}{10}}\, Y_{20}\, \chi_1 - \sqrt{\tfrac{3}{10}}\, Y_{21}\, \chi_0 + \sqrt{\tfrac{6}{10}}\, Y_{22}\, \chi_{-1} \right) \right]$$

Similarly using the orthogonality of the spin functions, $I_{11}(q')$ is then reduced to

$$I_{11}(q') = \int dr \sin\theta\, d\theta\, d\varphi \left[\frac{u^2}{4\pi} + \frac{2uw}{\sqrt{(40\pi)}} Y_{20} + w^2 \left(\frac{1}{10} Y_{20}^* Y_{20} + \frac{3}{10} Y_{21}^* Y_{21} + \frac{6}{10} Y_{22}^* Y_{22} \right) \right] \times e^{-irq'\cos\theta\cos\alpha} \times e^{-irq'\sin\theta\sin\alpha\cos\varphi} .$$

Integrating over the variable φ and using the formula

$$\int_0^{2\pi} e^{is\cos\varphi} e^{in\varphi} = \frac{2\pi}{(-i)^n} J_n(s) ,$$

we obtain,

$$I_{11}(q') = \int dr \sin\theta\, d\theta \left[\frac{u^2 + w^2}{\sqrt{2}} P_{00} + \frac{w(u - 8^{-1/2} w)}{\sqrt{5}} P_{20} \right] \times J_0(-rq' \sin\theta \sin\alpha)\, e^{-iq'r\cos\theta\cos\alpha} .$$

The Bessel function J_n and the spherical Bessel function j_n are related according to

$$\int_0^{\pi} e^{irq'\cos\theta\cos\alpha} J_m(-rq' \sin\theta \sin\alpha) P_{\ell m}(\cos\theta) \sin\theta\, d\theta = 2i^{\ell-m} P_{\ell m}(\cos\alpha)\, j_\ell(-rq')$$

thus,

$$I_{11}(q') = \int dr \; \frac{u^2 + w^2}{\sqrt{2}} \, 2P_{00}(\cos\alpha) \, j_0(rq')$$

$$- \frac{2w(u - 8^{-1/2} w)}{\sqrt{5}} \, P_{20}(\cos\alpha) \, j_2(rq')$$

$$= S_0(q') - \frac{P_{20}(\cos\alpha)}{\sqrt{5}} \, S_2(q')$$

and then

$$I_{11} = S_0(q') - \frac{(3\cos^2\alpha - 1)}{2\sqrt{2}} \, S_2(q') \quad ,$$

thus,

$$T_{2,11} = \frac{i}{2\pi k} \int d^2q' \; f_n(\tfrac{\vec{q}}{2} - \vec{q}') \, f_p(\tfrac{\vec{q}}{2} + \vec{q}') \left[S_0(q') - \frac{(3\cos^2\alpha - 1)}{2\sqrt{2}} \right.$$

$$\left. \times S_2(q') \right] \quad .$$

The expression for T_{11} is the sum of $T_{0,11}$ and $T_{2,11}$ and can be written as follows:

$$T_{11} = [f_p(\vec{q}) + f_n(\vec{q})] \left[S_0(\tfrac{q}{2}) - \frac{S_2(\frac{q}{2})}{\sqrt{2}} \right] + \frac{i}{2\pi k} \int q' dq' d\alpha$$

$$\times f_p(\tfrac{\vec{q}}{2} + \vec{q}') \, f_n(\tfrac{\vec{q}}{2} - \vec{q}') \left[S_0(q') - S_2(q') \, \frac{(3\cos^2\alpha - 1)}{2\sqrt{2}} \right] .$$

Similarly, for $M = M' = 0$,

$$T_{00} = T_{0,00} + T_{2,00}$$

$$= \left\langle \psi_0 \middle| f_n(\vec{q}) \exp(-\tfrac{1}{2}\vec{q}\cdot\vec{r})\, f_p(\vec{q}) \exp(-\tfrac{1}{2}\vec{q}\cdot\vec{r}) \middle| \psi_0 \right\rangle$$

$$+ \left\langle \psi_0 \middle| \frac{i}{2\pi k} \int d^2\vec{q}'\, f_n(\tfrac{\vec{q}}{2} - \vec{q}')\, f_p(\tfrac{\vec{q}}{2} + \vec{q}')\, e^{-i\vec{r}\cdot\vec{q}'} \middle| \psi_0 \right\rangle .$$

We can also write

$$T_{0,00} = (f_n(\vec{q}) + f_p(\vec{q})) \int \left\{ \left[\frac{1}{\sqrt{(4\pi)}} \frac{u}{r}^* \chi_0^* + \frac{w}{r}^* \left(\sqrt{\frac{3}{10}} Y_{2-1}^* \chi_1^* \right.\right.\right.$$

$$\left.\left.\left. - \sqrt{\frac{4}{10}} Y_{20}^* \chi_0^* + \sqrt{\frac{3}{10}} Y_{21}^* \chi_{-1}^* \right) \right] \times e^{-\frac{irq}{2}\cos\theta}$$

$$\times \left[\frac{1}{\sqrt{(4\pi)}} \frac{u}{r} \chi_0 + \frac{w}{r} \left(\sqrt{\frac{3}{10}} Y_{2-1} \chi_1 - \sqrt{\frac{4}{10}} Y_{20} \chi_0 + \frac{3}{10} Y_{21} \chi_{-1} \right) \right] \right\} d\vec{r}$$

Integrating over the variable φ and applying the orthogonality of the spin functions, $T_{0,00}$ is reduced to

$$T_{0,00} = (f_n(\vec{q}) + f_p(\vec{q})) \int dr \sin\theta\, d\theta \left[\frac{u^2 + w^2}{\sqrt{2}} P_{00} \right.$$

$$\left. - \frac{2}{\sqrt{5}} w(u - 8^{-1/2} w) P_{20} \right] e^{-\frac{iqr}{2}\cos\theta}$$

$$= (f_n(\vec{q}) + f_p(\vec{q})) \int dr \left[(u^2 + w^2)\, j_0(\tfrac{rq}{2}) \right.$$

$$+ \sqrt{2}\ 2w(u - 8^{-1/2}\ w)\ j_2(\tfrac{rq}{2})\Big]$$

or

$$T_{0,00} = (f_n(\vec{q}) + f_p(\vec{q}))[S_0(\tfrac{q}{2}) + \sqrt{2}\ S_2(\tfrac{q}{2})] \quad .$$

In evaluating $T_{2,00}$, we need only to evaluate $I_{00}(q')$ in the following expression

$$T_{2,00} = \frac{i}{2\pi k} \int d^2q'\ f_n(\tfrac{1}{2}\vec{q} - \vec{q}')\ f_p(\tfrac{1}{2}\vec{q} + \vec{q}')\ I_{00}(q')$$

where

$$I_{00}(q') = \int r^2 dr \sin\theta\ d\theta\ d\varphi \Big[\frac{1}{\sqrt{(4\pi)}} \frac{u}{r}^*\ \chi_0^* + \frac{w}{r}^* \Big(\sqrt{\tfrac{3}{10}}\ Y_{2-1}^*\ \chi_1^*$$

$$- \sqrt{\tfrac{4}{10}}\ Y_{20}^*\ \chi_0^* + \sqrt{\tfrac{3}{10}}\ Y_{21}^*\ \chi_{-1}^*\Big)\Big]$$

$$x\ e^{-irq'(\cos\theta\cos\alpha + \sin\theta\sin\alpha\cos\varphi)}$$

$$x \Big[\frac{1}{\sqrt{(4\pi)}} \frac{u}{r}\ \chi_0 + \frac{w}{r}\Big(\sqrt{\tfrac{3}{10}}\ Y_{2-1}\ \chi_1 - \sqrt{\tfrac{4}{10}}\ Y_{20}\ \chi_0$$

$$+ \sqrt{\tfrac{3}{10}}\ Y_{21}\ \chi_{-1}\Big)\Big] \quad .$$

Integrating over angular variables θ and φ we obtain,

$$I_{00}(q') = \int dr \left[(u^2 + w^2) \frac{1}{\sqrt{2}} P_{00}(\cos \alpha)\, j_0(-rq)\right.$$

$$\left. - \frac{2w(u - 8^{-1/2} w)}{\sqrt{5}} (-2)\, P_{20}(\cos \alpha)\, j_2(rq')\right] \quad ,$$

or

$$I_{00}(q') = S_0(q') + \frac{2}{\sqrt{5}} P_{20}(\cos \alpha)\, S_2(q')$$

$$= S_0(q') + \frac{\sqrt{2}}{2} S_2(q')(3 \cos^2 \alpha - 1) \quad ,$$

thus,

$$T_{00} = [f_p(\vec{q}) + f_n(\vec{q})][S_0(\tfrac{q}{2}) + \sqrt{2}\, S_2(\tfrac{q}{2})] + \frac{i}{2\pi k} \int q'dq'd\alpha$$

$$\times f_p(\tfrac{\vec{q}}{2} + \vec{q}')\, f_n(\tfrac{\vec{q}}{2} - \vec{q}') \left[S_0(q') + \frac{\sqrt{2}}{2} S_2(q')(3 \cos^2 \alpha - 1)\right] \quad .$$

It is easy to show that $T_{0,1-1} = T_{0,10} = 0$ because the orthogonality properties of the spin functions and the spherical harmonics.

$$T_{2,1-1} = \frac{i}{2\pi k} \int d\vec{q}'^{\,2}\, f_p(\tfrac{\vec{q}}{2} + \vec{q}')\, f_n(\tfrac{\vec{q}}{2} - \vec{q}')\, I_{1-1}(q')$$

where

$$I_{1-1}(q') = \int r^2 dr \sin\theta\, d\theta\, d\varphi \left[\frac{1}{\sqrt{(4\pi)}} \frac{u}{r}^{*} \chi_1^{*} + \frac{w}{r}^{*} \left(\sqrt{\frac{1}{10}}\, Y_{20}^{*}\, \chi_1^{*}\right.\right.$$

$$- \sqrt{\frac{3}{10}}\, Y_{21}^{*}\, \chi_{0}^{*} + \sqrt{\frac{6}{10}}\, Y_{22}\, \chi_{-1}^{*} \Big)\Big]$$

$$\times\, e^{-iq'r(\cos\theta\cos\alpha + \sin\theta\sin\alpha\cos\varphi)}$$

$$\times \Big[\frac{1}{\sqrt{(4\pi)}}\frac{u}{r}\,\chi_1 + \frac{w}{r}\Big(\sqrt{\frac{6}{10}}\, Y_{2-2}\,\chi_{-1} - \sqrt{\frac{3}{10}}\, Y_{2-1}\,\chi_0$$

$$+ \sqrt{\frac{1}{10}}\, Y_{20}\,\chi_1\Big)\Big] \quad .$$

$I_{1-1}(q')$ can be reduced to

$$I_{1-1}(q') = -\frac{3}{2\sqrt{2}}\, S_2(q')\, \sin^2\alpha$$

therefore,

$$T_{1-1} = 0 + \frac{(-i)}{2\pi k}\int q'dq'd\alpha\; f_p\Big(\frac{\vec{q}}{2} + \vec{q}'\Big)\, f_n\Big(\frac{\vec{q}}{2} - \vec{q}'\Big)$$

$$\times\Big[\frac{3}{2\sqrt{2}}\, S_2(q')\, \sin^2\alpha\Big] \quad .$$

We will show that $T_{2,10}$ is zero by writing $T_{2,10}$ as follows:

$$T_{2,10} = \frac{i}{2\pi k}\int d^2q'\; f_p\Big(\frac{\vec{q}}{2} + \vec{q}'\Big)\, f_n\Big(\frac{\vec{q}}{2} - \vec{q}'\Big)\, I_{10}(q')$$

where

$$I_{10}(q') = \int r^2 dr \sin\theta \, d\theta \, d\varphi \Big[\frac{1}{\sqrt{(4\pi)}} \frac{u}{r}^* \chi_1^* + \frac{w}{r}^* \Big(\sqrt{\frac{1}{10}} Y_{20}^* \chi_1^*$$

$$- \sqrt{\frac{3}{10}} Y_{21}^* \chi_0^* + \sqrt{\frac{6}{10}} Y_{22}^* \chi_{-1}^* \Big) \Big]$$

$$\times e^{-ir\vec{q}'(\cos\theta \cos\alpha + \sin\theta \sin\alpha \cos\varphi)}$$

$$\times \Big[\frac{1}{\sqrt{(4\pi)}} \frac{u}{r} \chi_0 + \frac{w}{r} \sqrt{\frac{3}{10}} Y_{2-1} \chi_1 - \sqrt{\frac{4}{10}} Y_{20} \chi_0$$

$$+ \sqrt{\frac{3}{10}} Y_{21} \chi_{-1} \Big) \Big] \quad .$$

$I_{10}(q')$ can be reduced to

$$I_{10}(q') = -i \int dr \Big[\sqrt{\frac{3}{5}} uw \, 2i^3 P_{2-1}(\cos\alpha) \, j_2(rq')$$

$$- \frac{w^2}{7\sqrt{5}} 2i^5 P_{4-1}(\cos\alpha) \, j_4(rq')$$

$$- \frac{9w^2}{56\sqrt{2}} 2i^3 P_{2-1}(\cos\alpha) \, j_2(rq') \Big] \quad .$$

Since P_{2-1} and P_{4-1} contain $\sin\alpha$ to the first power they are odd function of the variable α and therefore, when integrated over $d\alpha$ in d^2q' from 0 to 2π we find that $I_{10}(q') = 0$. It follows that,

$$T_{10} = 0 \quad .$$

Similarly

$$T_{2,10} = T_{2,-10} = T_{2,0-1} = 0 \quad .$$

By symmetry one can easily show that

$$T_{11} = T_{-1-1}$$

and

$$T_{1-1} = T_{-11} \quad .$$

In summary, the matrix elements of $T_{MM'}$ are shown as follows:

$$T_{11} = [f_p(\vec{q}) + f_n(\vec{q})] \left[S_0(\tfrac{1}{2} q) - \frac{S_2(\frac{q}{2})}{\sqrt{2}}\right] + \frac{i}{2\pi k} \int q'dq'd\alpha$$

$$\times f_p(\tfrac{\vec{q}}{2} + \vec{q}') \, f_n(\tfrac{\vec{q}}{2} - \vec{q}') \left[S_0(q') - S_2(q') \, \frac{(3 \cos^2 \alpha - 1)}{2\sqrt{2}}\right],$$

$$T_{-1-1} = T_{11} \quad ,$$

$$T_{00} = [f_p(\vec{q}) + f_n(\vec{q})][S_0(\tfrac{q}{2}) + \sqrt{2} \, S_2(\tfrac{q}{2})] + \frac{i}{2\pi k} \int q'dq'd\alpha$$

$$\times f_p(\tfrac{\vec{q}}{2} + \vec{q}') \, f_n(\tfrac{\vec{q}}{2} - \vec{q}')[S_0(q') + \tfrac{\sqrt{2}}{2} \, S_2(q')(3 \cos^2 \alpha - 1)] \, ,$$

$$T_{1-1} = \frac{i}{2\pi k} \int q'dq'd\alpha \, f_p(\tfrac{\vec{q}}{2} + \vec{q}') \, f_n(\tfrac{\vec{q}}{2} - \vec{q}') \left[\frac{3}{2\sqrt{2}} \, S_2(q') \sin^2 \alpha\right],$$

$$T_{-11} = T_{1-1} \quad ,$$

and $$T_{10} = T_{01} = T_{0-1} = T_{-10} = 0 \quad .$$

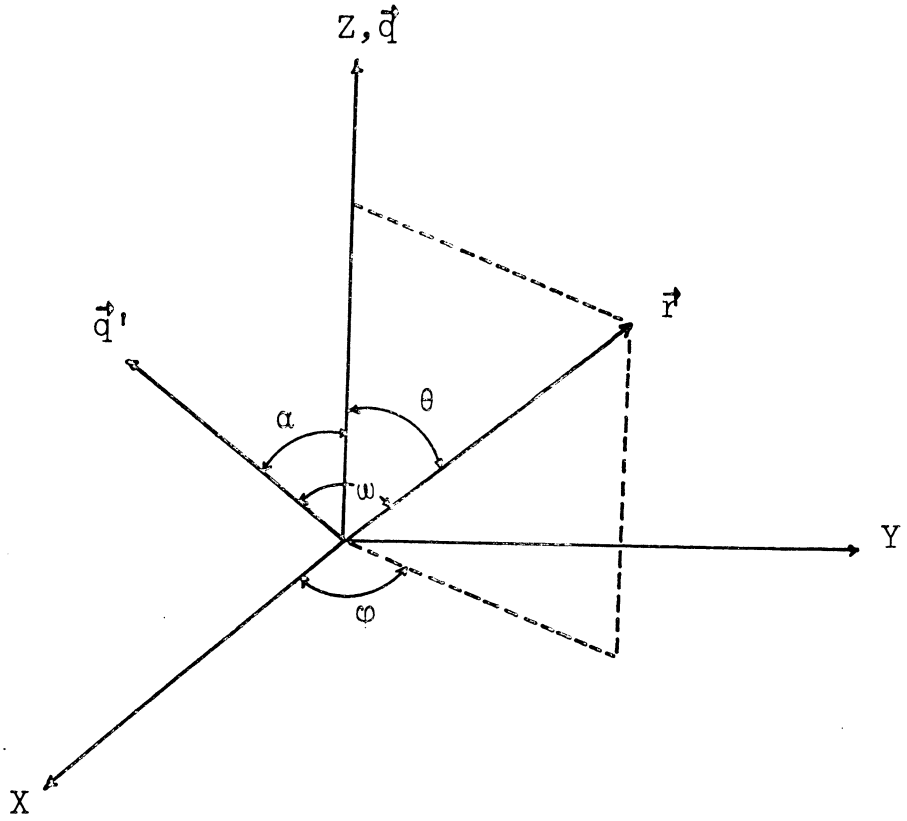

Figure 31. Coordinate system chosen for evaluating matrix elements $T_{MM'}$.

REFERENCES

1. G. F. Chew, Phys. Rev. 80, 196 (1950); S. Fernbach, T. A. Green, and K. M. Watson, ibid. 84, 1084 (1951).

2. P. K. Williams, D. M. LeVine, and J. A. Koschik, References and Some Two-body Data for High Energy Reactions (University of Michigan, 1967).

3. A. M. Sachs, H. Winick, and B. A. Wooten, Phys. Rev. 109, 1733 (1958).

4. K. C. Rogers and L. M. Lederman, Phys. Rev. 105, 247 (1957).

5. E. Arase, G. Goldhaber, and S. Goldhaber, Phys. Rev. 90, 160 (1953).

6. E. G. Pewitt, T. H. Fields, G. B. Yodh, J. G. Fetkovich, and M. Derrick, Phys. Rev. 131, 1826 (1963).

7. L. S. Dul'kova, I. B. Sokolova, and M. G. Shafranova, zh. Eksperim. i Teor. Fiz. 35, 313 (1958). [Translation: Soviet Phys. - JETP 8, 217 (1959).]

8. G. Vegni, et al., Physics Letters 19, 526 (1965).

9. R. J. Glauber, in Lecture in Theoretical Physics, ed. by W. E. Brittin and L. G. Dunham (Interscience, New York, 1959), Vol. 1, p. 315.

10. R. J. Glauber, Phys. Rev. 100, 242 (1955).

11. V. Franco and R. J. Glauber, Phys. Rev. 142, 1195 (1966).

12. V. Franco and E. Coleman, Phys. Rev. Letters 17, 827 (1966).

13. R. J. Glauber, High Energy Physics and Nuclear Structure, ed. by G. Alexander (North Holland, Amsterdam, 1967), p. 311.

14. B. P. Roe, University of Michigan Bubble Chamber Research Note No. 45/65, 1965 (unpublished).

15. A. Everett, Phys. Rev. 126, 831 (1962).

16. G. Chew and M. Goldberger, Phys. Rev. 87, 778 (1952).

REFERENCES (Continued)

17. M. Goldberger and K. Watson, Collision Theory (John Wiley and Sons, Inc., New York, N. Y., 1964).

18. R. Blankenbecler, M. Goldberger, and F. Halpern, Nuclear Physics 12, 629 (1959).

19. E. S. Abers, H. Burkhart, V. L. Teplitz, and C. Wilkin, Nuovo Cimento 42, 365 (1966); and Physics Letters 21, 339 (1966).

20. J. Pumplin, Phys. Rev. 173, 1651 (1968).

21. C. Baltay, H. N. Brown, J. Sandweiss, J. R. Sanford, M. S. Webster, and S. S. Yamamoto, in Proceedings of the 1962 Conference on Instrumentation for High Energy Physics at CERN, edited by F. S. M. Forley and M. E. Meyer (North Holland Publishing Company, Amsterdam, 1963), p. 37; C. Baltay, J. Sandweiss, J. Sanford, H. Brown, M. Webster, and S. Yamamoto, Nucl. Instr. Method 20, 37 (1963); C. Baltay, dissertation, Yale University, 1962 (unpublished).

22. G. C. Benson, Mesons and Spectator Protons in $\pi^+ d \rightarrow \pi^+\pi^-\pi^\circ pp$ at 3.65 BeV/c, dissertation (University of Michigan Technical Report C00-1112-4, 1966).

23. E. Hart, BNL-BCG Internal Report J-22 (1962).

24. R. Rau, BNL-BCG Internal Report J-18 (1961).

25. H. C. Hsiung, University of Michigan Bubble Chamber Group Research Note No. D-5 (1965).

26. Y. Lee, Investigation of Dipion Resonances in 3.7 BeV/c $\pi^+ p$ Collisions, dissertation (University of Michigan Technical Report 04938-1T, 1964).

27. J. C. Vander Velde, University of Michigan Bubble Chamber Group Research Notes HI-1 and HI-3 (1963).

28. W. D. C. Moebs, Four and Five-particle Production in 3.7 BeV/c $\pi^+ p$ Collisions, dissertation (University of Michigan Technical Report C00-1112-3, 1965).

29. A. H. Rosenfeld and W. E. Humphrey, Annual Review of Nuclear Science 13, 103 (1963).

REFERENCES (Continued)

30. R. Böck, GRIND Manual, DD/EXP/62/10 (CERN, Geneva, 1962) (unpublished).

31. D. M. Ritson, Techniques of High Energy Physics, p. 103 (Interscience Publisher, 1961).

32. T. Ferbel, Antiproton-proton Interactions at 3.25 BeV/c, dissertation, Yale University, 1963 (unpublished).

33. R. C. Chase, E. Coleman, T. G. Rhoades, M. Fellinger, E. Gutman, R. C. Lamb, and L. S. Schroeder, XIVth International Conference on High Energy Physics, Vienna (1968), (to be published).

34. G. Hohler, G. Ebel, and J. Giesecke, Z. Physik 180, 430 (1964).

35. A. Saulys, dissertation, University of Michigan, 1966 (unpublished).

36. M. J. Moravcsik, Nucl. Phys. 7, 113 (1958).

37. W. Baker et al., Proceedings of the Sienna International Conference on Elementary Particles (Societa Italiana di Fisica, Bologna, Italy, 1963).

38. G. Bennett, J. Frides, H. Palevsky, R. Sutter, G. Igo, W. Simpson, G. Phillips, R. Stearns, and D. Corley, Phys. Rev. Letters 19, 387 (1967).

39. David R. Harrington, Phys. Rev. Letters 21, 1496 (1968).

40. E. Coleman and T. G. Rhodes, Preprint (University of Minnesota).

41. C. Michael and C. Wilkin, Preprint (Rutherford High Energy Lab.).

42. W. Rarita and J. Schwinger, Phys. Rev. 59, 436 (1941).

43. N. K. Glendenning and G. Kramer, Phys. Rev. 126, 2159 (1962).

44. L. Bertocchi, Nuovo Cimenta, 50A, 1015 (1967).

REFERENCES (Concluded)

45. K. B. Mather and P. Swan, Nuclear Scattering (Cambridge University Press, Cambridge, England, 1958).

46. P. Sonderegger, Physics Letters 20, 75 (1966).

47. R. L. Eisner and D. D. Carmony, Preprint (Purdue University); D. D. Carmony (Private Communication).

48. Ian Butterworth et al., Phys. Rev. Letters 15, 500 (1965).

49. G. L. Kane (Private Communication).

ACKNOWLEDGEMENT

It gives me great pleasure to acknowledge the help and encouragement I have received from the following people, to all of whom I am deeply grateful:

Dr. Byron P. Roe for his inspiring guidance during the course of this work, and for serving as chairman of my doctoral committee,

Dr. John C. Vander Velde for many helpful discussions,

Drs. O. E. Overseth, M. Ross, D. Sinclair, and R. C. Tayler for serving as doctoral committee members,

Drs. E. C. Coleman, K. T. Hecht, G. L. Kane, J. C. Pumplin, M. Ross, and Y. Y. Yam for interesting conversations on the theoretical aspects of this work,

Drs. J. W. Chapman, J. Lys, E. Marquit, and C. T. Murphy for many discussions,

My graduate student colleagues: C. Arnold, G. Benson, M. Church, D. Falconer, A. Fisher, W. Gibbs, R. Kiang, J. Koschik, L. Lovell, W. Moebs, J. Morfin, and H. Ring,

Our programming and technical staff: particularly B. Bell, A. Loceff, L. Peterson, B. Stitt, J. Allen, D. Moebs, M. Rauer, V. French, and M. Brueckner,

The technical staff of Brookhaven National Laboratory,

The Bubble Chamber Group, under the direction of Dr. Daniel Sinclair, for supporting this study,

Drs. Chi-hua Hsiung and Hsien-chü Hsiung for their

assistance,

S. Morfin for typing the draft, J. Oh for drafting most of the figures in this report.